UNIVERSIDADE ESTADUAL DE CAMPINAS
Faculdade de Engenharia Elétrica e de Computação

Luisa Fernanda Suárez Uribe

New strategies for pre-processing, feature extraction and classification in BCI systems

Novas estratégias de pré-processamento, extração de atributos e classificação em sistemas BCI

Campinas

2018

UNIVERSIDADE ESTADUAL DE CAMPINAS
Faculdade de Engenharia Elétrica e de Computação

Luisa Fernanda Suárez Uribe

New strategies for pre-processing, feature extraction and classification in BCI systems

Novas estratégias de pré-processamento, extração de atributos e classificação em sistemas BCI

Thesis presented to the School of Electrical and Computer Engineering of the University of Campinas in partial fullfilment of the requirements for the degree of Doctor, in the area of Computer Engineering.

Tese apresentada à Faculdade de Engenharia Elétrica e de Computação da Universidade Estadual de Campinas como parte dos requisitos exigidos para a obtenção do título de Doutora em Engenharia Elétrica, na Área de Engenharia de Computação.

Supervisor: Prof. Romis Ribeiro de Faissol Attux

Este exemplar corresponde à versão final da tese defendida pelo aluno Luisa Fernanda Suárez Uribe, e orientada pelo Prof. Romis Ribeiro de Faissol Attux

Campinas

2018

Ficha catalográfica
Universidade Estadual de Campinas
Biblioteca da Área de Engenharia e Arquitetura
Rose Meire da Silva - CRB 8/5974

Su12n

Suárez Uribe, Luisa Fernanda, 1985-
New strategies for pre-processing, feature extraction and classification in BCI systems / Luisa Fernanda Suárez Uribe. – Campinas, SP : [s.n.], 2018.

Orientador: Romis Ribeiro de Faissol Attux.
Tese (doutorado) – Universidade Estadual de Campinas, Faculdade de Engenharia Elétrica e de Computação.

1. Interfaces cêrebro-computador. 2. Aprendizado de máquina. 3. Processamento de sinais. I. Attux, Romis Ribeiro de Faissol, 1978-. II. Universidade Estadual de Campinas. Faculdade de Engenharia Elétrica e de Computação. III. Título.

Informações para Biblioteca Digital

Título em outro idioma: Novas estratégias para pré-processamento, extração de atributos e classificação em sistemas BCI
Palavras-chave em inglês:
Brain-Computer Interfaces
Machine leaning
Signal processing
Área de concentração: Engenharia de Computação
Titulação: Doutora em Engenharia Elétrica
Banca examinadora:
Romis Ribeiro de Faissol Attux [Orientador]
Diogo Coutinho Soriano
André Kazuo Takahata
Gabriela Castellano
Rafael Ferrari
Data de defesa: 10-12-2018
Programa de Pós-Graduação: Engenharia Elétrica

Identificação e informações acadêmicas do(a) aluno(a)
- ORCID do autor: https://orcid.org/0000-0003-3403-8296
- Currículo Lattes do autor: http://lattes.cnpq.br/5586429932398441

COMISSÃO JULGADORA - TESE DE DOUTORADO

Candidato: Luisa Fernanda Suárez Uribe RA:123223

Data da Defesa: 10 de dezembro de 2018

Titulo da Tese: New strategies for pre-processing, feature extraction and classification in BCI systems

Prof. Dr. Romis Ribeiro de Faissol Attux
Prof. Dr. Diogo Coutinho Soriano
Prof. Dr. André Kazuo Takahata
Prof. Dr. Gabriela Castellano
Prof. Dr. Rafael Ferrari

A ata de defesa com as respectivas assinatiras dos membros da Comissão Julgadora, encontra-se no SIGA (Sistema de Fluxo de Dissertação/Tese) e na Secretaria de Pós-Graduação da Faculdade de Engenharia Elétrica e de Computação.

Dedico esta tese à minha familia

Acknowledgements

I would first like to thank God for helping me to fulfill this dream, my health, strength and motivation necessary to achieve complete this work came from Him. I would like to thank my friends and family for their support. For me being in Brazil, away from Colombia, there are many people that have been a family for their constant help, their kindness and affection with me. Thank you for counting on you in so many moments of these years. In particular, I would to thank my parents Ana and Carlos, my siblings Elizabeth and Federico, my nephew Cristobal and my uncles for their love, patience and words that has been a support in my life and a great motivation.

I thank CNPq for the financial support and UNICAMP for the infrastructure made available for this work. I also thank the university professors, especially FEEC professors, for the knowledge and experience received. Among these teachers, special thanks to my supervisor, Prof. Dr. Romis Attux, for the essential help at all times that I needed, with attention, patience and always in a very helpful way. Also, a special thanks to my colleagues DSPCom laboratory, thanks for your help, the tips and be able to share part of postgraduate student life with you.

Abstract

Brain-computer interfaces (BCIs) aim to control an external device by directly employing user's brain signals. Such systems require a series of steps to process and extract relevant features from the observed signals to correctly and efficiently interpret the user's intentions. Although the field has been continuously developing and some difficulties have been overcome, it is still necessary to increase usability by enhancing their classification capacity and increasing the reliability of their response.

The classical objective of BCI research is to support communication and control for users with impaired communication due to illness or injury. Typical BCI applications are the operation of interface cursors, spelling programs or external devices, such as wheelchairs, robots and different types of prostheses. The user sends modulated information to the BCI by engaging in mental tasks that produce distinct brain patterns. The BCI acquires signals from the user's brain and translates them into suitable communication. This thesis aims to develop faster and more reliable non-invasive BCI communication based on the study of different techniques that are employed in the signal processing stages, considering two principal aspects, the machine learning approach, and the reduction of the complexity in the task of learning the mental patterns by the user.

Research was focused on two BCI paradigms, Motor Imagery (MI) and the P300 event related potential (ERP). Signal processing algorithms for the detection of both brain patterns were applied and evaluated.

The aspect of the pre-processing was the first perspective studied to consider how to highlight the response of brain phenomena, in relation to noise and other sources of information that maybe distorting the EEG signal; this in itself is a step that will directly influence the response of the following blocks of processing and classification. Independent Component Analysis (ICA) was used in conjunction with feature selection methods and different classifiers to separate the original sources that are related to the desynchronization produced by MI phenomenon; an attempt was made to create a type of spatial filter that pre-processed the signal, reducing the influence of the noise. Furthermore, some of the classifications values were analyzed considering comparison when used other standard pre-processing methods, as the CAR filter. The results showed that it is possible to separate the components related to motor activity. The ICA proposal was, on average, 4% higher classification accuracy than those obtained using CAR, or when no filter was used.

The roles of methods that study the connectivity of different brain areas were evaluated as the second contribution of this work; this allowed us to consider aspects that contemplate the complexity of the brain response of a user. The area of BCI needs a deeper interpretation of what happens at the brain level in several of the studied phenomena. The technique used to build functional connectivity graphs was correntropy: this quan-

tity was used to measure similarity, a comparison was made using also, the Spearman and Pearson correlation. Functional connectivity relates different brain areas activity, so the study of the graph was evaluated using three measures of centrality of graph, where the importance of a node in the network is measured. In addition, two types of classifiers were tested, comparing the results at the level of classification precision. In conclusion, correntropy can bring more information for the study of connectivity than the use of the simple correlation, which brought improvements in the classification results especially when it was used with the ELM classifier.

Finally, this thesis demonstrates that BCIs can provide effective communication in an application where the prediction of the classification response was modeled, which allowed the optimization of the parameters of the signal processing performed using the xDAWN spatial filter and a FLDA classifier for the problem of the P300 speller, seeking the best response for each user. The prediction model used was Bayesian and confirmed the results obtained with the online operation of the system, thus allowing to optimize the parameters of both the filter and the classifier. In this way it was seen that using filters with few inputs the optimized model gave better results of acuraccy classification than the values initially obtained when the training ofthe xDAWN filter was made for the same cases.

The obtained results showed that improvements in the BCI transducer, pre-processing, feature extraction and classification methods constituted the basis to achieve faster and more reliable BCI communication. Improvements in the classification results were obtained in all cases, compared to techniques that have been widely used and had already shown effectiveness for this type of problems.

Keywords: Brain-computer interface; machine learning; signal processing.

Resumo

As interfaces cérebro-computador (BCIs) visam controlar um dispositivo externo, utilizando diretamente os sinais cerebrais do usuário. Tais sistemas requerem uma série de etapas para processar e extrair atributos relevantes dos sinais observados para interpretar correta e eficientemente as intenções do usuário. Embora o campo tenha se desenvolvido continuamente e algumas dificuldades tenham sido superadas, ainda é necessário aumentar a capacidade de uso, melhorando sua capacidade de classificação e aumentando a confiabilidade de sua resposta.

O objetivo clássico da pesquisa de BCI é apoiar a comunicação e o controle para usuários com comunicação prejudicada devido a doenças ou lesões. Aplicações típicas das BCI são a operação de cursores de interface, programas de escrita de texto ou dispositivos externos, como cadeiras de rodas, robôs e diferentes tipos de próteses. O usuário envia informações moduladas para a BCI, realizando tarefas mentais que produzem padrões cerebrais distintos. A BCI adquire sinais do cérebro do usuário e os traduz em comunicação adequada. Esta tese tem como objetivo desenvolver uma comunicação BCI não invasiva mais rápida e confiável baseada no estudo de diferentes técnicas que atuam nas etapas de processamento do sinal, considerando dois aspectos principais, a abordagem de aprendizado de máquina e a redução da complexidade na tarefa de aprendizado dos padrões mentais pelo usuário.

A pesquisa foi focada em dois paradigmas de BCI, Imagética Motora (IM) e o potencial relacionado ao evento P300. Algoritmos de processamento de sinais para a detecção de ambos os padrões cerebrais foram aplicados e avaliados.

O aspecto do pré-processamento foi a primeira perspectiva estudada, considerando como destacar a resposta dos fenômenos cerebrais, em relação ao ruído e a outras fontes de informação que talvez distorçam o sinal de EEG; isso em si é um passo que influenciará diretamente a resposta dos seguintes blocos de processamento e classificação. A Análise de Componente Independente (ICA) foi usada em conjunto com métodos de seleção de atributos e diferentes classificadores para separar as fontes originais relacionadas à dessincronização produzida pelo fenômeno de IM; esta foi uma tentativa de criar um tipo de filtro espacial que permitisse o sinal ser pré-processado, reduzindo a influência do ruído. Além disso, os resultados dos valores de classificação foram analisados considerando a comparação com métodos padrão de pré-processamento, como o filtro CAR. Os resultados mostraram que é possível separar os componentes relacionados à atividade motora. A proposta da ICA, em média, foi 4% mais alta em porcentagem de precisão de classificação do que os resultados obtidos usando o CAR, ou quando nenhum filtro foi usado.

O papel dos métodos que estudam a conectividade de diferentes áreas do cérebro foi avaliado como a segunda contribuição deste trabalho; Isso permitiu considerar aspectos que

contemplam a complexidade da resposta cerebral de um usuário. A área da BCI precisa de uma interpretação mais profunda do que acontece no nível do cérebro em vários dos fenômenos estudados. A técnica utilizada para construir grafos de conectividade funcional foi a correntropia, esta medida foi utilizada para quantificar a similaridade; uma comparação foi feita usando também, as medidas de correlação de Spearman e Pearson. A conectividade funcional relaciona diferentes áreas do cérebro analisando sua atividade cerebral, de modo que o estudo do grafo foi avaliado utilizando três medidas de centralidade, onde a importância de um nó na rede é medida. Também, dois tipos de classificadores foram testados, comparando os resultados no nível de precisão de classificação.

Em conclusão, a correntropia pode trazer mais informações para o estudo da conectividade do que o uso da correlação simples, o que trouxe melhorias nos resultados da classificação, especialmente quando ela foi utilizada com o classificador ELM.

Finalmente, esta tese demonstra que os BCIs podem fornecer comunicação efetiva em uma aplicação onde a predição da resposta de classificação foi modelada, o que permitiu a otimização dos parâmetros do processamento de sinal realizado usando o filtro espacial xDAWN e um classificador FLDA para o problema do speller P300, buscando a melhor resposta para cada usuário. O modelo de predição utilizado foi Bayesiano e confirmou os resultados obtidos com a operação on-line do sistema, permitindo otimizar os parâmetros tanto do filtro quanto do classificador. Desta forma, foi visto que usando filtros com poucos canais de entrada, o modelo otimizado deu melhores resultados de acurácia de classificação do que os valores inicialmente obtidos ao treinar o filtro xDAWN para os mesmos casos.

Os resultados obtidos mostraram que melhorias nos métodos do transdutor BCI, no pré-processamento, extração de características e classificação constituíram a base para alcançar uma comunicação BCI mais rápida e confiável. O avanço nos resultados da classificação foi obtido em todos os casos, comparado às técnicas que têm sido amplamente utilizadas e já mostraram eficácia para esse tipo de problema. No entanto, ainda há aspectos a considerar da resposta dos sujeitos para tipos específicos de paradigmas, lembrando que sua resposta pode variar ao longo de diferentes dias e as implicações reais disso na definição e no uso de diferentes métodos de processamento de sinal.

Palavras-chaves: Interfaces cérebro-computador; aprendizado de máquina; processamento de sinais.

List of Figures

List of Tables

List of Acronyms and Abbreviations

AAC Augmentative and Alternative Communications

ALS Amyotrophic Lateral Sclerosis

ANNs Artificial Neural Networks

AP Action Potential

AR Autoregressive Model

ARM Autoregressive Method

BC Betweenness Centrality

BCI Brain Computer Interface

BLDA Bayesian Linear Discriminant Analisys

BOLD Blood Oxygen Level-Dependent

BSS Blind Source Separation

CAR Common Average Reference

CD Correlation Dimension

CDF Cumulative Density Function

CLIS Complete Locked Syndrome

CNS Central Nervous System

CSP Common Spatial Patterns

DB Davies-Bouldin

DC Degree Centrality

DSLVQ Distinction-Sensitive Learning Vector Quantizer

DWT Discrete-Wavelet Transform

EC Eigenvector Centrality

ECoG Electrocorticography

EEG Electroencephalogram

ELM Extreme Learning Machine

EMG Electromyography

EOG Electrooculography

$EPSP$ Excitatory Postsynaptic Potential

ERD Event-Related Desynchronization

ERP Event Related Potential

ERS Event-Related Synchronization

FC Functional Conectivity

FD Fractal Dimension

FES Functional Electrical Stimulation

FFT Fast-Fourier Transform

$fMRI$ Functional Magnetic Resonance Imaging

GCF Generalized Correlation Function

$GEVD$ Generalized Eigenvalue Decomposition

$HMMs$ Hidden Markov Models

HOC Higher Order Crossings

HOS Higher Order Spectra

IC Independent Components

ICA Independent Component Analysis

IN Inion

$IPSP$ Inhibitory Postsynaptic Potential

ITL Information-Theoretic Learning

$JADE$ Joint Approximation Diagonalization of Eigen-matrices

KNN K-Nearest Neighbors Algorithm

$LCMV$ Linearly-Constrained Minimum Variance

LDA Linear Discriminant Analysis

$LFPs$ Local Field Potentials

LLE Largest Lyapunov Exponent

LMS Least Mean Square

$LORETA$ Low-Resolution Brain Electromagnetic Tomography

LVQ Learning Vector Quantizer

MC Meta-Classifier

MEG Magneto Encephalography

MI Motor Imagery

MLP Multilayer Perceptron

MUA Multi-Unit Activity

$NIRS$ Near-Infrared Spectroscopy

NS Nasion

PCA Principal Component Analysis

PDF Probability Density Functions

PET Positron Emission Tomography

PLV Phase-Looking Value

PSD Power Spectral Density

QDA Quadratic Discriminant Analysis

RBF Gaussian Radial Basis

$RKHS$ Reproducing Kernel Hilbert Space

ROC Receiver Operating Characteristic

SCI Spinal Cord Injury

SCP Slow Cortical Potential

$SINR$ Signal-to-interference-plus-noise Ratio

SIR Signal-To-Interference

SMR Sensory-Motor Rhythms

SNR Signal to Noise Ratio

$SOBI$ Second-Order Blind Identification

$SSVEP$ Support Vector Machine

$STFT$ Short-Time Fourier Transform

SUA Single-Unit Activity

SVD Singular-Value Decomposition

SVM Support Vector Machine

$SWLDA$ Stepwise Linear Discriminant Analysis

TBI Traumatic Brain Injury

VEP Visual Evoked Potential

WPD Wavelet Packet Decomposition

WT Wavelet Trasform

Contents

1 Introduction

Brain-Computer Interfaces (BCIs) are communication systems based on the interpretation of brain signals through the use of computers or electronic systems to obtain commands to control equipment such as wheelchairs, robotic arms or computer programs. BCIs find an important application by people who have some difficulty to control and to execute body movements, for example, those affected by diseases such as Amyotrophic Lateral Sclerosis (ALS) or even in diseases leading to progressive muscle weakness and paralysis of the body in general(WOLPAW *et al.*, 2002). The ability to interact with the outside world comes from the brain functions that were minimally compromised, allowing the recognition of certain expected brain activity patterns to create an alternative communication channel.

Proper operation of these systems leads to a precise classification scheme that is able to identify a useful brain response and associate it with, for example, the execution of specific commands. Its theoretical pertinence and its applicability have attracted great interest. Its application can be range from assistive technologies to computer games (MILLÁN *et al.*, 2010). Figure 1.1 shows the general scheme of a BCI system.

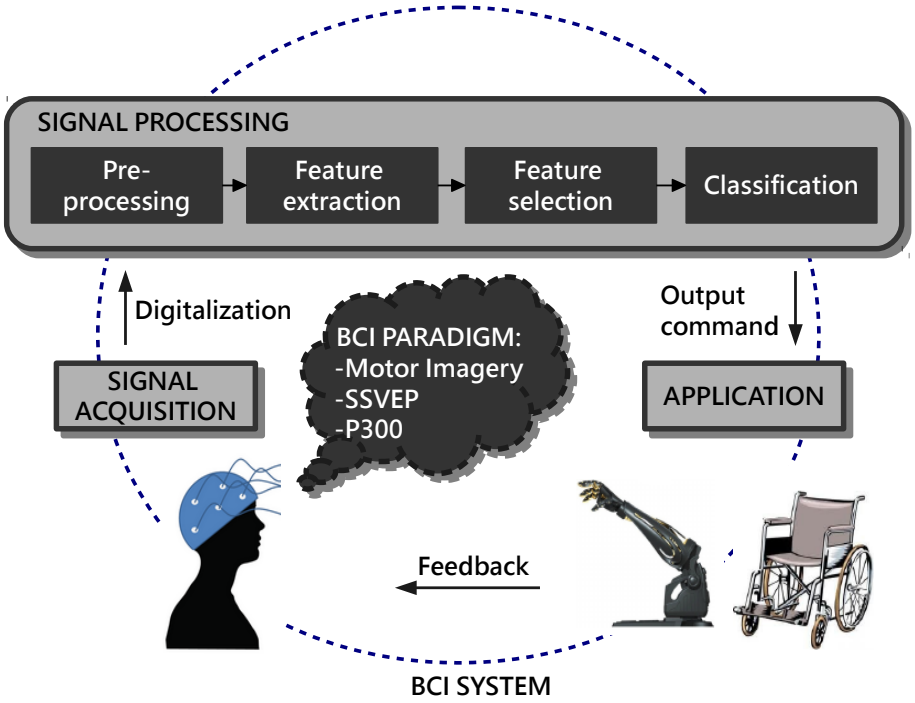

Figure 1.1 – Representation of a generic BCI system.

In fact, many people are unable to effectively interact, or even operate, assistive devices due to functional disabilities. Depending on the degree of illness or injury suffered

by a subject, the recovered capacity of movement will be defined and also the type of assistive device which can be used. There are two main categories into which different types of clinical users that can benefit from the use of BCI systems can be divided:

- The type affected by a degenerative neuromuscular disease like ALS. In these diseases the progressive motor neuron loss leads to a complete destruction of the peripheral and central motor system although sensory and cognitive functions are affected to a relatively minor degree (CHAUDHARY *et al.*, 2016). The loss of muscle activity is accompanied by deficiencies in communication and motor function; the last remaining muscular control is usually associated with the eye muscle. Patients with complete paralysis except for vertical eye movement and blinking but preserved consciousness are classified as having a locked-in syndrome. Total immobility and loss of eye movements with preserved awareness and cognition means that a patient has a complete locked-in syndrome (CLIS) (CHAUDHARY *et al.*, 2016).
- The type affected by severe central nervous system damage, such as stroke or spinal cord injury (SCI). These type of injuries may result from damage to the vertebrae, ligaments or disks of the spinal column or to the spinal cord itself, and often causes permanent changes in strength, sensation and other body functions below the site of the injury (MAYO CLINIC, 2017). Among their symptoms, there are loss or reduction of movement, altered sensation, including the ability to feel heat, cold and touch, loss of bowel or bladder control, inter alia, which leads to a drastic reduction of quality of life. Nowadays, treatments and rehabilitation allow many people with spinal cord injuries to recover some of their lost motor abilities.

Just in Europe, it is estimated that 300,000 people suffer from SCI, with 11,000 new injuries per year (MILLÁN *et al.*, 2010). In the United States, approximately 60% of spinal cord injuries are complete, while studies from Canada and Brazil report complete injuries in 18 and 87% of cases, respectively (SHOICHET *et al.*, 2008). Degeneration in the central nervous system (CNS) as a result of disease or trauma can have negative effects on quality of life. Every year 1.4 million new cases of Traumatic brain injury (TBI) are observed in the United States, resulting in more than 50,000 deaths, 80,000 disabilities and 10,000 new cases of SCI; with another 275,000 people living with an SCI. Most of the people affected by these injuries are young men and women (SHOICHET *et al.*, 2008).

Otherwise, the use of assistive technologies has allowed the work on critical aspects in different areas of life and treatment of patients who are affected by the aforementioned diseases. These applications, in general, cover aspects related with replacing, restoring, enhancing, supplementing, or improving natural (i.e., neuromuscular) CNS outputs.

There are four areas that include the types of application in which a BCI system could operate as an assistive device: (1) communication and control, (2) motor substi-

tution, (3) motor recovery (rehabilitation tools) and (4) entertainment (MILLÁN *et al.*, 2010). This shows that this type of application can also be useful to people who do not suffer from any disease that restricts their mobility. Consequently, contributions on this area have allowed the development of applications from videogames to alternative systems to explore communication between a human and a machine (MILLÁN *et al.*, 2010).

Concerning communication and control, there are several strategies that employ the residual motor functions of the subjects, and can be seen as augmentative and alternative communication (AAC) strategies. A practical application can be found in the eye trackers with speech-generating devices that have been used in joint operation with BCI signals (MILLÁN *et al.*, 2010). These communication interfaces may also allow the control of wheelchairs, mobility vehicles and the interaction with different types of environments (SAEEDI *et al.*, 2017; DOUD *et al.*, 2011). Generally, the control of these systems may be shared by two or even more input signals, e.g. cerebral signal, electromyography (EMG), electrooculography (EOG) or other type of biological signal captured from a user. However, AAC strategies do not work for patients with locked-in syndrome or CLIS owing to the loss of all motor channels: in these cases the BCI-based communication approach involves the exclusively use of brain signals by the patient as input to these systems.

Another application mentioned in the literature is the operation of prosthetic devices. In this context, the term neuroprosthesis is used to describe functional electrical stimulation (FES) systems aiming at the restoration of a weak or lost grasping function of the hand, or other limbs such as legs or feet, e.g. BCI-controlled exoskeleton, electrical orthosis and robotic arms (MULLER-PUTZ; PFURTSCHELLER, 2008; ORTNER *et al.*, 2011). A BCI might contribute to functional recovery in different ways. Some works mention that practical BCI systems could be employed as a tool to reinforce the use of spared neural representations or to insure that subjects were optimally prepared to execute a particular movement (CHAUDHARY *et al.*, 2016). In some cases, the possible users of these technologies do not have any residual movement which can be used as a basis for the control of these devices: therefore, the use of BCI has been evaluated to determine how this systems could be functional for different types of patients.

However, current BCIs are still restricted to laboratory applications. The main reason that prevents BCIs from being widely used is their low robustness and reliability (LOTTE, 2015). Frequent failures in recognizing user commands can result in low accuracy and decreased information transfer rate, even under laboratory conditions (BLANKERTZ *et al.*, 2010; ERP *et al.*, 2012).

There are different causes found to explain the low performance that BCI systems currently deal with. The high sensitivity to noise of some of the most used methods to record the brain signal can be mentioned as one of them. Electroencephalography (EEG) is one of these recording brain signal methods, and uses external electrodes placed on

the scalp. It is portable and relatively low in cost. Although the obtained signal presents a high temporal resolution, it suffers from low spatial resolution and high sensitivity to external noise, due to its low amplitude (TEPLAN, 2002). In addition to this, another factor could be considered problematic in relation to the EEG signal: the non-stationarity in the brain response.

In fact, when a BCI is configured with data from training sessions, it is very likely to have a reduction of performance over test data of other days or experimental contexts (HUEBNER *et al.*, 2018). The collection of numerous examples of the brain signal to train and calibrate the BCI specifically for a subject has been the strategy used to maximize the performance (SHAN *et al.*, 2015; LOTTE *et al.*, 2007). Therefore, to extend the practical use of BCIs, these systems must be robust in contexts adapted to the spatio-temporal differences of the response of a subject and the system itself. For the sake of simplicity, the procedures related to the actual sequences configured for the calibration and preparation of the subjects must be reduced.

1.1 Problem Statement

BCIs were introduced in 1964 (GRAIMANN *et al.*, 2010). Since then, great interest has been devoted to these systems. Remarkable advances in areas such as portability, non-invasiveness, cost and computing power were decisive for their performance improvement and usability up to present day (AMIRI *et al.*, 2013). Different approaches to building a BCI system have been established in the last years in the literature by some of the most prominent groups in this area: Wolpaw and the New York Group (WOLPAW *et al.*, 2002), the Graz Group (PFURTSCHELLER; NEUPER, 2001) and the Berlin Group (BLANKERTZ *et al.*, 2010). These groups have laid the foundation for what has been defined as a classic model for current BCIs: hence this topic has been able to advance in several research groups around the world.

Observing Figure 1.1, it can be seen that, from the analysis of the brain signal, it is expected that the patterns that are present in the brain response be discovered, for example, when an individual receives visual or auditory stimuli, and also when a specific mental task is performed. The paradigms used in BCI have been defined primarily by the use of certain recognized neurophysiological phenomena previously reported in literature, such as: the P300 waveform (CECOTTI *et al.*, 2010); steady-state visually evoked potentials (SSVEP) (CARVALHO *et al.*, 2015b; CARVALHO *et al.*, 2015a); slow cortical potentials (SCPs) (BIRBAUMER *et al.*, 1990); and motor imagery (MI) (PFURTSCHELLER; NEUPER, 2001). In this thesis, proposals related to two types of paradigms - MI and P300 - will be presented.

In view of the existence of multiple stages, BCI systems may change their strategy

depending on the used input paradigm and in the output application to be executed, e.g., control or rehabilitation. The specific variability of the problem has, in fact, favored a machine learning perspective in which, first, a brain pattern must be recognized from a training phase, and then an online session is performed where the trained system response is tested (LOTTE *et al.*, 2007). This adaptation process happens in such a way that recognition algorithms learn the subject's patterns, but, due to the feedback effect of online sessions, the subject also experiences a learning process associated with mental states required for BCI operation.

From the perspective of classic signal processing modeling for BCI systems, the fundamental stages are (FARWELL; DONCHIN, 1988): brain signal acquisition / digitalization, pre-processing, feature extraction / selection and classification. In this work, the focus was particularly on the methods related to the following stages:

- artifact removal: this part tries to deal with the low signal-to-noise ratio of the EEG signal, reducing the effects of the artifacts and the significant variability of the different acquisition configurations;
- feature extraction: this stage is responsible for converting the recorded signals into relevant features that are extracted to discriminate relevant brain activities;
- feature selection: this step optimizes the effectiveness of the features to be used in the classification stage - the analysis must be performed in each specific case;
- classification: these algorithms are used to identify patterns of brain activity by adopting techniques commonly used for machine learning.

The proposals for signal processing in BCI systems have advanced to deal with the challenges raised by an expanding practical frontier. The strategies of adaptation to the conditions of each session and subject are still evolving, leading to new methods that consider aspects like the changes of the response of these systems in several days of use, in a process that still has great variability since different conditions affect both the subject response and the processing implemented in the machine.

There is still a lack of a deeper understanding of how the subject can learn a mental pattern, so the effect of using different types of paradigms must be considered. Other factors that reduce the difficulty of using these systems by the subject should also be analyzed, minimizing the effects of fatigue caused by their prolonged use. These concepts will be addressed throughout the chapters of this thesis, where a clearer and deeper description of the used paradigms will be provided in the context of the contributions, the aim of which is to allow a BCI to be used in a daily operation for various types of applications.

Finally, there are some recent proposals in BCI systems leading to methods that allow an increase in the efficiency of information extraction, such as advanced methods of machine learning (SCHIRRMEISTER *et al.*, 2017), or supervised and unsupervised learning techniques (LOTTE *et al.*, 2007; HUEBNER *et al.*, 2018; YGER *et al.*, 2017). These methods present themselves as possible lines of action towards the definition of more robust BCIs. In this thesis, these directions will form an important basis of comparison.

1.2 Thesis objectives

The objectives of this work were:

General objective:

- To propose new approaches through the use and construction of techniques for signal pre-processing, feature extraction and classification in Motor Imagery and P300 BCIs. It is expected that there will be an increase in the Signal-to-interference-plus-noise (SINR) ratio of the BCI signal and, as a consequence also of the bit transmission capacity of the system.

Specific objectives:

- Analyze the classification performance when using a preprocessing spatial filter based on ICA and selection of features for a motor imagery BCI.
- To compare the performance of classification with different methods of extraction of features, and construction of graphs using analysis of functional connectivity for motor imagery BCI.
- Establish a classification prediction model using the practical values for a P300 speller system, so also a new form of model prediction optimization will be used to obtain the parameters of the spatial filter and classifier blocks.

This work will primarily focus on healthy subjects who have been volunteers for the experimental acquisition of the used databases, but it is expected that the obtained results can be extended to encompass patients.

Part I

Basis

2 Brain Computer Interfaces

The definition of the term "BCI" dates from 1999, during the first international meeting on BCI research and development (WOLPAW *et al.*, 2000). The definition established on this meeting was: "The brain-computer interface is a communication system that does not depend on the normal output of the brain to the peripheral nerves and muscles". A few years before this first official meeting on BCI systems, the interest in the exploration and study of brain signals had already begun.

In 1924, Hans Berger made a decisive finding with the development of EEG to enable the noninvasive recording of neuroelectrical signals from the human brain (BAMDAD *et al.*, 2015). One of the first experiments with humans related to BCI happened in 1969 with Kamiya and colleagues (CHAUDHARY *et al.*, 2016), who showed that healthy individuals could quickly learn to change the alpha waves in their brain (recorded with EEG) if they were given continuous sensory feedback, such as a rising and falling tone. These findings engendered extensive research into the link between brain physiology and behaviour using different experiments with instrumental learning. In this way, the foundations for the development of most current BCIs began to be established. In 1973, was the first time that the official term of BCI was presented by Jacques Vidal (VIDAL, 1977), when he introduced a system that could translate EEG signals into computer control signals.

In the following, the different components of a BCI system will be presented, explaining how the capture of signals works, the underlying brain phenomena and which are the signal processing steps generally employed for the interpretation and generation of a command response. In this way, the evolution of these systems through time and the considered state of the art in this research area will be introduced.

2.1 Signal Acquisition

The human brain is a complex system with billions of inter-connections of nerve cells (neurons) exhibiting rich spatiotemporal dynamics (SANEI; CHAMBERS, 2013). There are several invasive as well non-invasive techniques for mapping brain signals such as: Electroencephalography (EEG), Functional Magnetic Resonance Imaging (fMRI), Magneto Encephalography (MEG), Near-Infrared Spectroscopy (NIRS), Positron Emission Tomography (PET), electrocorticography (ECoG), among others. Before entering a detailed explanation of each of them, some aspects of the functional characteristics of the neuronal activity will be discussed.

2.1.1 Neural activity and action potentials

The CNS (which includes the brain and spinal cord) is composed of two basic types of cells: neurons and glia. Figure 2.1 shows some of these cells with their components and connections.

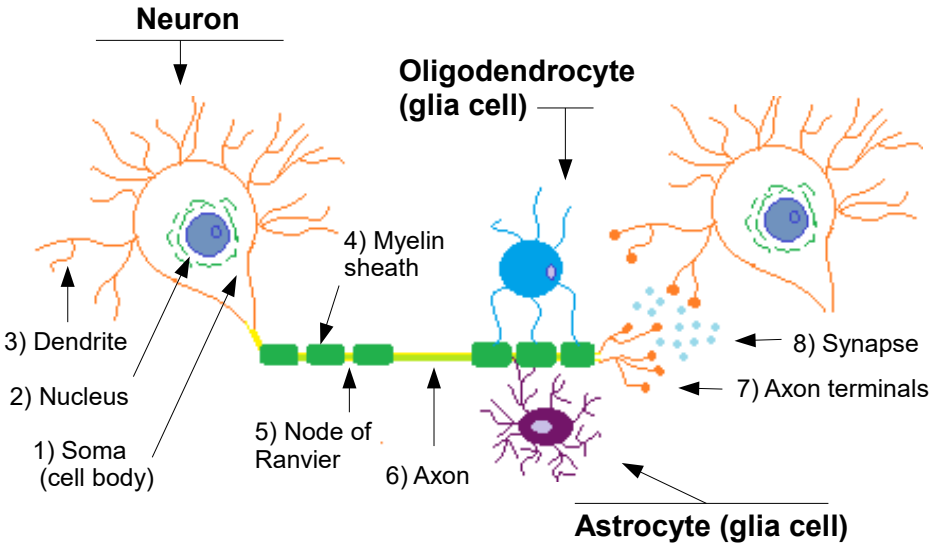

Figure 2.1 – Nerve cells components and connections. Adapted from: (THE NATIONAL INSTITUTE OF NEUROLOGICAL DISORDERS AND STROKE, NIH, 2018)

Neurons are information messengers. They use electrical impulses and chemical signals to transmit information between different areas of the brain, and between the brain and the rest of the nervous system. Everything that is thought, felt and done would be impossible without the work of neurons and their support cells, the glial cells called astrocytes and oligodendrocytes (THE NATIONAL INSTITUTE OF NEUROLOGICAL DISORDERS AND STROKE, NIH, 2018). The neurons have three basic parts:

- soma or cell body (1). Within the cell body is a nucleus (2), which controls the cell's activities and contains its genetic material;
- extension called axon (6). The axon is a long cylinder that is similar to a long tail and transmits messages through the cell;
- dendrites (3). These are also an extension of the cell and look like branches of a tree. These elements receive impulses from others nerves or convey the signals to other nerves. They are connected either to the axons or dendrites of other cells. In the human brain, each nerve is connected to approximately 10,000 other nerves, mostly through dendrites connections (SANEI; CHAMBERS, 2013).

The communication of the neurons with each other is started by sending chemicals, called neurotransmitters, across a space between the axons and dendrites of adjacent neurons, called a synapse (8).

Initially, a neuron can be in a rest state when the membrane of the cell body is polarized to a potential of 60-70mV with negative polarity. When a synaptic activation occurs, the neuron membrane potential changes, as well as the current flow. This transmission of information is called action potential (AP). Two types of action potentials can be found in the presynaptic connection, the excitatory and the inhibitory type. These types of connections can lead to an excitatory postsynaptic potential (EPSP) or an inhibitory postsynaptic potential (IPSP) (SANEI; CHAMBERS, 2013).

As described, the type of synapse indicates how a stimulus modifies the charge distribution within the body of a postsynaptic cell. If this change is large enough, then an AP will be triggered too. APs are caused by particular exchange of ions across the neuron membrane that creates differences of charge that change the potential of the membrane itself. This is usually initiated in the cell body and then travel in one direction along the axon. This process starts when the membrane depolarizes (becomes more positive), producing a spike. After this peak, the membrane repolarizes (becomes more negative), then the potential becomes more negative than the resting potential and next returns to normal (KA XIONG CHARAND, 2002). Figure 2.2 shows the stages of this process.

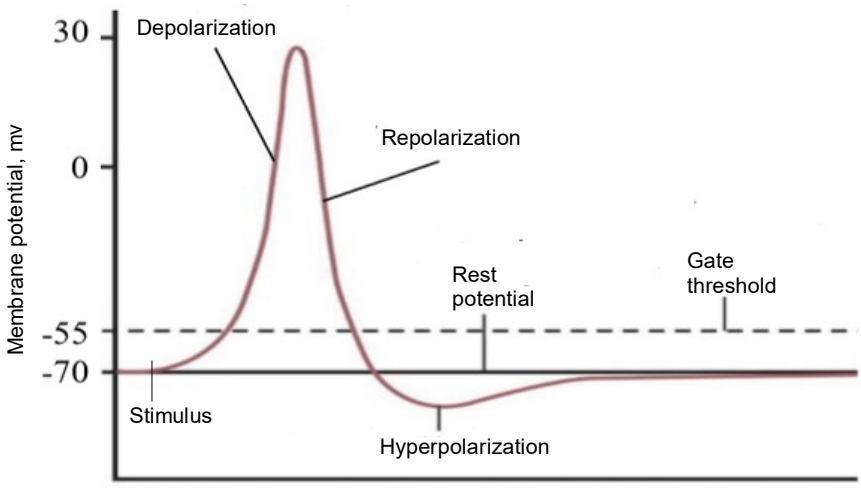

Figure 2.2 – Phases of action potential. Adapted from: (SANEI; CHAMBERS, 2013)

.

2.1.2 Non-invasive techniques for brain signal acquisition

The current methods for non-invasive acquisition most used in the area of BCI systems will be described below. These options stand out because they do not require

that the subject or patient who wants to be benefited by the use of a BCI suffer with devices that are implanted in their brain invasively. The non-invasive techniques can be used within a relatively small amount of time, and do not imply definitive life changes in the body of the subject. One of the most used options, for its speed and performance, is EEG, and this was the method used in this work. Among the current methods used to perform brain signals acquisition in a non-invasive form are: MEG, NIRS, fMRI and PET.

An EEG signal is a measurement of currents that flow in the dendrites of many pyramidal neurons in the cerebral cortex. When these cells are activated, the so called post-synaptic currents are produced within the dendrites. This current generates a magnetic field measurable by MEG machines and a secondary electric field over the scalp measurable by EEG systems (SANEI; CHAMBERS, 2013). To generate a signal that is detectable, approximately 50,000 active neurons are needed (LARSON; LEE, 2014). Currently, almost all noninvasive BCI communications are based on the EEG measure of brain activity, and more than 80% of BCI publications use electrical signals recorded on the scalp (MASON *et al.*, 2006).

Although EEG and MEG signals originate from the same neurophysiological processes, there are important differences between them (COHEN; CUFFIN, 1983). Magnetic fields are less distorted than electric fields by the skull and scalp. The human head consists of different layers including the scalp, skull, brain, and other thin layers in between. The skull attenuates the signals approximately one hundred times more than the soft tissue (SANEI; CHAMBERS, 2013). There are also different sources of noise from other internal brain activity and external interferences on scalp, so these signals must be usually amplified and then treated for their purposes of use. Finally, MEG is reference-free, while scalp EEG relies on a reference, which could make the MEG data interpretation difficult (GENÇER *et al.*, 2003).

For the acquisition of the EEG signal, gel-fixed electrodes on the scalp are commonly used, or even dry electrodes attached to a cap. Although they do not have the same signal quality, dry electrodes are more practical for use in research and BCI systems (PINEGGER *et al.*, 2016). The instrumentation used in the EEG acquisition also includes an amplifier and an analog-to-digital signal conversion system. Nowadays, there are different types and qualities of these equipments, and their simplicity of use allows that a computer be used for recording the data. Among the advantages of using EEG are its portability and low cost. However, some of its disadvantages are that, although the obtained signal has a high temporal resolution, it suffers from low spatial resolution and high sensitivity to external noise due to its low amplitude (TEPLAN, 2002).

There is a standard nomenclature for the EEG positioning scheme, the so-called international 10-20 system. This is based on an iterative arcs subdivision on the scalp

from four craniometric reference points: nasion (NS), inion (IN), and pre-auricular left (PAL) and right (PAR) points. In the international 10-20 system different electrodes are placed at a fixed distance from these points. The name "10-20" refers to the fact that the actual distances between the adjacent electrodes are 10 % or 20 % of the total NS-IN distances or PAL-PAR distances. Figure 2.3 presents what would be the distribution of the electrodes in the scalp for this type of system.

Each electrode has a letter identifying the lobe and an identification number of the location on the hemisphere. The letters F, T, C, P and O represent frontal, temporal, central, parietal and occipital, respectively. A "z" (zero) refers to an electrode placed in the midline. Even numbers (2,4,6,8) refer to electrode positions in the right hemisphere, while odd numbers (1,3,5,7) refer to those in the left hemisphere. For example, electrodes C3 and C4 are placed on the central part of the cortex (C), respectively, in the right (4) and left (3) hemispheres.

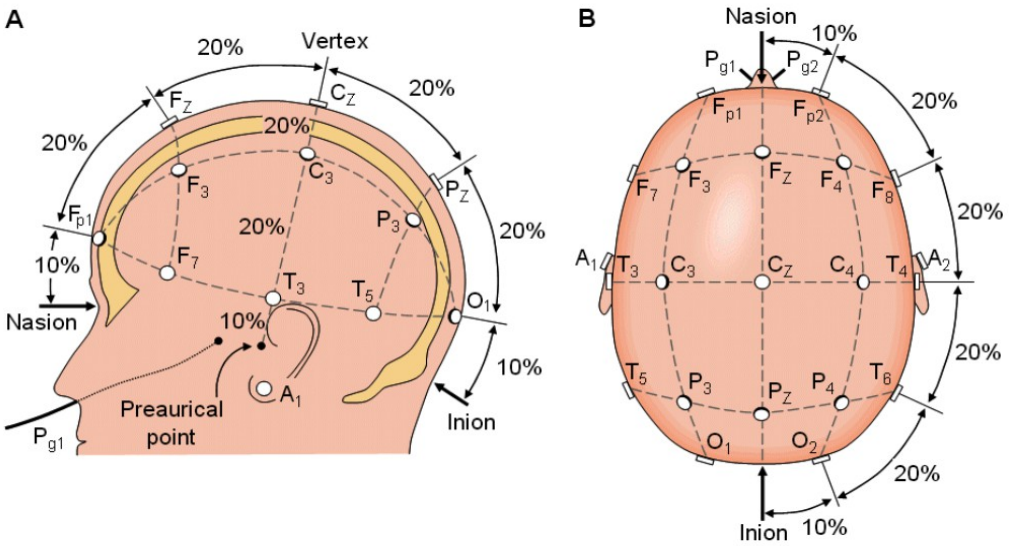

Figure 2.3 – Placement of the electrodes for EEG acquisition, according to the International Positioning 10-20 System. Source: (MALMIVUO; PLONSEY, 2017)

In addition, there are also functional measures that study the brain metabolism. This is the case of fMRI: this method reflects the brain activity indirectly, by measuring the oxygenation of blood flowing near active neurons. Another type of method is NIRS. It uses infrared light to identify fluctuations in cerebral metabolism during neural activity. Finally, the technique of positron emission tomography (PET) measures the blood glucose in activated parts of the brain (BAMDAD *et al.*, 2015). Some of these methods have been used in human neuroimaging showing that it is possible to accurately decode a person's conscious experience based only on non-invasive measurements of their brain activity (HAYNES; REES, 2006). The use of these techniques has been extended based on general sophisticated models that often exhibit higher sensitivity to detect information in brain signals (DIEDRICHSEN *et al.*, 2017; HAYNES, 2015). On many occasions, the use of

these methods has been presented in such a way that they can complement each other in their functions to obtain more precise models of some brain phenomena that are under study.

In BCI applications, MEG, fMRI and PET are generally not suitable for daily usage because of their complex technical requirements, high cost and limited real-time connection capabilities. But in the last few years, some of these methods have been used for BCI applications, because they offer some advantages regarding the quality of the signal in comparison with the most used method, which is EEG (CHAUDHARY *et al.*, 2016). fMRI has been explored for the development of BCIs. In some studies (SERENCES; SAPROO, 2012), patients with neuropsychiatric disorders have been successfully trained in an instrumental learning task that enables control of the blood oxygen level-dependent (BOLD) signal. The NIRS-based BCI, contrarily to the one based on fMRI, can be easily applied to patients who have severe impairments and who have difficulties to move, because its portability is superior to that of fMRI (KANOH *et al.*, 2009; SHIN *et al.*, 2016). Table 4.1 presents a comparison of different techniques for measuring brain activity, including also the invasive techniques.

Table 2.1 – Comparison of techniques to measure brain activity in BCI.

Method	Measured quantity	Invasive	Spatial resolution	Temporal resolution	Portable equipment
EEG	Electrical Pot.	No	-	++	Yes
ECoG	Electrical Pot.	Yes	+	++	Yes
Micro-electrodes	Electrical Pot.	Yes	++	++	Yes
MEG	Magnetic field	No	+	++	No
fMRI	Blood oxygen level	No	++	-	No
NIRS	Blood oxygen level	No	+	+	Yes

2.1.3 Invasive techniques for brain signal acquisition

The use of invasive BCIs involves surgical implantation of electrodes or multi-electrode grids. Invasive BCIs measure the pattern activity of groups of neurons, which encode behaviourally relevant information. Five main types of brain activity have been used as a measure for these types of BCIs: (1) local field potentials (LFPs), (2) single-unit activity (SUA), (3) multi-unit activity (MUA), (4) electrocorticographic oscillations recorded from electrodes on the cortical surface (electrocorticography, ECoG), and (5) calcium channel permeability (CHAUDHARY *et al.*, 2016).

All these methods share the common risk associated with the surgery for their implant. For this reason, their study started with animal subjects (YUAN; HE, 2014). Actually, its implementation has also been used in patients with great physical impairments (KENNEDY; BAKAY, 1998; GILJA *et al.*, 2015). The advantages associated with the use of a signal measured in such proximity to its origin are visible in the capacity to have both temporal and frequency high resolution in comparison with non-invasive methods. For this reason, are interesting to be used in BCI systems (YUAN; HE, 2014).

2.2 Operational protocol / stimulus

Next, some of the best known and used types of physiological phenomena for non-invasive BCI will be described, specifically when the EEG signal is used. Different neurophysiological phenomena can be explored to extract information from scalp EEG signals. In some cases, these phenomena are generated consciously by the user (endogenous system). In other cases, there is an unconscious mechanism in response to an external stimulus (exogenous system). Exogenous BCIs are based on Event-Related Potentials (ERP); on the other hand, the main endogenous BCIs are based on slow cortical potentials (SCP) and sensory-motor rhythms (SMR).

Because each paradigm is associated with the neuronal cortical response of certain brain regions to stimuli, Figure 2.4 shows how these regions are separated in a general way according to certain functions in the brain.

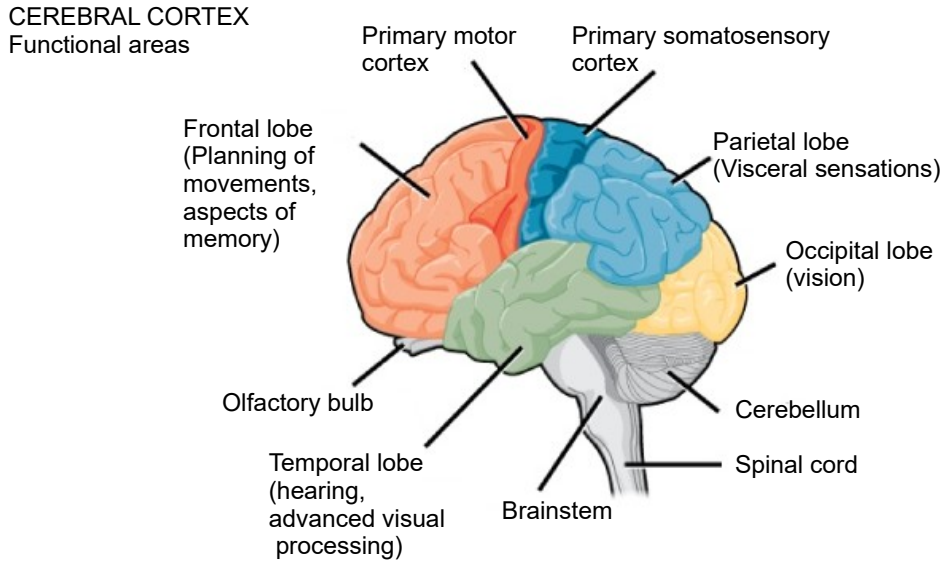

Figure 2.4 – Lobes of the cerebrum and functional areas of the cerebral cortex. Adapted from: (LUMEN, 2018).

2.2.1 Event-Related Potentials (ERPs)

Natural automatic responses from the brain to external stimuli are known as ERPs and are widely used as paradigms for BCI systems. ERPs are associated with experiences that usually involve the presentation of different types of sensory stimuli (visual and auditory), and it is assumed that there is a typical spatial-temporal pattern that is delimited in time for each type of stimulus (also called an event) (RIVET; SOULOUMIAC, 2013). There are distinct types of ERPs: some of the most commonly used are the steady-state visually evoked potentials (SSVEP) and P300, which are visual ERPs. These paradigms have the advantage of providing a more stable response among different subjects, and

also a relatively simple training process. One of the main drawbacks of these approaches is that they require control of the movement of the eyes: this makes them unsuitable for certain types of users, e.g., patients with CLIS.

The SSVEP oscillations are evoked in the occipital electrodes and induced by the observation of repetitive visual stimulation. Stimuli flashing at a certain frequency leads to oscillations in the EEG signal at the same frequency and in harmonics and sub-harmonics of the stimulation frequency (BIN *et al.*, 2009). Users can select a stimulus by focusing on it, which leads to an increase in amplitude in the frequency bin corresponding to the stimulus frequency. Figure 2.5 shows how the SSVEP signal looks like for a subject that fixes his attention on a stimulus that is blinking. The visually evoked potentials (VEP) includes positive (Pi) and negative (Ni) deflections that going to steady stable state oscillation in the EEG signal that is linked to the attended stimulus frequency (NG *et al.*, 2012).

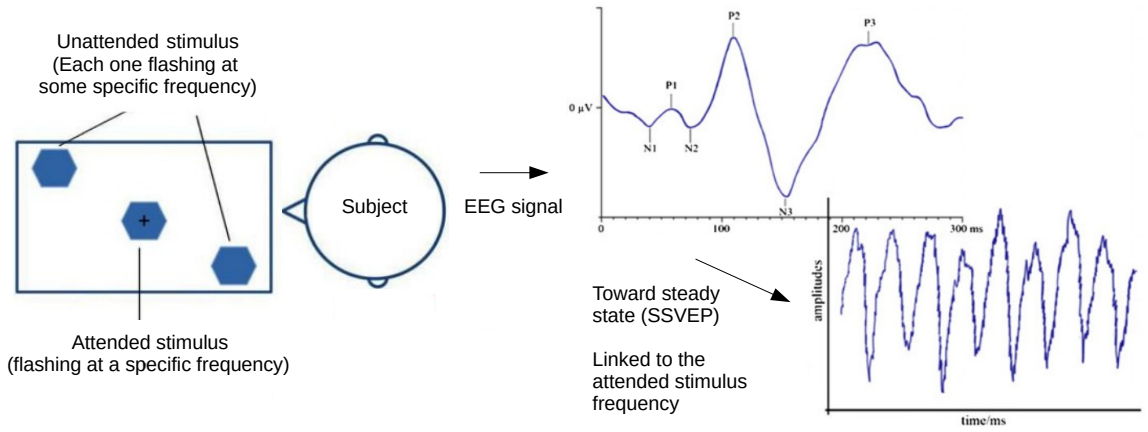

Figure 2.5 – Typical waveforms with visually evoked potentials (VEP) positive (Pi) and negative (Ni) deflections going to steady stable state. Adapted from: (NG *et al.*, 2012).

The P300 wave is a positive deflection that is typically detectable in the EEG measured around the parietal lobe, around 300 ms after the occurrence of an unexpected stimulus (KINDERMANS *et al.*, 2012). Its application is based on the oddball paradigm, in which a rare target stimulus is presented between common stimuli that are not of interest. A typical use consists of a speller where an array containing the symbols of the alphabet is displayed on a screen. Rows and columns of the matrix shine in random order and flashes of the line or column containing the desired symbol (letter) constitute the rare stimulus, while all other flashes constitute normal stimuli (RIVET *et al.*, 2009). Figure 2.6 shows the most typical application of the P300 wave and the brain response associated with this type of stimulation.

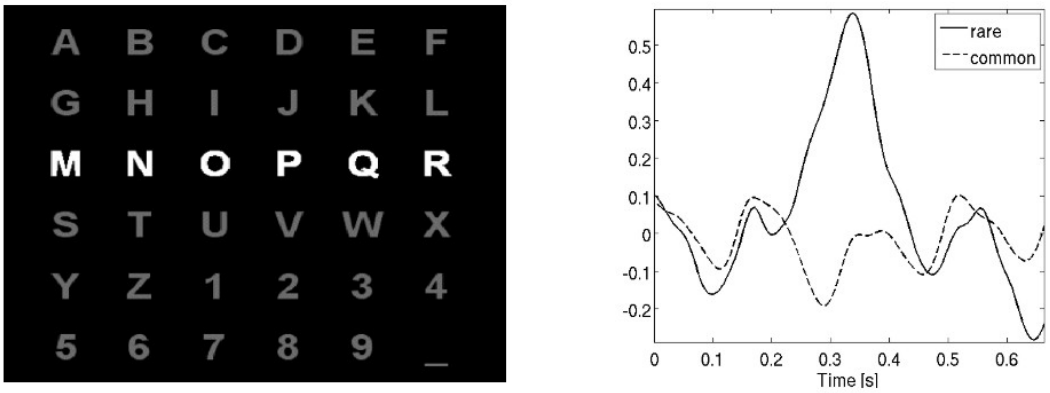

a) Graphical user interface b) P300 evoked potentials

Figure 2.6 – P300-BCI Speller. (a): Screen display, recognition step, (b): The outputs of the P300 classification are represented in the average P300 response on Cz. Source: (CECOTTI *et al.*, 2010).

2.2.2 Slow cortical potentials (SCP)

SCP refer to the slow voltage changes of the EEG signal occurring in the 1-2 Hz frequency range. Negative SCPs correspond to a general decrease in cortical excitability, while positive SCPs correspond to a general increase in cortical excitability. It has been proven that individuals can learn to voluntarily control their SCPs when they are trained with visual or auditory feedback of their brain potential (PFURTSCHELLER; NEUPER, 2001).

2.2.3 Sensory-motor rhythms and motor imagery

Oscillatory brain activity occurs in many regions of the brain following the state changes of the subject (e.g. between wakefulness and sleep or between concentrated and rest work). This EEG activity is usually classified into different frequency bands or rhythms: delta (1-4 Hz), theta (4 -8 Hz), mu (8-13 Hz), beta (13-25 Hz) and gamma (25-40 Hz).

Sensory-motor rhythms (SMR) are observed oscillatory activities in the cortex specific to the sensory-motor (parietal lobe) areas, focused on the frequency of the mu and beta bands. The motor stimulation, behavior, and mental imagery are associated with the modulation of SMR. The Motor Imagery (MI) task results in an amplitude suppression [event-related desynchronization(ERD)] or in an amplitude enhancement [event-related synchronization (ERS)] of mu and central beta rhythms in the motor cortex. Figure 2.7A presents the temporal representation of the ERD and ERS signal for MI events in the mu-band.

Often, hands, feet or tongue MI are investigated: these members require very fine motor control, with detailed sensory information. Hence, they are mapped onto large

regions of the sensorimotor cortex (STIPPICH *et al.*, 2002). More specifically, hand MI has been shown to produce short-lasting ERDs in the mu and central beta rhythms (HALDER *et al.*, 2011). For the case of separate MI of left and right hands, since neurons from the motor cortex are crossed in the medulla, this response can be observed in the contralateral brain hemisphere to which the limb MI is performed (PFURTSCHELLER *et al.*, 1997; PFURTSCHELLER; ARANIBAR, 1977). Figure 2.7B presents the distribution of brain areas related to movement and sensations of different limbs in the human body in the motor and somatosensory cortex.

A common strategy used in the MI-BCI community for signal processing using this type of paradigm involves employing the EEG signal power in specific frequency bands for assessing distinct MI tasks (CINCOTTI *et al.*, 2001; CHENG *et al.*, 2004). Although this phenomenon has the advantage of not needing any external stimulus to provoke it, its biggest disadvantage is the fact that to date no evidence has been found of an easy way to train mental tasks for all types of users, hindering the tasks of BCI, due to the use of more time to adjust, train and detect the classes for each subject (VIDAURRE; BLANKERTZ, 2009).

2.3 Processing and translation

The choice of the adopted paradigm not only influences the acquisition stage of the data, but also the techniques that will be used in the signal processing blocks. Figure 2.8 shows a general view of the components that describe different stages of signal processing used on BCI systems and some of the methods and characteristics of each one of them. These stages will be shortly described next.

2.3.1 Pre-processing

The first stage of signal pre-processing generally includes the mitigation of artifacts. These may appear due to noise introduced by recording equipment, sources of biological origin, or due to changes in electrode impedance. Physiological artifacts are caused by a number of biological processes, such as: ocular movement caused by the blink of an eye, movements of the pupil and the muscle artifacts generated by the movement of any part of the body, including muscles of the face, jaw and tongue. Artifacts can be avoided or removed. In the first case, the segments of corrupted EEG are identified and rejected. The simplest way to do this is to record simultaneously the electrooculography (EOG), electromyography (EMG) and EEG signals. One option is to reject the EEG signal in the time window in which the artifact occurs, which is done primarily for off-line analysis. It is also possible to try to keep interesting neurological phenomena intact using other strategies, such as temporal filtering, regression and blind source separation (BSS)

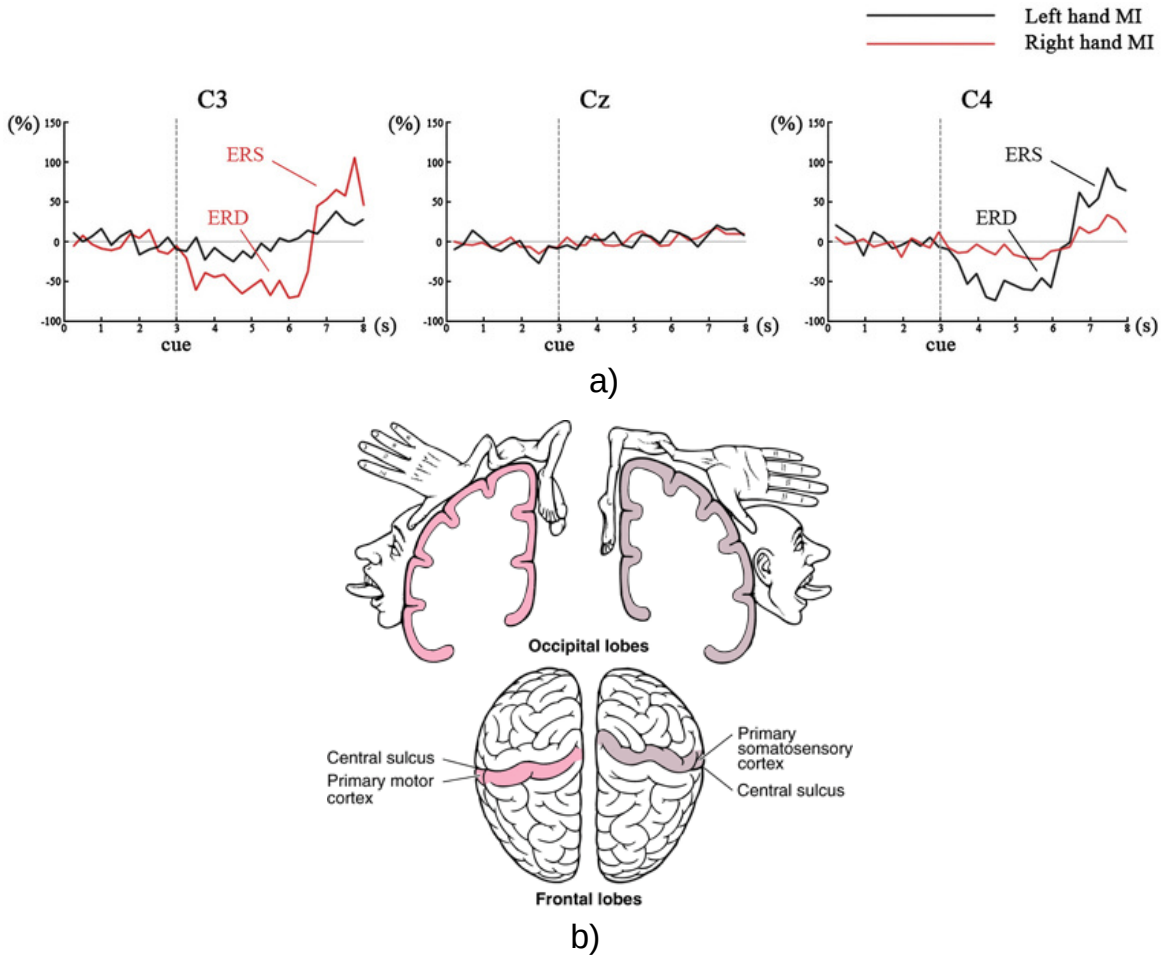

Figure 2.7 – Motor imagery response. a) EEG power of C3, Cz and C4 within 8-12Hz frequency band is averaged over the time and is displayed relative (as percentage) to the power of the same EEG derivations recorded during the reference period. Source: (TANG *et al.*, 2017). b) Sensory-motor regions are illustrated by a "somatosensory homunculus" indicating which regions are assigned to process sensory information from the respective body parts. Source: (MERCK MANUALS, 2018).

(SCHLÖGL *et al.*, 2007; FABIANI *et al.*, 2004).

As previously mentioned, the EEG signal has a low spatial resolution: only half the contribution of a scalp electrode comes from sources within a 3-centimeter radius. Due to this problem, spatial filtering is used as a way to improve signal quality, trying to find the signal at its spatial origin, removing some of the sources of interference that reduce its signal-to-noise ratio.

There are a number of spatial filters available in the literature, most of which apply a linear transformation in the EEG signal, recalculating the contribution of each channel to a specific electrode (DORNHEGE G., 2007). Some spatial filters (MCFARLAND *et al.*, 1997), such as the Common Average Reference (CAR) or Laplacian filters, preserve the original number of channels and produce output signals that are still related to

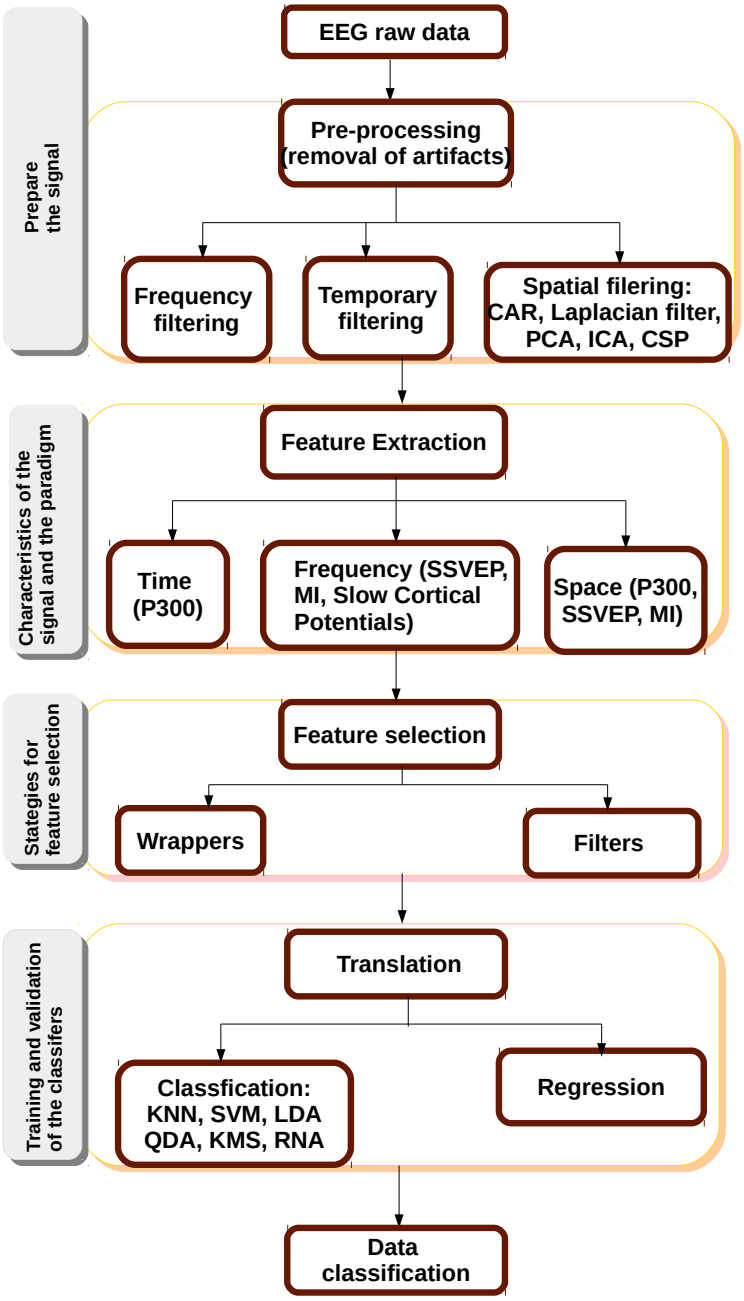

Figure 2.8 – Characteristics of processing and translation stages in a BCI system.

their sources. Other spatial filters lose this direct reference; examples of these are Principal Component Analysis (PCA), Independent Component Analysis (ICA), and Common Spatial Patterns (CSP) (GUGER *et al.*, 2000). This second class of filters is commonly employed when the output channels are designed to be used as discriminative features.

2.3.2 Feature extraction

After pre-processing, feature extraction can be performed to discriminate the user's intentions from other brain activity. The relevant features need to be extracted from

the EEG so that the underlying neurophysiological phenomena can be identified and successfully translated into control signals.

The algorithms used for this task on BCIs are based on an a priori knowledge about the characteristics of the respective neurophysiological phenomena. These characteristics can be obtained from the analysis in time, frequency or space domain (RAMOSER *et al.*, 2000; FABIANI *et al.*, 2004; GROSSE-WENTRUP; BUSS, 2008).

The features extracted in the time domain relate the amplitude of the EEG signal to temporal modifications associated with the presentation of stimuli. Time domain features are commonly used when the underlying neurophysiological phenomena are based on event-related potentials such as P300, since they usually occur within precise time windows after the presentation of a stimulus.

Features in the frequency domain are related to changes in the oscillatory activity of the EEG signal. Such changes can be generated by an external stimulus, or self-induced by the user by concentrating on a specific mental task. Features in the frequency domain are mainly employed in BCI systems based on MI and SSVEP.

On the other hand, features in the spatial domain combine information from different EEG channels in order to identify patterns in brain activity related to distinct neurophysiological phenomena. As already mentioned, several spatial filtering techniques are employed for this purpose: among the most common are PCA, ICA and CSP. Like the frequency features, spatial features have been widely used, as they have proved to be a good strategy to improve the quality of signal discriminative information (BLANKERTZ *et al.*, 2008; WANG *et al.*, 2012; ANG *et al.*, 2012). In the next chapters, where the contributions reported in this thesis will be presented, several methods for the extraction of features using each of the domains mentioned above will be discussed.

2.3.3 Feature selection

After extracting several features, an essential task is to choose the most relevant for the best differentiation between classes (THEODORIDIS; KOUTROUMBAS., 2008). In some cases, the amount of features available to design a classification system can be large when compared to the restricted number of features required to ensure suitable generalization properties of the classifier, reasonable computational complexity and processing time. For this reason, feature selection is applied in order to yield the most relevant features for designing the classification system. Its use is not mandatory and must be evaluated in each case and strategy.

Feature selection exploits the mutual (linear and/or nonlinear) correlation among features by selecting those that convey more class discriminatory information. Strategies for performing this selection usually follow two approaches: filters or wrappers (KOHAVI;

JOHN, 1997; GUYON; ELISSEEFF, 2003). The first uses statistical measures to quantify the relevance of each feature and is probably the simplest technique to operate on the feature space (GUYON; ELISSEEFF, 2003; THEODORIDIS; KOUTROUMBAS., 2008). Filters operate with metrics directly obtained from features, being, therefore, independent of the classifier to be employed. They usually outline statistic functions that yield a relevance index matching each feature and label. This approach tacitly assumes independence between features and, therefore, ignores the correlation between variables, which can affect the prediction performance. The wrappers approach takes into account the performance of the trained classifier to rank the features. Later, on the following chapters, these methods will be discussed in more detail.

2.3.4 Classification

In the sequence of tasks performed in the signal processing stages of a BCI system, there is a final block responsible for defining or categorizing the states that were identified to later convert them into a control signal. This block is related either to regression or classification. In regression, the features of the EEG signal are evaluated in real time and used to generate a continuous control signal. Classification is a more popular approach in BCI research. The corresponding algorithms adopt commonly used techniques for pattern recognition and machine learning. A large number of classification algorithms have been used in BCI systems (DORNHEGE G., 2007). These can be classified into memory-based methods, discriminant functions, and dynamic models. An example of a memory-based method is k-nearest neighbor (KNN). On the other hand, discriminant functions are related to classifiers based on linear, quadratic and other models. Linear models include Linear Discriminant Analysis (LDA), where linearly separable classes are assumed. Quadratic class boundaries are employed by Quadratic Discriminant Analysis (QDA), while general nonlinear boundaries are generated by artificial neural networks (ANNs) and kernel methods (Support Vector Machines, SVMs). Finally, dynamic models assume that the system being considered evolves over time and that its behavior can be modeled through a set of states, such as those described by hidden Markov models (HMMs), Kalman and autoregressive models. The review work (BASHASHATI *et al.*, 2007) discusses a number of BCI works that have used these techniques.

2.3.5 Feedback and / or output

Depending on the type of BCI system, there may exist a feedback and / or a pacing module. When brain activity is produced by self-induced modulations, as in MI, feedback is often provided to assist the user in his/her task, thereby engendering closed-loop control. When the neurophysiological phenomena of interest are derived from external events, a

stimulation module is needed and is generally connected to the feedback module in the physical structure of the BCI.

Otherwise, adaptation is a concept that needs to be considered for BCI systems (HUEBNER *et al.*, 2018). Two different types of adaptation exist: the adaptation of the machine to the user, that consists on the parameterization for each user of the learning algorithm (signal processing block); and the adaptation of the user to the machine when the subject learns to regulate the specific activities of the brain by means of a feedback signal that is provided in real time by the BCI system. The feedback offers continuous information about the change in brain activity, thus allowing a conscious or unconscious training process of the user (PERRIN *et al.*, 2010).

The use of feedback is still a topic of intense study in BCI, since it has been observed that the user is significantly affected by this process to change his mental strategy of accomplishment of the task. Naturally, in the case of erroneous feedback, the learning process would be affected. The best way to deal properly with this complex problem of co-adaptation is still an open question in the field of BCI research (GUGER *et al.*, 2001; ACQUALAGNA *et al.*, 2016; HUEBNER *et al.*, 2018).

Part II

Contributions

3 Combined use of ICA based pre-processing and feature selection for motor imagery BCI

3.1 Introduction

The characterization of spatial and time-frequency properties of the EEG signal recorded in the context of the BCI systems can be complex. The adoption of a robust adaptation process using spatial filters and classifiers has been considered to help in the analysis of some distinctive parameters, such as noise, interference, and the experimental and subject-specific features used to recognize the cerebral patterns of interest. Thus, the study of the signal characteristics can also be considered in the signal processing performed in some of the different stages of the BCI system (RAMOSER *et al.*, 2000). The specific variability of the problem has, in fact, directed the focus of these systems to a machine learning perspective in which a brain pattern must first be recognized from a training phase and then a session of testing is executed in which the trained system response is tested (LOTTE *et al.*, 2007).

Therefore, one of the first difficulties signal processing methods must deal with, in the analysis of the EEG signal, is the existence of undesirable potentials that can contaminate it. Such signals may compromise the identification of the neurophysiological phenomena explored by the BCI. The contamination by different artifacts such as EOG (electrooculography) or EMG (electromyography) is an important issue in EEG data analysis (LOTTE *et al.*, 2007). The artifacts are not necessarily originated from physiological sources: there exist artifacts associated with non-physiological sources, such as the electric noise generated at 60 Hz (powerline noise). To handle this situation, the effect of some parameters of each session has to be considered.

In the specific case of EEG signals recorded from the motor cortex in experiments of MI, these are known for exhibiting complex spatiotemporal patterns. The absence of a precise activity associated to the band frequency analysis of each subject and the uncertainty related with the precise time in which the expected response will appear, create difficulties from the standpoint of classification results. For this reason, the use of techniques like spatial filters, electrode selection, or even the use of feature selection methods its seen in the literature works for BCI systems (PFURTSCHELLER; NEUPER, 2001).

Consequently, a proposal for studying and exploring the frequency bands and the

temporal and spatial properties of the EEG signal over the motor cortex during different kinds of motor imagery is presented in this chapter. The objective of this study is to propose signal processing techniques that improve the quality of the communication between brain and computer. These techniques are expected to operate in the time, space and frequency domains. It is also expected to find the specific responses for each type of motor imagery for different subjects. Considering this information, the novel approach will operate on the entire BCI cycle, including the test of several techniques for feature extraction, feature selection and classification. The comparison between different approaches will allow the analysis of the paradigm from distinct perspectives.

3.1.1 Sensorimotor rhythms (SMR) and Motor Imagery

Oscillatory EEG activity is caused by complex networks of neurons that create feedback loops (TEPLAN, 2002). The synchronized firing of the neurons in these feedback loops generates observable oscillations. A change in the synchronization of these neurons can cause a decrease or an increase in the power of specific frequency bands. Sensorimotor rhythms are part of this oscillatory EEG activity and comprise mu (8–12 Hz) and beta (18–25 Hz) rhythms. These are found in the primary sensory or motor cortical areas and are related to the execution or the imagination of movement. As defined in chapter 2, a decrease in mu and beta rhythms is termed ERD; the opposite is the increase of the rhythms that is associated with relaxation, which is an ERS (PFURTSCHELLER; NEUPER, 2001). Figure 3.1 presents the EEG signal observed for different brain rhythms including beta and alpha.

Since EEG recordings can be modified by motor imagery (MI) (PFURTSCHELLER *et al.*, 1993), this strategy has been considered for patients with severe motor impairments to aid them communicate with their environment. It has been shown that this paradigm can be used as a mental strategy to control a brain-computer interface (BCI). Figure 3.2 shows how the EEG signal looks when an MI task is executed. The subsequent subsection summarizes some of the different researches and progresses made in the field of BCI and MI in these last years.

3.1.2 Summary of works in literature

Next, some of the first works done in BCI with MI will be highlighted. The most recent techniques specifically in the sense of feature extraction will be explored in the next chapter: for now, the main objective is to make clear the importance of some of the methods used in the classification of the data and to give a perspective of the signal processing methods used for the EEG signal.

In the early 1990s, Wolpaw and his colleagues developed the first motor-imagery

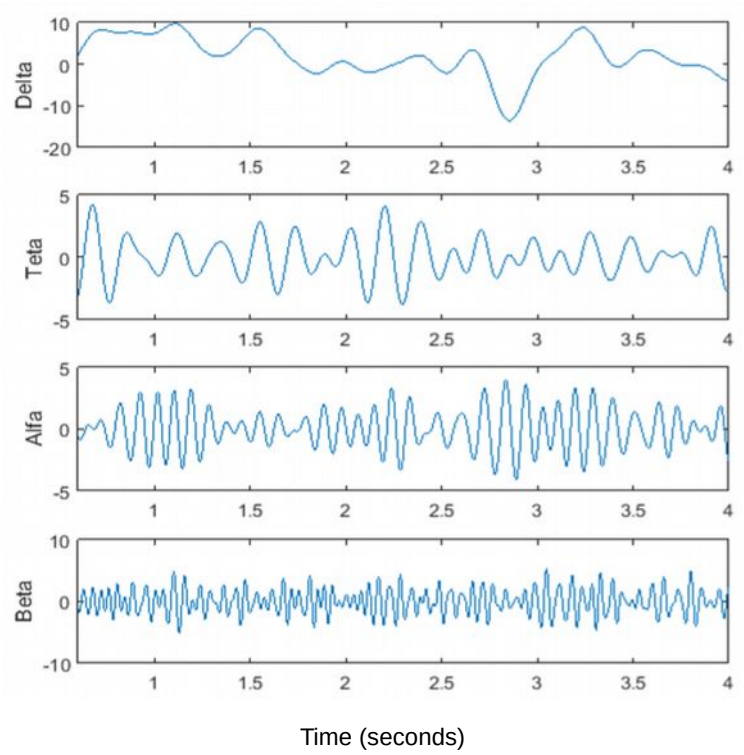

Figure 3.1 – EEG signals observed in the delta, theta, alpha and beta band. Source:

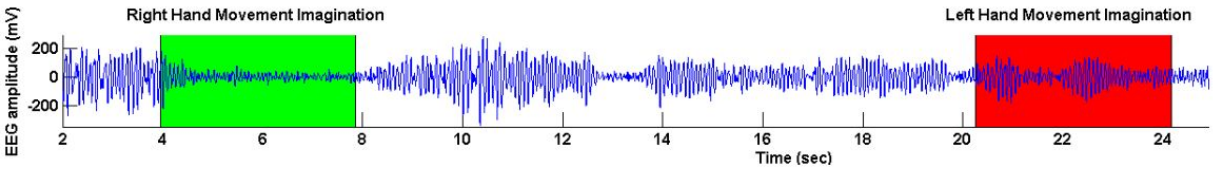

Figure 3.2 – Example of EEG oscillations in the 8-30Hz band (i.e., the sensorimotor rhythm), over the left motor cortex (after spatial filtering). The decrease in signal amplitude in that band during right hand motor imagery is clearly visible and can thus be exploited to operate a BCI. Source: (LOTTE, 2015)

BCI for an EEG-based cursor control (WOLPAW *et al.*, 1991). This work intended to determine whether people could develop the capacity to increase and decrease the mu rhythm reliably and rapidly. The cursor movements were executed based on one-dimensional control; the increase of mu rhythm moved the cursor towards a top target, and a decrease towards a bottom target. In a normal session, the subject was asked to make the cursor move up or down along the screen as fast as possible, to hit targets in each 3-minute run. The signal processing stage was carried out based on frequency analysis. The square root of power expressed in volts was compared with five voltage ranges initially set. Based on this comparison, there was a translation of the amplitude into one of 5 possible cursor

movements. The training sessions made per week were 1 to 3.

In 1993, the same group presented a study with a more advanced form of mu rhythm control. Subjects learned to use the mu rhythm to move a cursor up or down in order to intercept a target moving horizontally across the screen at a randomly determined height (MCFARLAND *et al.*, 1993). The task not only involved moving the cursor but also holding it at a specific location until the target arrived. Each subject participated in eight sessions over a period of several weeks. In the final sessions, all four subjects had improved their performances with respect to the initial day. Subsequently, in 1994, the experiments were focused on showing that humans can learn to control separately the mu rhythm activity of two channels of EEG simultaneously with a degree of independence sufficient to support 2-dimensional cursor movement. Two channels of bipolar EEG were placed across the central sulcus of each hemisphere (FC3/CP3 and FC4/CP4) (WOLPAW; MCFARLAND, 1994).

Meanwhile, the Graz University group (PFURTSCHELLER *et al.*, 1993) developed a BCI also to control the movement of a one-dimensional cursor. Different motor imagery tasks such as imagination of left-hand and right-hand movement were used to elicit the brain activity in the sensorimotor areas in response to a visual cue. The principal difference between the New York BCI (Wolpaw and colleagues) and the Graz BCI is the adaptation of the latter to the user. Feature extraction was performed using band power values; the speed was better compared to other tested methods. Pattern classification was made using a Learning Vector Quantizer (LVQ), a type of artificial neural network. After four sessions of half an hour each, an 85% rate of correct movements was reached, the initial performance being around 70%. By using this technique, it can be said that the progress at which a user could use these systems was considerably increased in relation to previous works. The reliability given by the precision value of classification was improved.

For the Graz BCI, different ways to increase the classification accuracy were tested later. In the case when only one or two EEG channels are available, more advanced algorithms for the extraction of discrimination-relevant features were tested (e.g., adaptive autoregressive filtering) and/or better classifiers were employed (e.g., multilayer perceptrons) . A work that mixed these two aspects was (PFURTSCHELLER *et al.*, 1997). In this, a type of distinction-sensitive learning vector quantization (DSLVQ) was used on spectral components of the recorded data. The DSLVQ weight values were analyzed to find the most relevant frequency components for each subject, for the discrimination between right and left motor imagery. They found out that imagination of a movement triggers a significant ipsilateral ERS in parallel with the contralateral ERD.

(RAMOSER *et al.*, 2000) used multiple EEG channels to acquire additional information about the state of the brain. In this approach, specifically-designed spatial filters obtained by the method of common spatial patterns (CSP) were used to construct new

time-series whose variances contained the most discriminative information. These were classified by a linear discriminator. Other methods for referencing the channel signals were also tested - small Laplacian, large Laplacian, bipolar, and common average reference (CAR). The data were previously visually checked for EEG artifacts during the MI period. For each of the subjects, an accuracy of more than 90% was achieved using the referential methods and the CSP method. The best classification results for the online feedback sessions were 91.3% for subject S1, 83.7% for S2, and 89.9% for S3. The advantages of the CSP method were demonstrated in (GUGER *et al.*, 2000) when analyzing the EEG in real time in order to give feedback to the subject. The method was utilized to give fast, continuous, and accurate feedback during left- and right-hand movement imagination. Furthermore, a significant classification accuracy was achieved after only three days of training when the CSP filter was adapted between sessions. In (GUGER *et al.*, 2001), a summary of the methods to build an online BCI-MI system was presented, includingthe Adaptive Autoregressive Model with Linear Discrimination, which had good results but showed a relatively slow adaptation speed when the subject was not healthy .

In 2004, reports appeared concerning a pilot study for classification of motor imagery for BCI applications, by means of source analysis of scalp-recorded EEGs. Independent component analysis (ICA) was used as a spatio-temporal filtering technique to extract signal components relevant to left or right motor imagery (MI) tasks. Source analysis methods including equivalent dipole analysis and cortical current density imaging were applied to reconstruct equivalent neural sources corresponding to MI, and classification was performed based on the inverse solutions. The obtained source signals had better SNR than the scalp EEG data and could be safely related to cortical regions. ICA appears to play an important role in extracting the useful information, enabling effective source estimation to identify the origins of the expressed brain activities and the difference between them (QIN *et al.*, 2004).

Later, data related to the BCI 2005 competition was used to test the classification of 4 types of MI. The adopted strategy was based on the comparison between different types of classifiers: LDA, SVM and KNN. The features were extracted using an adaptive autoregressive model (AAR). From the data of 60 channels, feature vectors with 180 features were obtained. Only for the case of LDA individual channel performance tests were made, and also bipolar electrodes were used. The results showed that SVM was the method who provided the best classification results, followed by LDA and finally KNN. Previous studies showed that KNN together with AAR parameter estimation can generate a low classification rate. In this case, the success of SVM was attributed to the fact that the set of analyzed data had not many samples in the time domain but a considerable amount of features when all channels were used (SCHLÖGL *et al.*, 2005).

Between 2007 and 2008, improvements were reported in literature related to the

spatial filter CSP. Some problems had already been found in this algorithm, such as the adequate selection of channels and frequency bands. Thus, in (NOVI *et al.*, 2007), the use of filter banks was proposed to divide the power spectrum for finding the best bands for a subject. Fusion methods such as recursive removal of bands and a Meta-Classifier (MC) were used. To evaluate the methods, data from the 2005 BCI competition III was used. The results indicated a small increase in the classification accuracy. This result was associated with the use of effective feature selection and classification methods.

Another group joined in BCI research with MI, the group of Berlin. Their research began by proposing a BCI using different types of MI, for both hands and feet (BLANKERTZ *et al.*, 2008). The goal of this work was to make subjects who were never trained in this type of BCI achieve, from their first session, good results for online control. The strategy was based on the selection of the two best classes for a subject, using also the best frequency bands individually. The features were obtained with CSP, where the selection of channels was semiautomatic. The results show that 57% of the population of their group achieved 84% classification accuracy in the first session. A comparison against the strategies used by the Graz group was made using a kind of bipolar electrode selection that did not give better results. The subject of the joint learning of machine and user was left open.

The Berlin BCI group (BLANKERTZ *et al.*, 2010) also explored the issue of the capacity of each subject to control MI based BCI, as nearly 15 to 30% of subjects using this technique cannot obtain a good classification result. The proposal of a predictor of SMR, from two channels C3 and C4 filtered with a Laplacian filter, was made. This filter is based on the spectral power from the idle state, during which the baseline noise that exists in this spectrum is calculated and estimated. The high peaks found in the activity in the alpha band are the references of comparison for the other states of imagination. The results show no increase in the capacity of classification - in fact, there was a decrease in the values, which reached only 75% in the best cases, this result being for an online test.

With respect to ICA, a work in 2009 was focused on finding independent components to separate noise from other potential MI activity (QI *et al.*, 2009). ICA was used over several EEG channels, then the mutual information of the independent components was employed to cluster the components; finally, the original channels were reconstructed keeping only the components having no noise characteristics. In 2012, a type of spatial filter using ICA was proposed using the independent components of each of the states of imagination used, and the resting state (WANG *et al.*, 2012). The components that had MI features were searched by the type of spectrum corresponding to these characteristics. From these, the filters were built. In an offline experiment, a classification accuracy of 87% was reached, slightly higher than that of the experiment conducted by the same

group with CSP. Finally, other similar work was found with offline data analysis of three types of motor imagery, using variance features in the independent components and an SVM classifier (ZHOU *et al.*, 2014). The independent components with MI features were selected by visual inspection. The best classification results were about 86%.

In the last years, from a general analysis of the research of these different groups, there are still many questions to be solved in the processing stages for the BCI and MI problem. Since it was mentioned that the strategies based on machine learning allowed the direct learning of the mental patterns of a subject, it has been found that the task of MI also requires a process in which the subject also has to adapt through the feedback received. Thus, in online systems, the task of control requires the use of new approaches, some of which have been designed to incorporate adaptive learning. The purpose in the adaptation of the subject-specific model is to address the session-to-session non-stationarity in the EEG signal (LIYANAGE *et al.*, 2013; SHENOY *et al.*, 2006). The idea is to determine the parameters of the subject-specific model using the EEG data recorded from a calibration session as well as EEG data recorded from subsequent feedback sessions. Some of these works related to adaptive learning include the use of a modification of the CSP filter (ANG; GUAN, 2017), known as FBCSP, also a proposal using feature selection with a method called IterRelCen (SHAN *et al.*, 2015). Finally a compilation work shows us the advantages of including new classification perspectives using this kind of adaptive strategy (AHN; JUN, 2015).

3.1.3 Proposal

The use of Independent Component Analysis (ICA) for pre-processing or selecting features of EEG signals derived from motor imagery tasks has been a relevant option used in the literature. In the next sections, it is shown that the combined use of ICA and feature selection techniques is capable of enhancing task imagery responses in BCI systems, which implied in overall better classification performance for a two class motor imagery system. To evaluate the mentioned signal processing framework, a complete motor imagery-based BCI was implemented, which also allowed the comparison of different techniques for signal pre-processing, feature extraction, feature selection and classification. Figure 3.3 shows a summary of the methods used and the combinations proposed to execute the different processing steps of the EEG signal.

3.2 Materials

3.2.1 Experiment setup

Six healthy subjects (3 men and 3 women with ages between 19 – 30 years, average of 25 years and standard deviation of 4.83) contributed as volunteers for this

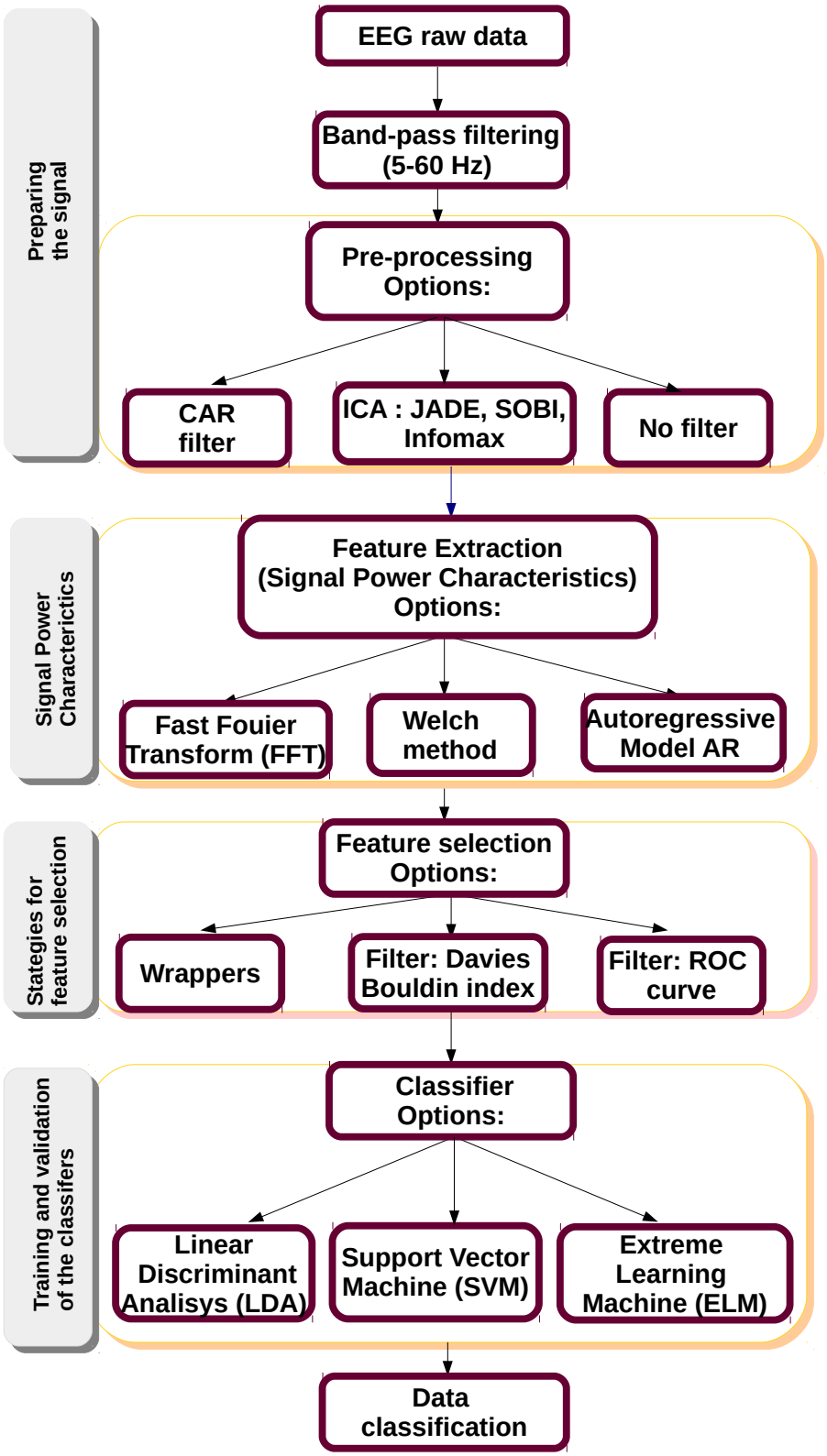

Figure 3.3 – Summary of the different combinations of methods used for the different EEG signal processing blocks in this proposal.

study, approved by the Ethics Committee of the University of Campinas (UNICAMP) (n. 791/2010). Data acquisition started with each subject seated in front of a monitor placed two meters ahead with relaxed arms and hands. The sequence of events that characterized each trial is shown in Figure 3.4 , which includes: 2s for task preparation - cross at the center of monitor changes color -, task imagery – cross highlighted at the right (right hand movement imagery) or at the left (left hand imagery) for 6s. The experiment comprised 20 left and 20 right trials per subject.

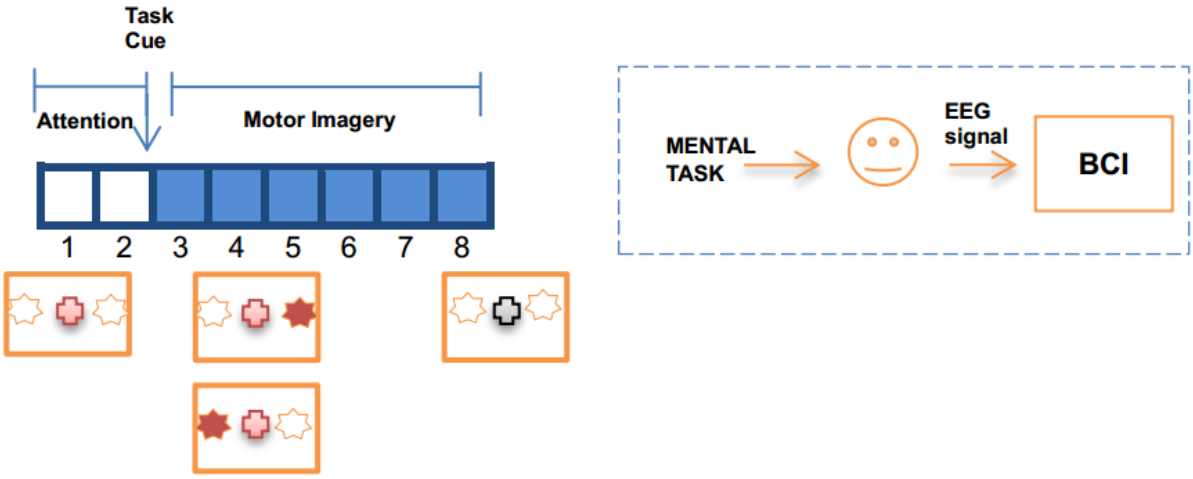

Figure 3.4 – Experimental paradigm of motor imagery-based BCI used.

3.2.2 Data recording

The EEG was recorded using the g.tec g.USBamp amplifier with a sample rate of 256 Hz, with a 16-channel dry-electrode cap. The electrodes were distributed on the subject scalp, aiming to capture the electrical activity of the sensorimotor region and also of the occipital and frontal regions. Figure 3.5 shows the arrangement of the electrodes at FC3, FC4, Fz, POz, Pz, C4, C3, CP4, CP3, C6, C5, Cz, C1, C2, CPz, FCz, according to the international 10-20 system (OOSTENVELD; PRAAMSTRA, 2001).

3.3 Methodology

The signal-processing framework proposed here is shown in Figure 3.6, where the steps and blocks used are presented. This methodology was described also in Figure 3.4. The raw EEG recorded signal was pre-processed by the amplifier with an analog band-pass filter (5 – 60 Hz) and a notch filter at 60 Hz. The performed analysis included: (1) use of spatial filters comparing common average reference (CAR) and ICA-based spatial filters; (2) feature extraction using spectral analysis by means of FFT, Welch method

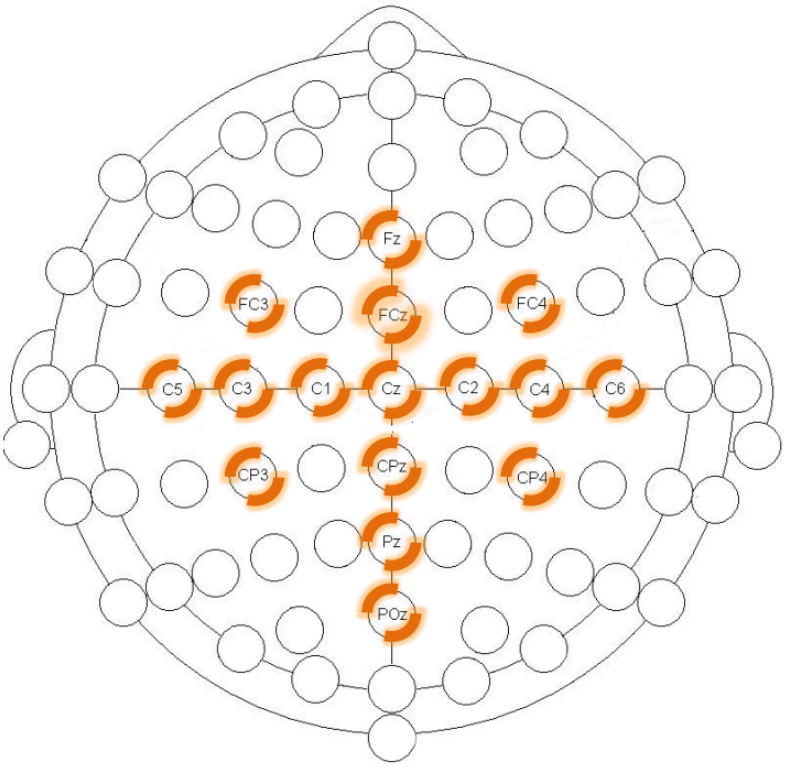

Figure 3.5 – Cap configuration with 16 electrodes.

and autoregressive model (AR); (3) feature selection using filters Davies-Bouldin (DB) index and Receiver Operating Characteristics (ROC) curve and a progressive wrapper; (4) classification based on linear discrimination analysis (LDA), extreme learning machines (ELMs) and support vector machines (SVMs).

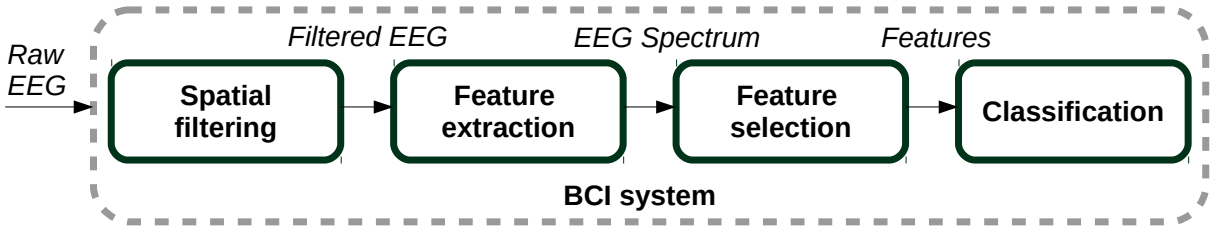

Figure 3.6 – BCI processing pipeline.

3.3.1 Pre-processing and spatial filtering

Scalp potentials are associated with low spatial resolution and low signal to noise ratio (SNR) (TEPLAN, 2002). The contamination of different artifacts such as EOG or EMG is an important issue in EEG data analysis. Spatial filters are commonly used to

reduce the impact of these issues improving signal localization and the SNR of the EEG signal. Other techniques that are usually employed are the temporal filters.

Temporal filters: Temporal filters are used both in noise elimination and in the extraction of signals associated with specific frequency bands or EEG rhythms. The information extracted in different frequency bands can be obtained by using high-pass, low-pass or band-pass filters. Typically, in motor imagery, the mu and beta bands reflects the activity associated with this task. The signal energy estimated at the output of the filter can define a classification strategy (GRAIMANN *et al.*, 2010).

Spatial filters: This strategy attempts to use the signals from different electrodes in order to emphasize local activity, reduce common noise among channels, decrease data dimensionality, search for projections that maximize discrimination among different classes, among other objectives (RAO, 2013). Some examples of spatial filters are common spatial patterns (CSP), Laplacian and common average reference (CAR) filters. Figure 3.7 shows how the distribution of the electrodes is represented for different types of spatial filters.

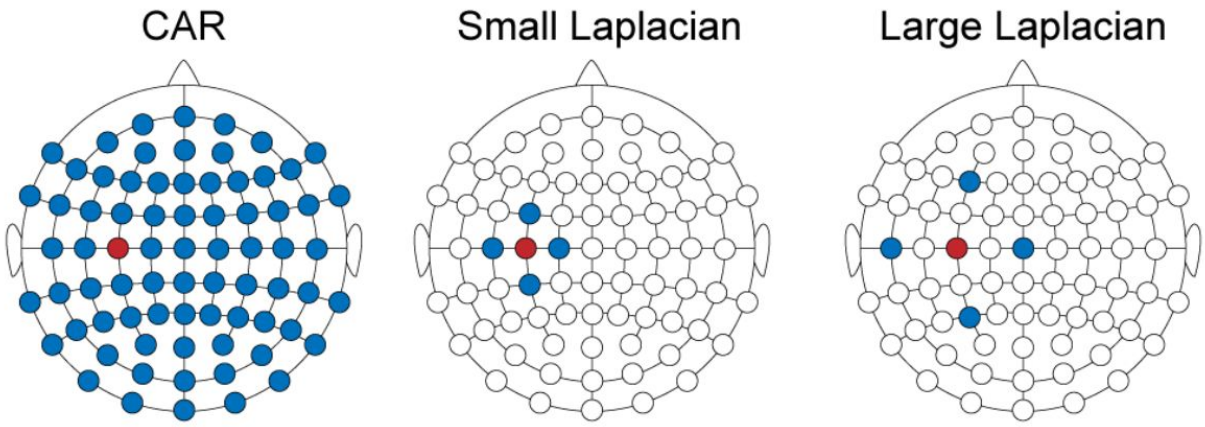

Figure 3.7 – Electrodes used to calculate the CAR and Laplacian filter using the red electrode as reference. Adapted from: (MCFARLAND *et al.*, 1997)

The CAR and the Laplacian methods preserve the physiological meaning of the channels and not necessarily change the original number of inputs. CAR references all channels to their common average (obtained from all channels). The expression (3.1) describes mathematically the CAR operation (MCFARLAND *et al.*, 1997).

$$V_i^{CAR} = V_i^{ER} - \frac{1}{N}\sum_{j=1}^{N} V_j^{ER} \tag{3.1}$$

where V_i^{ER} is the electric potential difference between the electrode i and the reference. When the scalp is entirely covered by spaced electrodes, as shown in Figure 3.7, the result is a zero-mean spatial voltage distribution. While the influence of far field sources is

reduced, CAR may introduce some undesired spatial smoothing, since the artifacts of one channel may be spread all other channels caused by disproportionate isolated components that can deform the signal after the global mean.

Laplacian filters, instead, are computed subtracting from each electrode i the average of its surrounding electrodes:

$$V_i^{LAP} = V_i^{ER} - \frac{1}{|S_i|} \sum_{j \epsilon S_i} V_j^{ER} \tag{3.2}$$

where S_i corresponds to a neighborhood of electrode i. The choice of the neighborhood S_i determines the characteristics of the spatial filter. The Laplacian filter determines for each electrode the second derivative of the instantaneous electric space potential distribution, emphasizing the radial activity near the electrode (MCFARLAND *et al.*, 1997). This filter can be used with electrodes more or less spaced depending on the purpose (small Laplacian and large Laplacian), as shown in Figure 3.7.

3.3.2 Independent component analysis (ICA)

ICA is very often employed as a Blind Source Separation (BSS) method. The goal of BSS is to recover sources from mixtures (observations) of signals with no information about the mixing matrix, considering only certain general assumptions and conditions (WANG *et al.*, 2012). For an N-dimensional unknown vector of independent sources $\mathbf{S_N} = [s_1, \ldots, s_N]^T$, the measured multi-channel EEG signals $\mathbf{X_N} = [x_1, \ldots, x_N]^T$ are assumed to be the following linear mixture of sources

$$\mathbf{X_N} = \mathbf{AS_N} \tag{3.3}$$

If assume that the mixing system is linear, time invariant and memoryless, i.e., that the mixing system can be represented by a $M \times N$ matrix $\mathbf{A}$. This matrix is the unknown mixing matrix. If the matrix is square, i.e., $M = N$, so that the number of the sources and mixtures is the same, as well as invertible, then the BSS problem may be cast as the estimation of the inverse matrix $\mathbf{A^{-1}}$, only from the mixtures given by the vector $\mathbf{X_N}$. In (COMON, 1994), it was shown that analogously to the case of the unsupervised deconvolution,if the source signals, $\mathbf{S_N}$, are mutually independent and non-Gaussian, then it is possible to find such matrix up to some ambiguities analogous to the gain and delay factors in unsupervised deconvolution.

The goal of ICA is to obtain the latent sources with a separating matrix $\mathbf{W}$ obeying the following matrix transformation.

$$\mathbf{U_N} = \mathbf{WX_N} \quad \text{with} \quad \mathbf{W} = \mathbf{A}^{-1} \tag{3.4}$$

being the unmixed signals $\mathbf{U_N}$ an estimate of $\mathbf{S_N}$. Each row of $\mathbf{W}$ is a spatial filter for estimating independent components (ICs) (WANG *et al.*, 2012). These ICs can be estimated by different ICA algorithms in order to achieve the condition of statistical independence for the estimated sources U_i $(i = 1, 2, ...N)$. The obtained ICs will be considered the filtered signals for the context of signal processing that it is proposed in this chapter. Figure 3.8 shows the block diagram of the process made for the ICA algorithm.

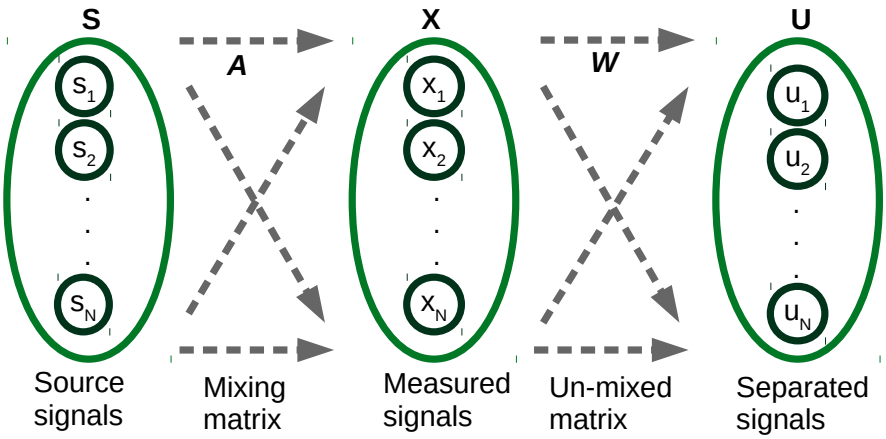

Figure 3.8 – Independent component analysis (ICA) block diagram. **S** are the sources. **X** are the recordings, **U** are the estimated sources, **A** is the mixing matrix and **W** is the un-mixing matrix. Adapted from: (NAIK, 2012)

In this case, the original sources are recovered up to a scale factor and permutations, as scaling and changing the order of the signals it will not change the fact that these signals are statistically independent.

If equation (3.3) is not valid, a linear transformation, as the presented in Eq.(3.4), that performs the decomposition into strictly independent components (STÖGBAUER *et al.*, 2004), is not possible. However, there is still a possibility to search for the least dependent components. Even if Eq.(3.3) is valid, the problem of blind source separation (BSS), to find the matrix $\mathbf{W}$ without explicitly knowing $\mathbf{A}$, is not trivial. Basically, it requires that $\mathbf{X_N}$ is such that the components of any superposition $\mathbf{U_N}' = \mathbf{W}'\mathbf{X_N}$ with $\mathbf{W}' \neq \mathbf{W}$ are not independent. Since linear combinations of Gaussian variables are also Gaussian, BSS is possible only if the sources are not Gaussian (STÖGBAUER *et al.*, 2004). Otherwise, any rotation (orthogonal transformation) $\mathbf{U_N}' = \mathbf{R}\mathbf{U_N}$ would again lead to independent components, and the original sources $\mathbf{U_N}$ could not be uniquely recovered. Thus, any ICA algorithm tries to find a more or less meaningful solution to this problem.

Usually, as a first step, the matrix $\mathbf{W}$ could be decomposed into two factors, $\mathbf{W} = \mathbf{RV}$, where the prewhitening $\mathbf{V}$ could be just a principal component analysis (PCA)

together with a rescaling (STÖGBAUER *et al.*, 2004). Thus, the ICA problem itself reduces to finding a suitable rotation for the prewhitened data. The motivation for this is that any reasonable contrast function used for ICA will give least dependent components which are also uncorrelated. The choice to use whitening depends mainly on several factors that are determined by each algorithm; there are also reasons why it is also not necessary or efficient to perform this processing in some cases (STÖGBAUER *et al.*, 2004).

Figure 3.9 shows the approach used for the ICA spatial filter implemented in the proposal presented in this chapter. There are two stages, the training , and, afterwards, a validation stage. ICA was executed on the data obtained by collecting the information of the two MI classes. All the trials together of the two classes reached 320 s. ICA was performed using: Logistic Infomax algorithm with natural gradient (BELL; SEJNOWSKI, 1995); Second Order Blind Identification (SOBI) (BELOUCHRANI *et al.*, 1997); and Joint Approximate Diagonalization of Eigenmatrices (JADE) (CARDOSO, 1999). The principal differences between these methods are related to two key issues of ICA, the definition of an independence measure and the design of algorithms to find the change of basis (or separating matrix) **W** to optimize this measure.

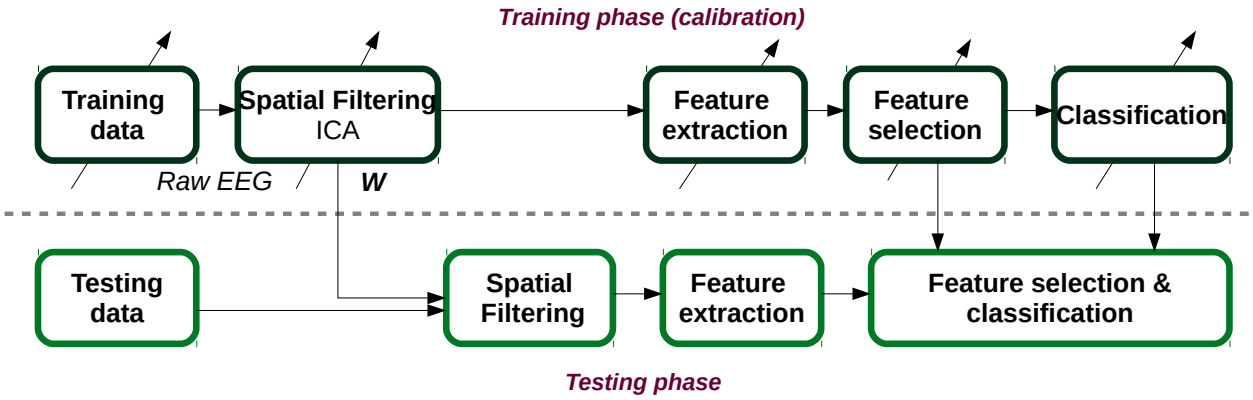

Figure 3.9 – Using spatial filtering with ICA in BCI - MI experiments.

- **Logistic Infomax ICA algorithm of Bell & Sejnowski (1995) with the natural gradient feature of Amari, Cichocki & Yang**: The Infomax method separates unknown source signals from a number of signal mixtures by maximizing the entropy of a transformed set of signal mixtures. Assuming the technically simplest statistical consideration about the probability distribution of $\mathbf{U_N}$, P_{U_N} is selected as fixed densities $r_1, ..., r_N$ for each component, possibly on the basis of prior knowledge. Then P_{U_N} is a fixed distributional assumption, and the choice of **W** such that $\mathbf{U_N} = \mathbf{WX_N}$ is as close as possible in distribution to the hypothesized model distribution P_{U_N} (CARDOSO, 1999). The algorithm used was 'runica.m', which is based in Super Gaussian activity distribution (MAHAJAN *et al.*, 2018).

- **Joint Approximate Diagonalization of Eigenmatrices (JADE) algorithm**: this is a statistical technique that is based on the joint diagonalization of cumulant matrices under the assumption that the sources have non-Gaussian distributions. After whitening and possible dimension reduction, a set of matrices obtained from eigenmatrices of the fourth-order cumulant tensor is approximately diagonalized with a single orthogonal transformation. (CARDOSO, 1999).
- **Second Order Blind Identification (SOBI) by joint diagonalization of correlation matrices**: SOBI relies only on stationary second order statistics that are based on a simultaneous diagonalization of a set of covariance matrices for the computation of an estimate of the unmixing matrix **W**. The basis of the SOBI algorithm is a set of time-lagged covariance matrices. To estimate the sources, a joint diagonalisation of the time-lagged covariance matrices is performed, similarly to the JADE algorithm (NAIK, 2012).

3.3.3 Feature extraction

The oscillations in the alpha and beta bands are particularly important to discriminate between different brain states during activity. Thus, the use of methods for spectral estimation was investigated in this study: classic FFT; Welch's method; Burg method for AR spectral estimation. The signals were windowed at 3 seconds with 1 second of overlap. The Hamming window was used for the Welch method.

Short-time Fourier transform: The short-time Fourier transform allows the estimation of the power spectrum via the computation of the Fourier transform on segments of the signal, normally with an overlap to reduce artifacts at the boundary (HAYKIN, 2008). The obtained complex values provide information concerning the magnitude and phase of each point in time and frequency. The STFT is given by

$$X(m,\omega) = \sum_{n=-\infty}^{\infty} x[n]w[n-m]exp(-j\omega n) \tag{3.5}$$

in which $x[n]$ is the signal, $w[n]$ is the window, m is the segment length and ω is the angular frequency. The squared magnitude of the STFT is given by the spectrogram as:

$$spectrogram = |X(m,\omega)|^2 \tag{3.6}$$

and provides an estimate of the power spectrum of the signal.

Welch's method: Welch's method estimates the power spectral density (PSD) applying the fast Fourier transform (FFT) algorithm (HAYKIN, 2008; WELCH, 1967).

The method splits the input data into N segments, computes modified periodograms of segments via FFT and estimates the PSD by the average of the resulting periodograms. The mathematical formulation of the PSD can be expressed by:

$$\hat{S}(\omega) = \frac{1}{KNU} \sum_{k=1}^{K} \left| \sum_{k=1}^{K} W(n)x(n+kD)exp(-j\omega n) \right| \tag{3.7}$$

in which the signal is divided into K segments of length N and shifted of D points. $W(n)$ is a window function and U is a constant given by:

$$U = \frac{1}{N} \sum_{n=1}^{N} |W(n)|^2 \tag{3.8}$$

In the present study, the data were windowed by Hamming windows with 3s and 1s of overlap. The PSD was estimated for each MI class using a spectral resolution of 1 Hz in the mu and beta bands. The cumulative value of the power in each band was added to obtain only two features for each electrode analyzed.

Autoregressive Spectrum Estimation: An $AR(p)$ process may be represented as the output of an all–pole filter driven with unit variance white noise. The AR model assumes that the current value of the process, x_n, can be described by a finite linear aggregate of the previous values of the process ans the current value of a white driving source n_n. An AR process of zero mean and order p is defined as:

$$x_n = n_n - a_1 x_{n-1} - a_2 x_{n-2} - a_3 x_{n-3} \cdots a_p x_{n-p} \tag{3.9}$$

The AR model contains $p+1$ parameters which have to ve estimated from the data: the coefficients and the variance of the white noise. (SCHLINDWEIN; EVANS, 1992).

There are some reasons beacuse this method could be consider superior in some cases that other classic methods for spectral estimation (SCHLINDWEIN; EVANS, 1992): (1) The estimation of the AR parameters results in linear eqution, which are easy to implement in efficient computer algorithms. (2) The AR model is equvalent to a maximum entropy (ME) model for the unidimensional case and the spectral estimate based on ME model it is optimally smooth. (3) Finally, the AR is a predictive model, being suitable for forecasting the behaviour of the time series outsidethe known sample interval.

Its spectrum is given by:

$$Pxx(\omega) = \frac{|b(0)|^2}{\left|1 + \sum_{k=1}^{p} a_p(k)exp(-j\omega k)\right|^2} \tag{3.10}$$

Since $b(0)$ and $a_p(k)$ can be estimated from the data, an estimate of the power spectrum becomes

$$\hat{P}_{AR}(\omega) = \frac{\left|\hat{b}(0)\right|^2}{\left|1 + \sum_{k=1}^{p} \hat{a}_p(k) exp(-j\omega k)\right|^2} \tag{3.11}$$

The model parameters of P_{AR} can be precisely estimated, so as to be consistent with the data generation process. To guarantee the accuracy, it is necessary to work on the methods used to estimate all-pole model coefficients. The AR coefficients are found by solving the autocorrelation function (ACF) normal equations: this can be done by several methods as the Yule–Walker method (STOICA; MOSES, 2005).

3.3.4 Feature selection

Each method of spectral analysis generates two different features related to two frequency bands (mu and beta) in every one of the 16 channels used, yielding a total of 32 features per subject. Although it is not a large number, a feature selection algorithm was used to find the best combination of them. Two approaches for feature selection were used: filters and wrappers (THEODORIDIS; KOUTROUMBAS., 2008).

Feature selection exploits the mutual (linear and/or nonlinear) correlation among features selecting those that retains more class discriminatory information. As previously mentioned in Chapter 2, the strategies for performing this selection follow two approaches: filters or wrappers (KOHAVI; JOHN, 1997; GUYON; ELISSEEFF, 2003). Filters operate with metrics directly obtained from the features, being, therefore, independent of the classifier to perform the choice. The filters usually outline statistic functions that return a relevance index matching each attribute and label. This approach tacitly assumes independence between features and, therefore, ignores the correlation between variables, which can affect the prediction performance. The second approach takes into account the performance of the trained classifier to rank the features. In the following, two filter techniques are described – ROC curve and Davies Bouldin –, as well as the forward wrapper algorithm used in this study.

Davies Bouldin index: The DB Index was used to rank the features according to their estimated ability in discriminating the classes. This measure combines in a single expression two main relevant aspects of data clustering: the minimization of the intra-class distance and the maximization of the distance between the classes (DAVIES; BOULDIN, 1979). For the classes w_i with $i = 1, 2, \ldots, m$ the DB index can be described by:

$$DB = \frac{1}{m} \sum_{i=1}^{m} \left(\max_{j=1,\ldots,m \; j \neq i} \frac{s_i + s_j}{d_{ij}} \right) \tag{3.12}$$

in which s_i is the average distance between each point of the class i and the centroid of this class, and s_j is the same for the class j. The parameter d_{ij} is the Euclidean distance between the centroids of classes i and j. Then, the DB index presents the average similarity between each class and its most similar. As it is intended to make classes least similar between them, small values of DB index are indicative that the average similarity is low and the data sets are compact and well separated.

In this work, the DB index was used to rank the features. Actually, for the heuristics introduced here, the inverse of this index (DBinv) was used (as a maximization criterion). Based on this rank, the feature vectors that will feed the classifiers can be constructed.

ROC curve: The other filter method used was the ROC curve that works with the probability density functions describing the distribution of a feature in two classes (THEODORIDIS; KOUTROUMBAS., 2008). It measures the overlap between the probability density functions (pdfs) describing the data distribution of the feature in two classes. This overlap is quantified in terms of an area between two curves, also known as AUC (area under the receiver operating curve). For complete overlap, the AUC value is 0, and for complete separation it is equal to 0.5 (THEODORIDIS; KOUTROUMBAS., 2008).

Figure 3.10(a) illustrates an example of overlapping probability density functions describing the distribution of a feature in two classes. The class w_1 is related to the values on the left and class w_2 for the values on the right. The decision for one of the classes is associated with an error probability, α, of reaching a wrong decision concerning class w_1 (the probability of a correct decision is $1 - \alpha$). Similarly, let $\beta(1 - \beta)$ be the probability of a wrong (correct) decision concerning class w_2 (THEODORIDIS; KOUTROUMBAS., 2003). By moving the threshold of decision beetwen the two classes over different possible positions, different values of α and β result. When two distributions have complete overlap, then for any position of the threshold get $\alpha = (1 - \beta)$, that case can be represented in Figure 3.10(b), where is also presented how the ROC curve looks for probability distributions that are overlapping.

Wrappers: The employed wrapper was based on forward selection (THEODORIDIS; KOUTROUMBAS., 2008). The algorithm is based on a "bottom–up" approach, which means that it starts with an empty feature set. In each step, one feature is added until 24 features are reached. The wrapper methodology performs feature selection in terms of the performance of the classifier. The three aspects to define its implementation (KOHAVI; JOHN, 1997) are: (i) the search strategy employed at the feature space, (ii) the stopping criterion and (iii) the classifier structure.

The first step concerns performing an efficient search on the feature space due to the large number of possibilities - $2^M - 1$ - with M being the number of features. There are many ways to carry out this search, such as genetic algorithms, simulated annealing

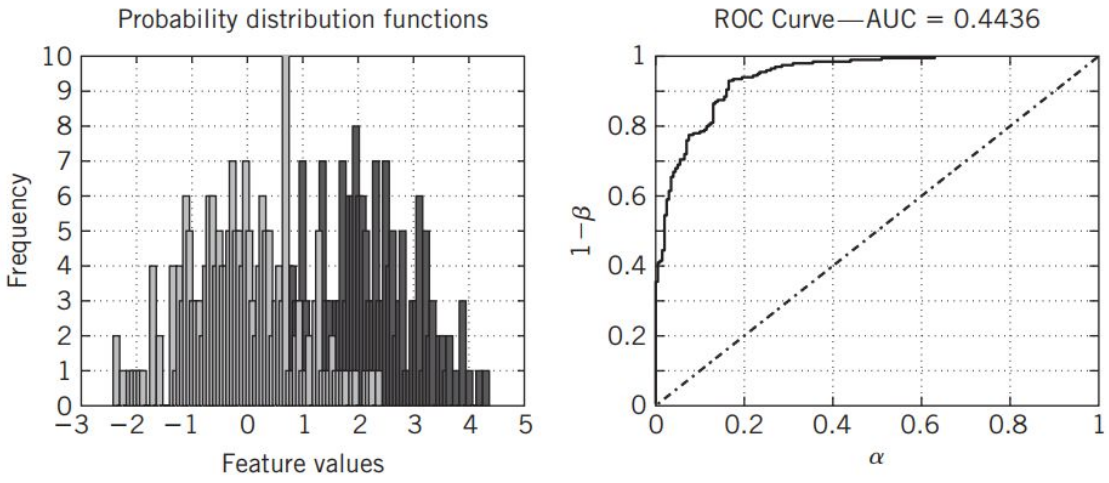

Figure 3.10 – (a) Distributions with partial overlap between pdfs of the two classes. (b) Corresponding ROC curve. Source: (THEODORIDIS *et al.*, 2010)

or greedy heuristics. In this study, the greedy heuristic based on forward selection - as mentioned - was chosen in view of the trade-off between computational simplicity and achievable performance. The simplest stopping criterion consists of the rule "if no improvement, then stop". This approach can, however, lead to local convergence. A more robust stopping criterion considers k consecutive steps without performance gain. In this study, $k = 2$ was adopted. The third aspect, the classifier structure, has a strong influence on feature selection, since the performance of the classifier is constantly evaluated each time a new feature has to be incorporated. It is important to note that there is no guarantee of global convergence.

3.3.5 Classification

The classification was based on LDA, ELM and SVM classifiers. The total data set of one session was divided into two sets of 70% for training and 30% for test. This division was done ten times, i.e., the elements that were part of the two sets were different in each case. This procedure is similar to k-fold cross-validation, with the difference that our second set is for test and not for validation.

Linear Discriminant Analysis

Linear Discriminant Analysis (LDA) is a machine learning technique usually employed to design a classifier, a mathematical structure that receives vectors belonging to a feature space and assigns them to one of the possible classes. The LDA method consists in finding the parameter vector $\mathbf{w}$ that, according to a specific optimization criterion, gives rise to hyperplanes that work as efficient decision boundaries.

LDA is one of the most used strategies in BCIs systems due to its simplicity and low computational cost (THEODORIDIS; KOUTROUMBAS., 2008; BISHOP, 2006). In simple terms, it consists in finding the vector $\mathbf{w}$ that best linearly separates the classes, which implies in establishing a decision surface in the form $\mathbf{w}^T\mathbf{x} + c = 0$, for a constant threshold value c. For instance, if we assume two normal multivariate distributions with means $\boldsymbol{\mu_1}$ and $\boldsymbol{\mu_2}$ and correlation matrices $\mathbf{C_1}$ and $\mathbf{C_2}$, respectively, the LDA approach aims to establish $\mathbf{w}$ that maximizes the ratio between the inter-class and intra-class variance, which can be described by:

$$S = \frac{\sigma^2_{between}}{\sigma^2_{within}} = \frac{(\mathbf{w}^T(\boldsymbol{\mu_1} - \boldsymbol{\mu_2}))^2}{\mathbf{w}^T(\mathbf{C_1} - \mathbf{C_2})\mathbf{w}} \tag{3.13}$$

It is possible to show that maximization of S is reached for $\mathbf{w} \propto (\mathbf{C_1} + \mathbf{C_2})^{-1}(\boldsymbol{\mu_1} + \boldsymbol{\mu_2})$ and $c = \frac{1}{2}\mathbf{w}^T(\boldsymbol{\mu_1} + \boldsymbol{\mu_2})$ (THEODORIDIS; KOUTROUMBAS., 2008). There are also different criteria that can be used to set $\mathbf{w}$ for obtaining linear decision surfaces, such as the one provided by support vector machine strategies with linear kernel functions. When a Gaussian distribution is assumed, the covariance and the mean fully describe the model. However, non-Gaussian random variables can be assumed in this model, as the use of their statistical structure up to second order might be enough to solve the problem at hand.

Extreme Learning Machine

Structurally, an extreme learning machine (HUANG *et al.*, 2006)(HUANG *et al.*, 2011) (ELM) can be defined as a multi-layer perceptron neural network with a single hidden layer and a linear output layer. The parameters of the neurons that form the hidden layer are randomly chosen (HUANG *et al.*, 2006), and the process of training the output layer is essentially equivalent to the adaptation of a linear classifier. Figure 3.11 presents the basic structure of an ELM.

In simple terms, the hidden layer generates a number of nonlinear random projections that map the input vector space onto a feature space over which the output layer operates as a linear discriminant. It has been proved , that single- hidden layer feedforward neural networks (SLFNs) with arbitrarily assigned input weights, hidden layer biases and with almost any nonzero activation function can universally approximate any continuous functions on any compact input sets. These research results imply that in the applications of feedforward neural networks input weights may not be necessarily adjusted at all (HUANG *et al.*, 2003).

For N arbitrary distinc samples $\mathbf{x_i}, \mathbf{d_i}$, where $\mathbf{x_i} = [x_{i1}, x_{i2}, \cdots, x_{in}]^T \in \mathbb{R}^n$ and $\mathbf{d_i} = [d_{i1}, d_{i2}, \cdots, d_{in}]^T \in \mathbb{R}^m$. A standard SFLNs with N' hidden neurons and activation

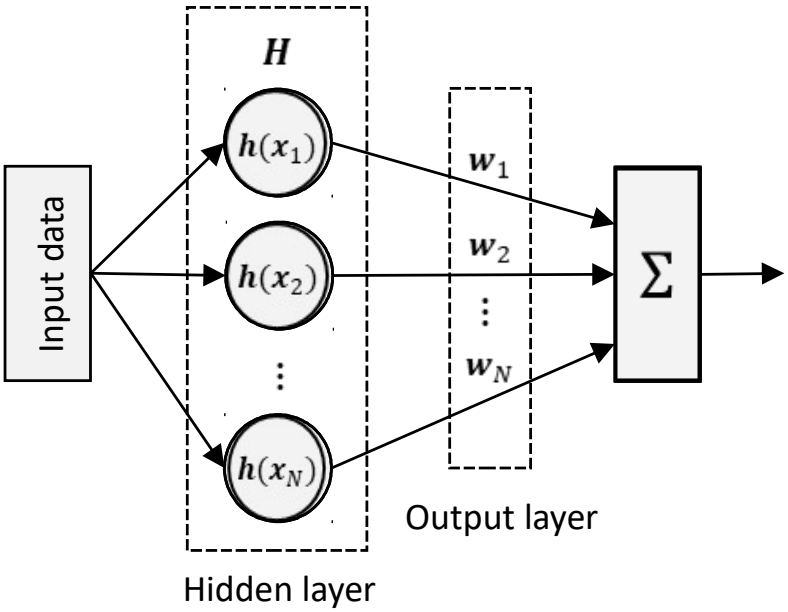

Figure 3.11 – ELM basic structure.

function $g(x)$ are modeled as:

$$\sum_{i=1}^{N'} \beta_i g(\mathbf{w_i} \cdot \mathbf{x_j} + b_i) = \mathbf{o_j},\ j = 1, \cdots, N, \tag{3.14}$$

where $\mathbf{w_i} = [w_{i1}, w_{i2}, \cdots, w_{in}]^T$ is the weigth vector connecting the ith hidden neuron and the input neurons $\beta_i = [\beta_{i1}, \beta_{i2}, \cdots, \beta_{im}]^T$ is the weight vector connecting the ith hidden neuron and the output neurons, and b_i is the threshold of the ith hidden neuron. For a standard SFLNs with N' hidden neurons with activation function $g(x)$ can approximate these N samples with zero error mean with $\sum_{j=1}^{N'} \|\mathbf{o_j} - \mathbf{d_j}\| = 0$ (HUANG *et al.*, 2003), i.e., there exist $\beta_i, \mathbf{w_i}$ and b_i, such that

$$\sum_{i=1}^{N'} \beta_i g(\mathbf{w_i} \cdot \mathbf{x_j} + b_i) = \mathbf{d_j},\ j = 1, \cdots, N, \tag{3.15}$$

Equation (3.15) can be written as:

$$\mathbf{H}\beta \simeq \mathbf{D} \tag{3.16}$$

where

$$\mathbf{H}(\mathbf{w_1}, \cdots, \mathbf{w_{N'}}, b_1, \cdots, b_{N'}, \mathbf{x_1}, \cdots, \mathbf{x_N}) = \begin{bmatrix} g(\mathbf{w_1} \cdot \mathbf{x_1} + b_1) & \cdots & g(\mathbf{w_{N'}} \cdot \mathbf{x_1} + b_{N'}) \\ \vdots & \cdots & \vdots \\ g(\mathbf{w_1} \cdot \mathbf{x_N} + b_1) & \cdots & g(\mathbf{w_{N'}} \cdot \mathbf{x_N} + b_{N'}) \end{bmatrix}_{N \times N'} \tag{3.17}$$

$$\beta = \begin{bmatrix} {\beta_1}^T \\ \vdots \\ {\beta_{N'}}^T \end{bmatrix}_{N' \times m} \quad \text{and} \quad \mathbf{D} = \begin{bmatrix} {\mathbf{d}_1}^T \\ \vdots \\ {\mathbf{d}_N}^T \end{bmatrix}_{N \times m} \tag{3.18}$$

where $\mathbf{H}$ is called the hidden layer output matrix of the neural network. Considering that for most of the cases the number of the hidden neuron is less than the number of distinct training samples, $N' \ll N$, then $\mathbf{H}$ is a non squared matrix and there may not exist $\mathbf{w_i}, b_i, \beta_i (i = 1, \cdots, N')$ such that $\mathbf{H}\beta = \mathbf{D}$. Thus, could be find a specific parameters $\hat{\mathbf{w}}_\mathbf{i}, \hat{b}_i, \hat{\beta}_i (i = 1, \cdots, N')$ such that

$$\left\| \mathbf{H}(\hat{\mathbf{w}}_\mathbf{1}, \cdots, \hat{\mathbf{w}_{N'}}, \hat{b_1}, \cdots, \hat{b_{N'}})\hat{\beta} - \mathbf{D} \right\| = \min_{\mathbf{w_i}, b_i, \beta} \|\mathbf{H}(\mathbf{w_1}, \cdots, \mathbf{w_{N'}}, b_1, \cdots, b_{N'})\beta - \mathbf{D}\| \tag{3.19}$$

The parameter vector β of the output layer is, as a rule is obtained by solving the optimization problem of Equation 3.19 (HUANG *et al.*, 2003).

Its solution can be calculated as a projection of the label vector $\mathbf{D}$ carried out with the aid of an operator based on the Moore-Penrose pseudo-inverse (THEODORIDIS; KOUTROUMBAS., 2008). If the number of neurons in the hidden layer (N') is larger than the number of available data samples, there will be multiple optimal solutions to the problem shown in (3.19), and the pseudo-inverse has the desirable property – from a regularization perspective – of generating a minimal norm solution. In this study, the value of N' was chosen in accordance to a cross-validation criterion.

As outlined above, the solution to the least squares problem is given in terms of the Moore-Penrose pseudo-inverse. For the case in which the number of data samples (N) is larger than N', the solution is:

$$\hat{\beta} = (\mathbf{H}^T\mathbf{H})^{-1}\mathbf{H}^T\mathbf{D} \tag{3.20}$$

Because the parameters of the hidden layer are randomly generated, some of their realizations might result in classifiers that do not satisfy a desired performance criterion. To overcome this difficulty, we decided to generate ten sets of random parameters in order

to generate ten ELMs, which form a machine committee responsible for the final decision. This approach reduces the chances that a single inefficient ELM negatively affects the overall performance.

Support Vector Machine

The SVM is a learning structure that can be used to solve classification and regression tasks (BURGES, 1998). In the context of classification, it can be understood as a maximal margin classifier whose linear/nonlinear structure is defined by a kernel function. The design of a classifier of this kind gives rise to a quadratic constrained optimization task that can be solved using a number of efficient computational tools. In a classification system, the SVM follows two stages: training and classification. In the training, labeled data are used in order to determine the hyperplane in a high-dimensional feature space that distinguishes the classes with maximal margin. The mapping function is expressed as follows:

$$\mathbf{x} \mapsto \phi(\mathbf{x}) \ \in H \tag{3.21}$$

where the dimension of H is higher than $\mathbb{R}^l$ and, depending on the choice of the (nonlinear) $\phi(\mathbf{x})$, can even be infinite (THEODORIDIS *et al.*, 2010). Moreover, if the mapping function is carefully chosen from a known family of functions that have specific desirable properties, the inner product between the images $(\phi(x_1), \phi(x_2))$ of two points x_1, x_2 can be written as,

$$\langle \phi(x_1), \phi(x_2) \rangle = k(x_1, x_2) \tag{3.22}$$

where $\langle \cdot, \cdot \rangle$ denotes the inner product operation in H and $k(\cdot, \cdot)$ is a function known as kernel function. That is, inner products in the high-dimensional space can be performed in terms of the associated kernel function acting in the original low-dimensional space. The space H associated with $k(\cdot, \cdot)$ is known as a reproducing kernel Hilbert space (RKHS).

Different kernel functions are used, such as: linear, quadratic, polynomial, multilayer perceptron (MLP) or Gaussian radial basis (RBF) (CRISTIANINI; SHAWE-TAYLOR, 2000). In this study, the RBF kernel was selected after preliminary tests with all the methods, in view of its stability for multiple trials. The RBF kernel is defined as:

$$k(\mathbf{x_i}, \mathbf{x_j}) = exp\left(-\frac{\|\mathbf{x_i} - \mathbf{x_j}\|^2}{\sigma^2}\right) \tag{3.23}$$

where σ is a user-defined parameter that specifies the rate of decay of $k(\mathbf{x_i}, \mathbf{x_y})$ toward zero, as $\mathbf{x_i}$ moves away from $\mathbf{x_j}$. The value of this parameter was obtained through a process of testing and validation, using the method of cross validation, in this way an

optimal value of $\sigma = 1.5$ was determined. The machines found in the training phase are then used to classify new data on the classification stage.

Solving a linear problem in the high-dimensional space is equivalent to solving a nonlinear problem in the original space. Thus, the hyperplane computed by the SVM method in the high-dimensional space H is

$$\mathbf{w} = \sum_{i=1}^{N_s} \lambda_i y_i \phi(\mathbf{x_i}) \tag{3.24}$$

To obtain the discriminant function given $\mathbf{x}$, it is necessary to first map $\mathbf{x}$ to $\phi(\mathbf{x})$ and then test whether the following is less than or greater than zero:

$$\begin{aligned} g(\mathbf{x}) \equiv \langle \mathbf{w}, \phi(\mathbf{x}) \rangle + w_0 &= \sum_{i=1}^{N_s} \lambda_i y_i \langle \phi(\mathbf{x}), \phi(\mathbf{x_i}) \rangle + w_0 \\ &= \sum_{i=1}^{N_s} \lambda_i y_i k(\mathbf{x}, \mathbf{x_i}) + w_0 \end{aligned} \tag{3.25}$$

where the $\lambda_i, n = 1, 2, ..., N_s$ are the nonzero Lagrange multipliers associated with the support vectors. For the case of a binary clasification task y_n is described by

$$y_n = \begin{cases} +1, & \text{if } \mathbf{x_n} \in w_1 \\ -1, & \text{if } \mathbf{x_n} \in w_2 \end{cases} \tag{3.26}$$

Figure 3.12 shows the corresponding architecture of this classifier. This is a special case of the generalized linear classifier. The number of nodes is determined by the number of support vectors N_s. The nodes perform the inner products between the mapping of $\mathbf{x}$ and the corresponding mappings of the support vectors in the high dimensional space, via the kernel operation. Different constrains and methods for optimization could to be considered to find the solution that describe the optimal margin classifiers of Equations 3.24, 3.25 (THEODORIDIS, 2015).

3.4 Results

As previously discussed, motor imagery is mainly associated to a de-synchronization of the rhythms mu and beta in the areas of the motor cortex that are contra-lateral to the movement. Moreover, stronger rhythmic activities may be also observed in the areas of the cortex that are ipsi-lateral to the movement (VIDAL, 1977). In the case of left hand motor imagery, an attenuation of the signal power in the mu/beta frequency bands is expected generally on channel C4, while the same frequency bands should show power

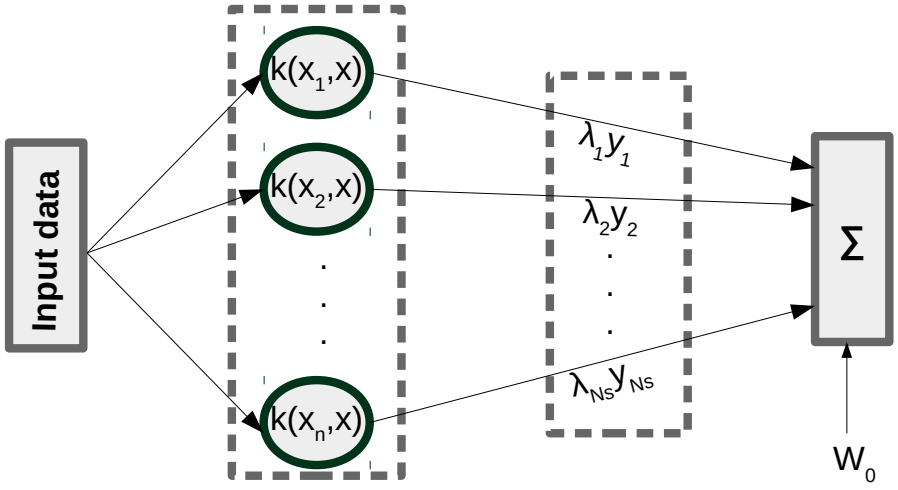

Figure 3.12 – The SVM architecture employing kernel functions. Adapted from: (THEODORIDIS; KOUTROUMBAS., 2008)

peaks on channel C3. Similarly, attenuated mu/beta peaks on C3 and peaks on C4 should characterize right hand motor imagery.

To know more about the spectral response of the different channels that were recorded during data capture and to study about the possible features that will be computed based on this response, in the following section the average spectra of different subjects will be presented. The analysis of the spectral response was made to find the differences and similarities between the two motor-imagery tasks. All electrodes mentioned in the section of materials were used. The electrodes that are near to the motor cortex were expected to be sources of relevant information.

3.4.1 Spatial Patterns

On the imagination of left or right hand movement, the reduced amplitude of sensorimotor rhythms appears over the primary sensorimotor area related to hand movement, and it is contralateral (PFURTSCHELLER; NEUPER, 2001). This corresponds to a spatial response centered mainly at channel C3 (left hemisphere) for right hand movement imagination and channel C4 (right hemisphere) for left hand movement imagination. Figures 3.13, 3.14, 3.15 show the estimation of band power for these channels using CAR filtering for a clear enhanced SNR condition for three of the subjects (1,2,6). These figures were obtained with the sum of all the mean power calculated over segments of 3s with an overlap of 1s.

By observing the spectral response of Subjects 1, 2 and 6, it can be seen that there are few who had desynchronization for the two MI tasks performed. Only Subject 1 (Figure 3.13) presents a spectrum that had the “correct” characteristics for the two

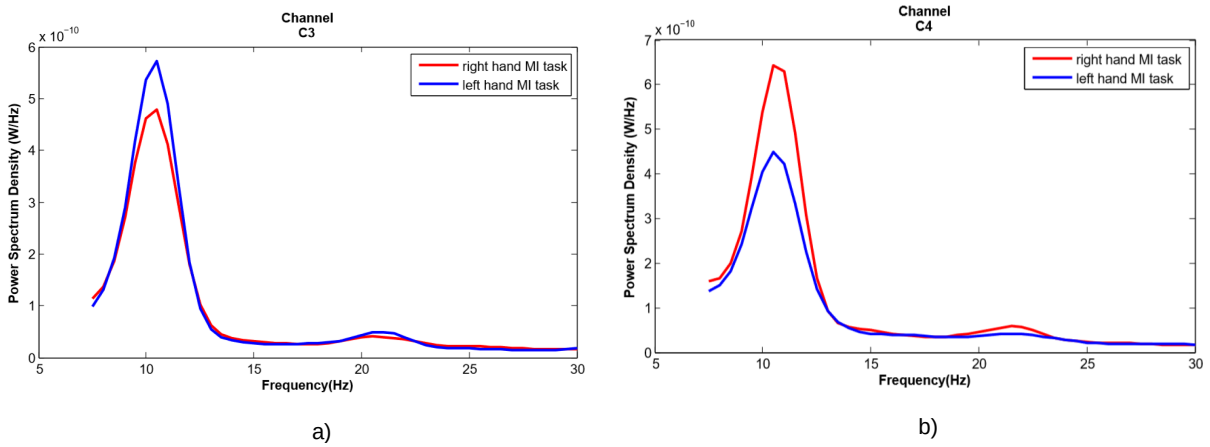

Figure 3.13 – PSD for Subject 1, using CAR filtering. (a) Channel C3 (b) Channel C4.

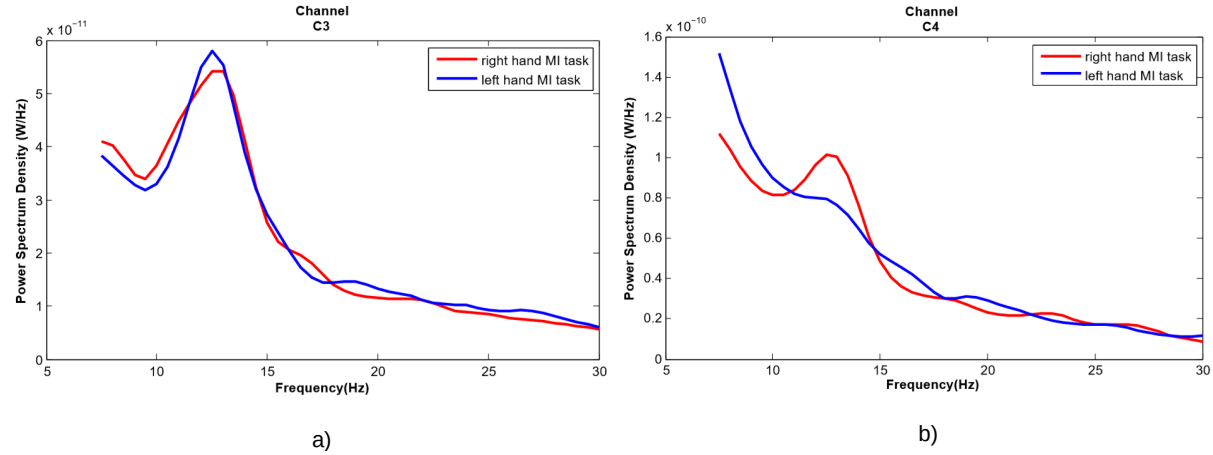

Figure 3.14 – PSD for Subject 2, using CAR filtering. (a) Channel C3 (b) Channel C4.

channels (C3, C4). It is also interesting to observe how each subject presents a particular synchronization in each frequency band, which can vary a bit where the desynchronization starts or ends. These two channels (C3, C4) were observed because they are the ones where the MI response is expected to be strongest, but it could also be observed that in other channels it was possible to find some features of this de-synchronized response.

Alternatively, when ICA is used, different components had a similar kind of spectral band power associated with MI. Figures 3.16, 3.18, 3.20 show the average spectra for some of the IC that were found for Subjects 1,2 and 6, where the expected response for motor-imagery tasks is present.

For Subject 1 (Figure 3.16), the IC 2 and IC 6 had band power characteristics of right hand imagination (Figure 3.16 (a) and (b)). In the case of IC5 and IC16, the band power characteristics are from left-hand imagination (Figure 3.16 (c) and (d)). To explore the relation of the IC and the original channels for revealing the spatial response associated with MI activity, the matrix $\mathbf{W^{-1}}$ is used. Each column of $\mathbf{W^{-1}}$ consists of

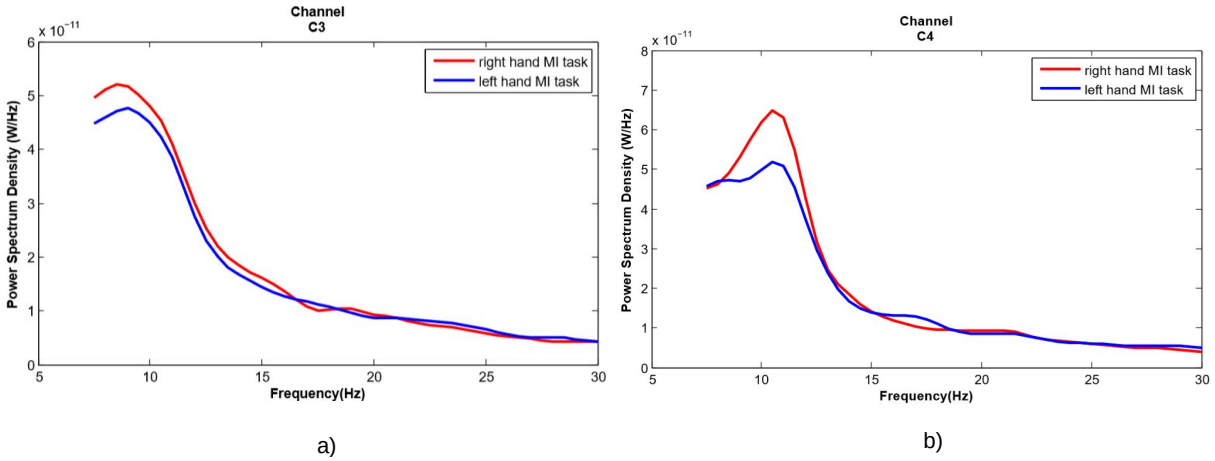

Figure 3.15 – PSD for Subject 6, using CAR filtering. (a) Channel C3 (b) Channel C4.

electrode weights of an independent component. Observing Figure 3.17, the relation of the components IC 2 and IC6 with channels CP3 and C3 can be seen. For IC5 and IC16, the relation comes from C6 and C4. These correspond to a contralateral response of MI activity.

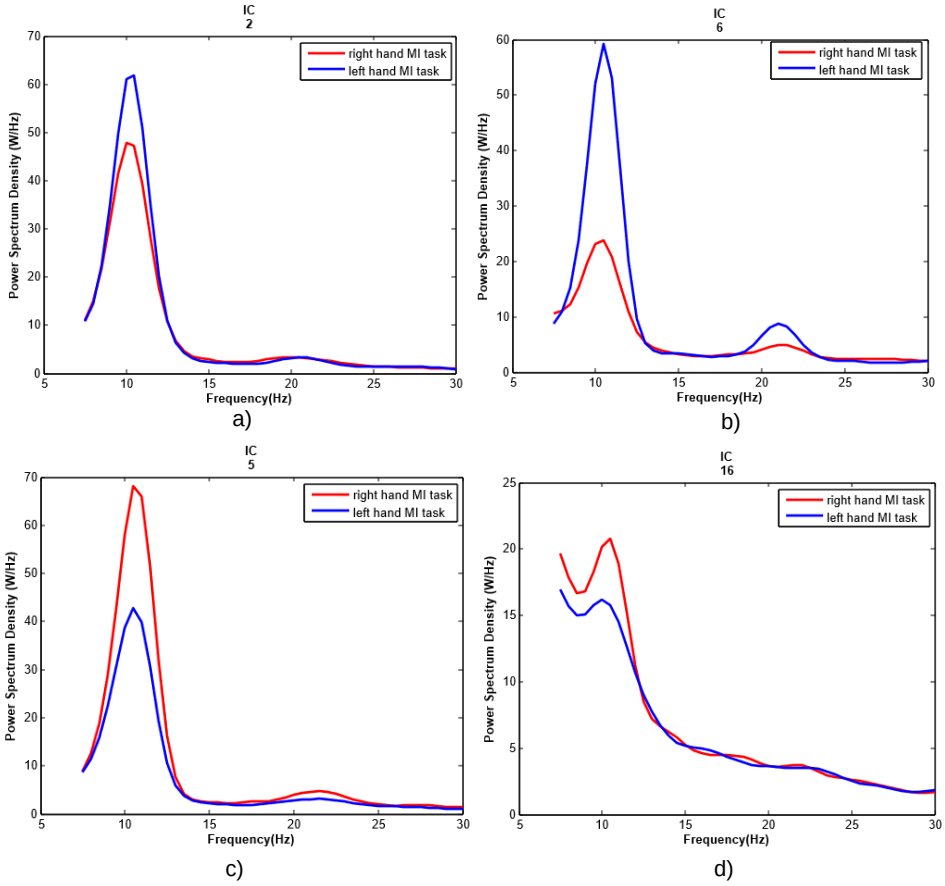

Figure 3.16 – PSD for Subject 1 using ICA-JADE. (a) IC2, (b) IC6, (c) IC5, (d) IC16.

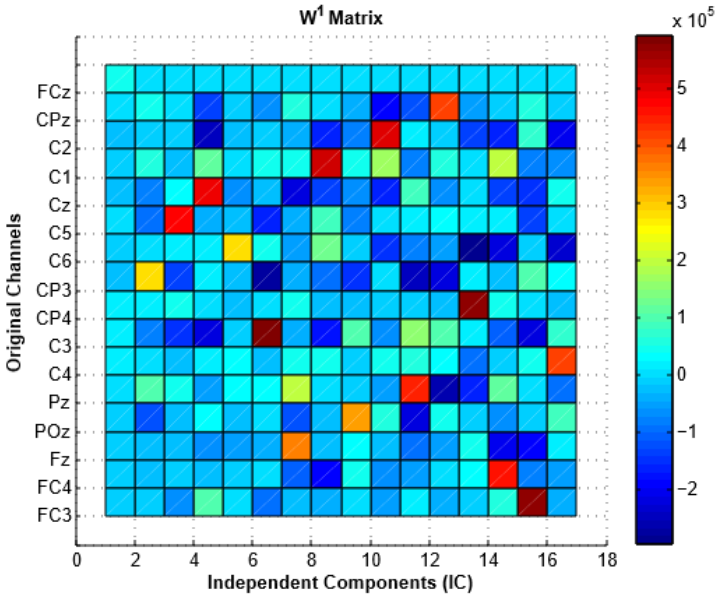

Figure 3.17 – Matrix $\mathbf{W^{-1}}$ for Subject 1.

A comparison, for Subject 1, between the figures of the power spectrum obtained with the CAR and the ICA filter show that, for these cases, the C3 channel (Figure 3.13 a)) associated with IC6 has its power enhanced more strongly on the IC compared to when using CAR filter (Figure 3.16 a) and b)), but in the case of the C4 channel (Figure 3.13 b)) occurred just the opposite and it was a generally loss of power in their associated component IC16, the large desynchronization in fact, was associated with IC5 that is related with C6 (Figure 3.16 c) and d)). This could mean that, according to the ICA filter the real desynchronization was concentrated in a neighboring electrode and not specifically in C4.

In the case of Subject 2, the PSD of the IC are presented in Figure 3.18. The characteristics of the left–hand motor imagination (Figure 3.18 c) and d)) appears to be stronger than for right-hand 3.18 a) and b)). This response is similar to the results with the CAR filter (Figure 3.14), in relation to the kind of synchronization found. However, e.g., the difference in the relation of the IC3 and IC8 with the electrodes FC4 and CP4 respectively (Figure 3.19), indicates that the synchronization response is present for this subject but the electrodes where it can be seen most markedly include a region a bit more extensive than electrodes C4 and C3.

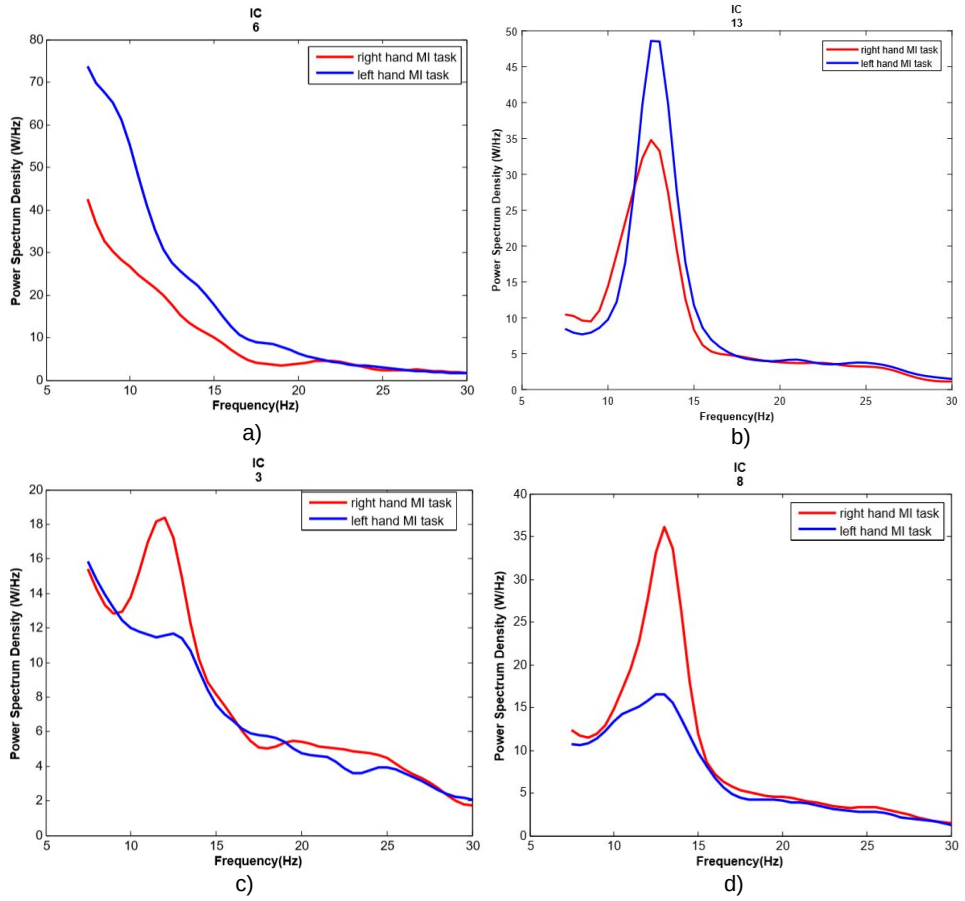

Figure 3.18 – PSD for Subject 2 using ICA-JADE. (a) IC6, (b) IC13, (c) IC3, (d) IC8

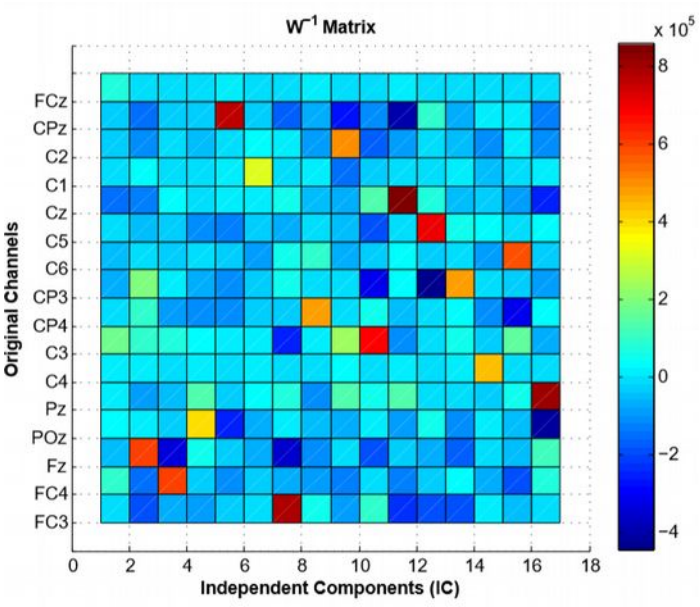

Figure 3.19 – Matrix $\mathbf{W^{-1}}$ for Subject 2.

Subject 6 is the last case to be shown (Figure 3.20). It presents a reduced number

of IC with MI response. In addition, there does not exist a synchronization or desynchronization effect so pronounced as in the two previously discussed subjects. The spectrum of IC11 (Figure 3.20 a)) and IC 9 (Figure 3.20 d)) had a response associated with the electrodes CP4 and CP3, this was clear in Figure 3.21.

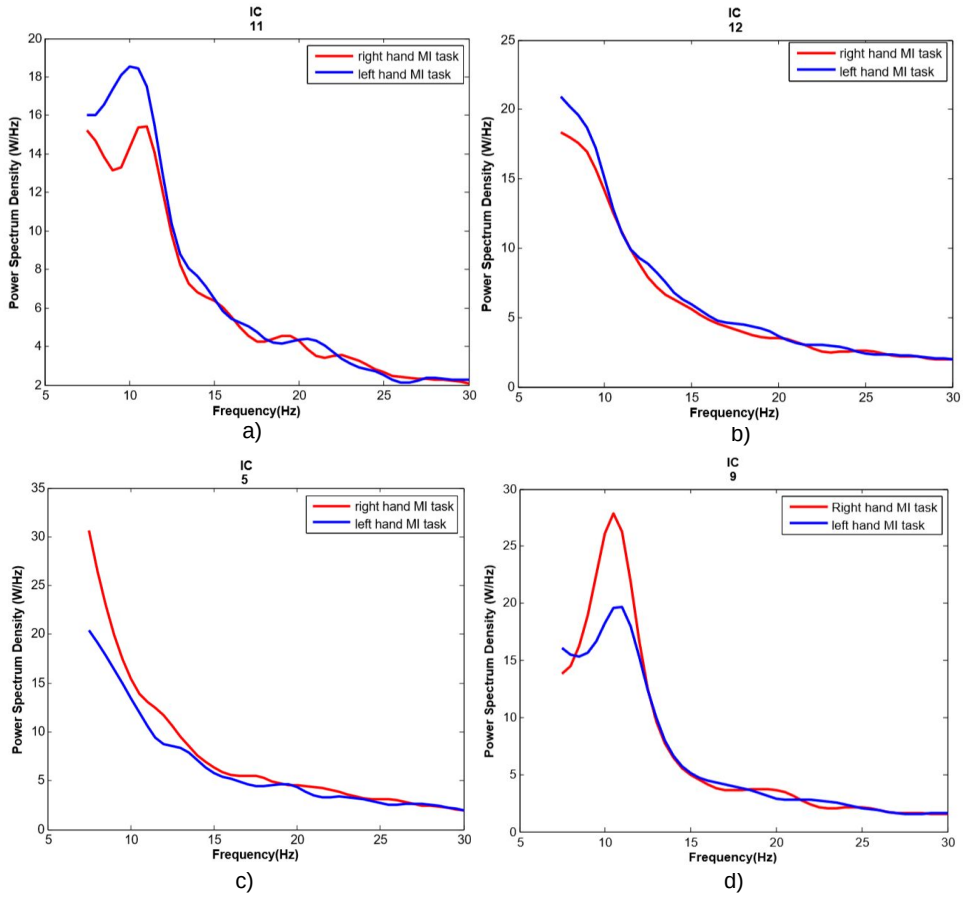

Figure 3.20 – PSD for Subject 6 using ICA-JADE. (a) IC11, (b) IC12, (c) IC5, (d) IC9

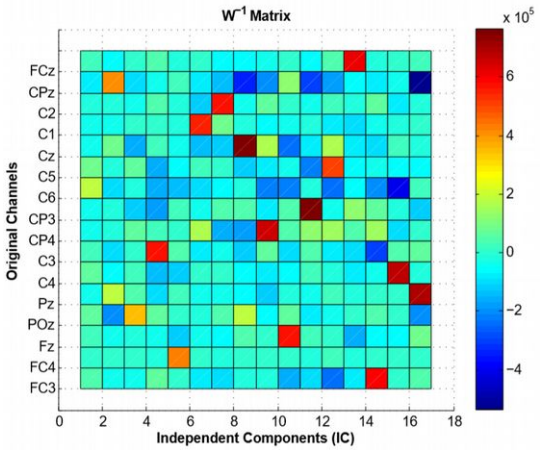

Figure 3.21 – Matrix $\mathbf{W^{-1}}$ for Subject 6.

3.4.2 Classification of left- and right-hand imagery movements

Tables 3.1 and 3.2 present the results of mean accuracy of classification between subjects for the tested cases. Table 3.1 shows the different cases of spatial filtering on each line: No filter, CAR Filter, ICA filter with JADE, INFOMAX and SOBI. The best value for classification was 91.4% using ICA-JADE in combination with LDA, FFT and wrappers. But it can be observed that the use of different kind of strategies for feature selection present a similar behavior; the results with DB-index usually lie below wrappers and ROC below DB-index. The difference between the FFT and Welch method is distinct for each case and for each subject.

Table 3.1 – Total mean accuracy classification for the different case tested.

		LDA			**SVM**			**ELM**		
		FFT	**Wel**	**AR**	**FFT**	**Wel**	**AR**	**FFT**	**Wel**	**AR**
NFilter	**Wra**	85.4	**86.3**	86.0	**77.5**	76.5	75.8	**83.1**	76.2	71.9
	DB	82.2	84.3	**85.8**	**73.2**	71.9	70.5	**63.6**	62.0	62.5
	ROC	81.6	84.1	**84.3**	**72.7**	71.2	72.0	**59.8**	60.7	61.7
CAR	**Wra**	90.4	**90.7**	89.6	**80.7**	80.6	77.9	**88.6**	79.1	78.2
	DB	**88.7**	87.4	86.4	**76.2**	76.0	65.8	**68.8**	63.8	64.2
	ROC	**87.3**	85.8	84.8	**74.6**	72.4	74.0	**67.2**	64.9	63.9
JADE	**Wra**	**91.4**	90.9	90.3	**85.8**	85.7	84.2	77.5	**81.0**	77.6
	DB	**89.3**	87.8	86.3	**82.4**	80.5	80.3	67.9	**69.1**	66.3
	ROC	**87.2**	85.2	86.2	**79.2**	77.3	78.5	69.6	**70.8**	69.0
INFO	**Wra**	**89.6**	89.0	87.8	84.4	**84.7**	82.6	75.4	**80.9**	76.2
	DB	**87.9**	86.3	86.1	**78.7**	78.5	77.4	68.9	**69.6**	68.3
	ROC	**87.4**	85.8	83.9	**78.5**	77.3	75.8	68.8	**71.3**	70.1
SOBI	**Wra**	**89.4**	85.6	86.4	**81.9**	81.7	78.2	74.1	**83.0**	79.7
	DB	**85.2**	84.0	84.4	**79.0**	75.3	75.4	62.5	62.2	**64.5**
	ROC	**84.6**	83.3	83.6	**76.1**	75.8	70.8	61.4	62.0	**62.2**

Table 3.2 shows the mean classification accuracy for the three specific cases of no filter, CAR and ICA-JADE using a wrapper for feature selection. The results are the best found for each one of the subjects who took part in this experiment.

The subjects with the best classification result are S1 and S4: checking their results when using the different filters shows a consistent superiority in relation to other subjects. Remembering the results of the figures with the spectral response of the IC, S1 was one of the cases that had up to 4 components that showed a marked desynchronization (Figure 3.17). S2 was in third place in relation to classification performance, according to the results of Figure 3.19. This shows that S2 had a strong desynchronization, indicating to be stronger for one of the classes.

The results of classifcation performance between subjects seem quite even when using LDA as classifier and ICA-JADE and CAR filter, however the option of ICA-JADE

Table 3.2 – Mean classification accuracy - best case for each subject using feature selection with wrappers.

	No Filter			CAR			ICA-JADE		
Subject	**LDA**	**SVM**	**ELM**	**LDA**	**SVM**	**ELM**	**LDA**	**SVM**	**ELM**
1	0.90	0.78	0.86	0.97	0.78	0.89	0.99	0.96	0.9
2	0.85	0.68	0.8	0.9	0.82	0.84	0.95	0.83	0.76
3	0.86	0.77	0.76	0.9	0.78	0.83	0.88	0.88	0.77
4	0.94	0.93	0.91	0.96	0.95	0.98	0.96	0.93	0.89
5	0.83	0.75	0.84	0.9	0.72	0.87	0.93	0.79	0.82
6	0.9	0.78	0.83	0.9	0.83	0.94	0.87	0.87	0.74
Mean	**0.88**	**0.77**	**0.85**	**0.87**	**0.81**	**0.89**	**0.93**	**0.87**	**0.81**

was superior for LDA and SVM classifiers. Additionally, in Table 3.3, the amount of attributes used by each of the tested selection methods and classifiers is shown. After running 4 times each one of the cases tested, the smallest and largest values found among all the runs are registered in this table.

Table 3.3 – Number of features selected, best case for each subject using different methods for feature selection and ICA-JADE.

	Wrappers			DB Index			ROC		
Subject	**LDA**	**SVM**	**ELM**	**LDA**	**SVM**	**ELM**	**LDA**	**SVM**	**ELM**
1	9/15	9/16	4/10	8/10	8/17	3/8	32	32	32
2	17/19	14/17	4/22	21	21	4/8	5/9	21/29	2/23
3	5/17	13/22	9/20	7/11	19/24	9/15	27/32	17/21	24/31
4	16/21	15/23	4/22	16/21	17/27	8/17	6/31	22/27	32
5	9/19	9/20	5/9	27/31	29/32	12/30	31	25/30	30
6	11/20	15/19	13/17	22/29	22/25	9/29	30	30	27/30

Observing the data in Table 3.3 for feature selection with wrappers, it can be seen that no more than 22 features were reached for any subject with any classifier. In relation to the number of features selected, with two features to be used for channel (the two frequency bands mu and beta), a 22 features selection are equivalent to a number of 11 channels used. This number of channels may seem excessive considering that the spectra seen before in some subjects does not present more than seven IC with typical motor imagery response. However, this must be studied for each particular subject, since in some subjects the components with desynchronization are few and for this same reason other type of features of other components had to be considered. It remains to investigate why other attributes or more channels appear to improve the performance of classification. In the case of the other techniques used for feature selection (DB Index and ROC), for some subjects, all features were used. ROC in general was the technique that selected the largest number of features.

Another test for the ICA-Filter was made with data from more days of experiments.

In these days, the quantity of trials per subject was lower with 10 left and 10 right trials. Only Subjects 1, 5 and 6 were part of this other experiment. In the days 3 and 4, these subjects also performed online test. In this kind of test, feedback was included in the form of a bar that appeared indicating which was the direction selected (left or right hand). These results are presented in Table 3.4.

Table 3.4 – Mean classification accuracy with ICA-JADE filter, best case using other days data.

	Filter and classifier from day itself			**Using filter first day**		
Subject	**DAY1**	**DAY2**	**DAY3**	**DAY1**	**DAY2**	**DAY3**
1	0.96	1	0.98	0.8	0.78	0.92
5	0.92		0.95	0.74		0.81
6	0.95	1	0.98	0.81	0.82	0.84

The results of Subject 1 confirm their level of execution of the MI task, that remained consistent even in new days of experiment. Also, Subject 6 showed continuity in their results, indicating that, in some way, MI patterns detected in the initial filter could be used on other days as well.

3.5 Conclusion

In some cases, the recovered ICs were comparable to or superior in their MI activity to the signal found with CAR filters, especially on subjects with a clear MI activity where it is possible to say that the IC enhanced the response of the raw EEG signals. Despite this, some subjects were an exception, with no evident MI activity even in the ICs. In these cases, maybe the strategy to select attributes explores at maximum the components achieving improvements on the classification rates. The lower mean classification accuracy obtained for a subject in the best strategy of signal processing was 88%, for Subject 3. Further steps include to verify the performance of these filters in an online session with feedback, trying to take into account the adaptation of each subject to the system and the influence of a process of continuous training on the improvement of the MI response.

4 A comparative analysis for feature extraction in graph-based motor imagery brain-computer interfaces

4.1 Introduction

In order to discriminate pertinent brain activities, the feature extraction stage is responsible for converting the recorded signals into relevant features that are obtained and used in the classification stage. For a BCI, it is important to ensure a feature extraction process that allows the identification of a subject's response to a particular paradigm. This is part of the establishment of the correct response of the total BCI system.

To this date, several works with non-invasive BCIs have used features derived from the analysis of individual channels (electrodes) in a separate way. These approaches allow studying and extracting different types of features depending on each type of specific paradigm (LAKSHMI *et al.*, 2014). This approach specifically oriented to the domain where the features are expected could reduce the study of the brain phenomena as a whole, which could influence the quality of the response of the BCI system, reducing the classification performance (VAID *et al.*, 2015).

Therefore, to increase BCIs' usage, which could be achieved by improving the reliability of their response, brain functional connectivity (FC) measures derived from graph theory have been recently suggested as a potential option. FC reflects statistically related activity of brain areas (BILLINGER *et al.*, 2013). This allows the brain signal to be analyzed statistically in the time domain mainly, but the frequency and spatial relationships could be included also, giving a deeper idea of a cerebral phenomenon in several domains and oriented to a connected brain response analysis. Thus, in this chapter, some of the methods commonly used for feature extraction and also a specific proposal oriented to the application of FC using correntropy as a similarity measure for building graphs from electroencephalography (EEG) data obtained from a motor imagery (MI) based BCI will be presented.

In the next sections, some of the classic techniques used for feature extraction will be mentioned. Then, methods related to graphs and functional connectivity will be discussed. Finally, the FC-correntropy research effort and the obtained results will be presented in detail.

4.1.1 Proposal

This proposal is based on the experiments focused on exploring the feasibility of using a FC approach to generate features for a MI-BCI (URIBE *et al.*, 2017; STEFANO FILHO *et al.*, 2018; RODRIGUES *et al.*, 2017). Preliminary findings indicated that using correntropy instead of Pearson correlation for building graphs results in a better classification performance. This probably comes from the introduction of higher-order statistics in the information carried by the adjacency matrix, thus providing more favorable scenarios for the correntropy usage. Motivated by these initial results, the investigation of such a perspective is continued by incorporating different analysis setups regarding the feature extraction and classification stages, which include:

- First analysis setup: data from 2-command (left / right hand MI) BCI obtained with 64-channel EEG for 8 subjects, in which the classification performance was investigated under: (1) different mu and beta frequency bands; (2) evaluation of three different FC methods: correntropy, Pearson and Spearman correlations; (3) feature extraction based on three different graph measures: degree, betweenness and eigenvector centrality; (4) classification performance using either linear discriminant analysis (LDA) or extreme learning machines (ELMs);
- Second analysis setup: a comparison between the proposed approach - correntropy / graph based measures / LDA and ELM - with alternative frameworks in the benchmark defined by the BCI competition IV - dataset 2a (TANGERMANN *et al.*, 2012).

A summary of the methods used for the different implemented stages is shown in Figure 4.1. The methodological details of this work will be described in the following sections.

4.2 Feature analysis

Each paradigm of BCI includes different features that must be interpreted in the feature extraction stage. In this process, several factors must be considered, such as the domain where the information can be suitable for interpretation; the amount of generated features; and the simplicity of the process considering an online and offline operation. For this reason, this stage can determine the real capacity of use of a BCI system. An analysis excessively demanding in terms of processing capacity can make the system slow and difficult or impossible to use in an online BCI application (LOTTE, 2015). For a clearer description of this process, some of the methods used in this stage will be explained by dividing them into two types of strategies: first considering solely feature extraction, and,

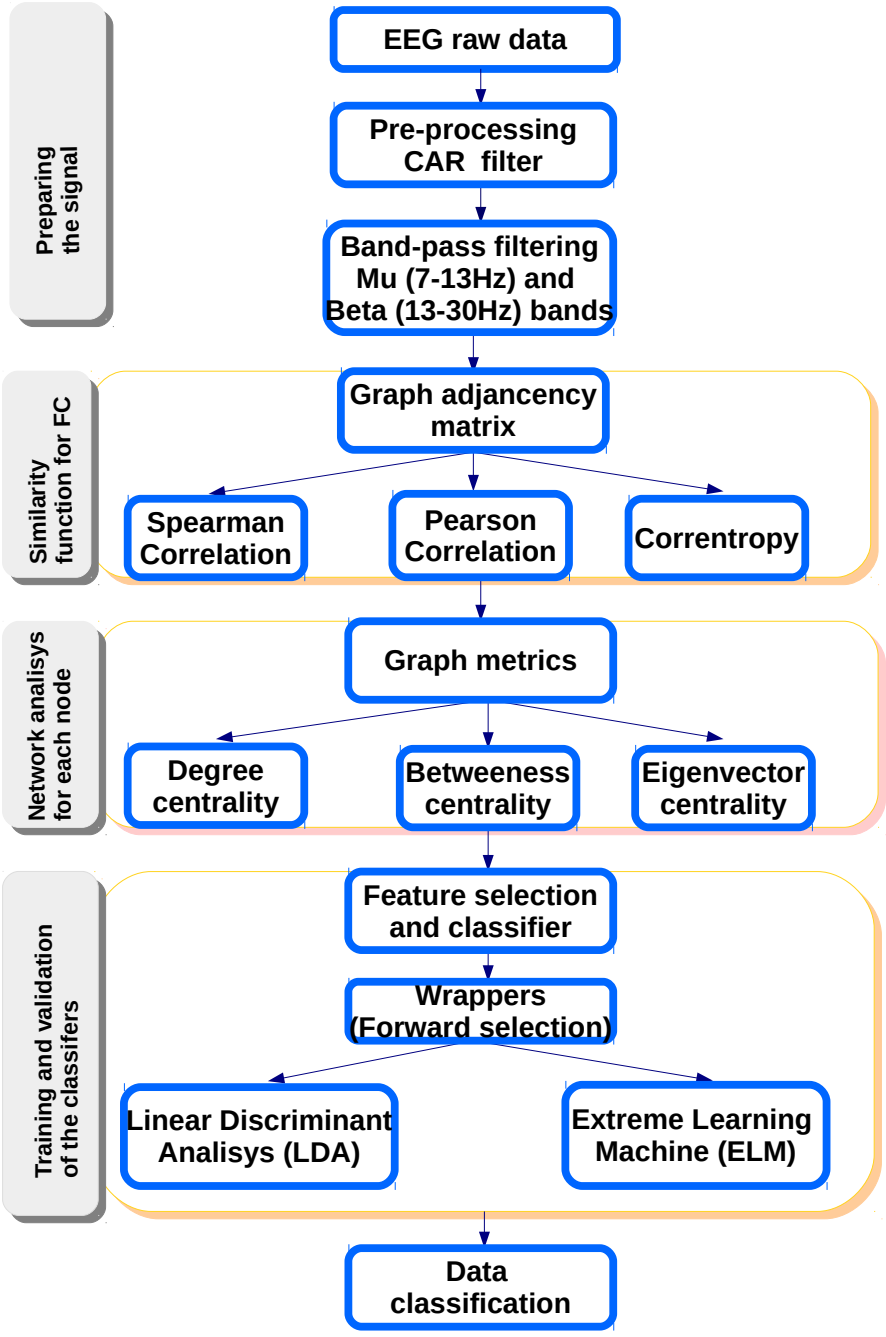

Figure 4.1 – Methodology used in these proposal.

second, gathering and considering information about the separation of the classes using different forms of optimization and other techniques related to spatial filters.

4.2.1 Approaches for feature extraction in BCI systems

The direct estimation of the features of interest can be done by several parametric and non-parametric methods. The simplest methods include basic techniques for extracting information in time and frequency domain, in which case linear methods have already

been used, including: fast Fourier transform (FFT), eigenvector analysis, auto-regressive model (AR), wavelet transform (WT), wavelet packet decomposition (WPD), principal component analysis (PCA) (VAID *et al.*, 2015). Nonlinear methods include the correlation dimension (CD), Hurst (H) exponent, largest Lyapunov exponent (LLE), different entropies, higher order spectra (HOS), fractal dimension (FD), space recurrence diagrams (URIBE *et al.*, 2014) and phase analysis (VAID *et al.*, 2015).

Table 4.1, taken from (VAID *et al.*, 2015), summarizes some of the features that compose the different types of analysis that have been worked for some BCI systems. It can be observed that the analysis of these brain phenomena for BCI systems are not only composed of a single domain to be used, and including more information could be useful. For the case of the two phenomena in which the frequency is studied, which are MI and SSVEP, the inclusion of temporal information can give more precision to the estimate, or it can also allow to recognize the phenomenon of interest in a clearer way, giving a precise image of what is happening with the brain response, for example, the spectrogram map, where the evolution of the spectra in time can be seen.

Table 4.1 – Attributes and methods for feature extraction in BCI systems.

Different domain	**Feature extraction method**	**Features**
TIME DOMAIN (t-domain)	1- Linear Prediction (LP) 2- Independent Component Analysis (ICA)	1- Event Related Potentials (ERP) 2 - Statistics of signal Power - Mean - Standard deviation - 1st difference - Normalized 1st difference - 2nd difference - Normalized 2nd difference 3- Hjorth features - Activity - Mobility - Complexity 4- Fractal Dimension 5- Higher Order Crossings (HOC)
FREQUENCY DOMAIN (f-domain)	1- Fast Fourier Transform (FFT) 2- Autoregressive method (ARM) 3- Eigenvector	1- Band power 2- Higher Order Spectra (HOS)
TIME-FREQUENCY DOMAIN (t-f domain)	1- Short-Time Fourier Transform (STFT) 2- Spectrogram 3- Wigner Ville Distribution 4- Scalogram 5- Hilbert-Huang Spectrum 6- Discrete-Wavelet Transform (DWT) 7- Wavelet Packet Decomposition (WPD)	Combination of time and frequency features
SPACE-TIME FREQUENCY DOMAIN (s-t-f domain)	For multichannel EEGs, in which spatial dimension is calculated by the geometrical positions of the electrodes	Combination of time and frequency features

In P300 EEG signal processing, the ERPs were commonly extracted by signal av-

eraging based on the data recorded on some expected electrodes of the parietal region like Pz or POz (DUNCAN-JOHNSON; DONCHIN, 1982). The number of electrode channels used can be established also using techniques such as PCA, and methods for automatic channel selection (THULASIDAS; GUAN, 2005). The information of P300 is mainly in the temporal domain, therefore, usually, features from other domains are not included, but due to the influence of noise, ways should be found to maximize the information extracted. The proposals in the literature consider the use of preprocessing strategies that reduce especially certain types of outliers (THULASIDAS *et al.*, 2006). The use of classifiers has also been considered in relation to feature extraction, ensuring that a large number of attributes can be handled (RAKOTOMAMONJY; GUIGUE, 2008).

The SSVEP paradigm is based on the detection of oscillating patterns within EEG waves, hence the use of spectral features is a natural choice. Figure 4.2 shows the spectral features of the SSVEP responses observed on channel O2 for the evoked frequencies 12 and 15 Hz (CARVALHO *et al.*, 2015b). It is important to notice that the spectral content is concentrated around the evoked frequencies. Works in the literature show that the inclusion of the power spectrum information of some harmonics of the stimulation frequencies and the use of different methods to combine electrode channels can bring information that increases the accuracy of the classification value (FRIMAN *et al.*, 2007). Also, for SSVEP, there are works in which not only the frequency of the stimuli is analyzed, but also the difference in phase (KLUGE; HARTMANN, 2007).

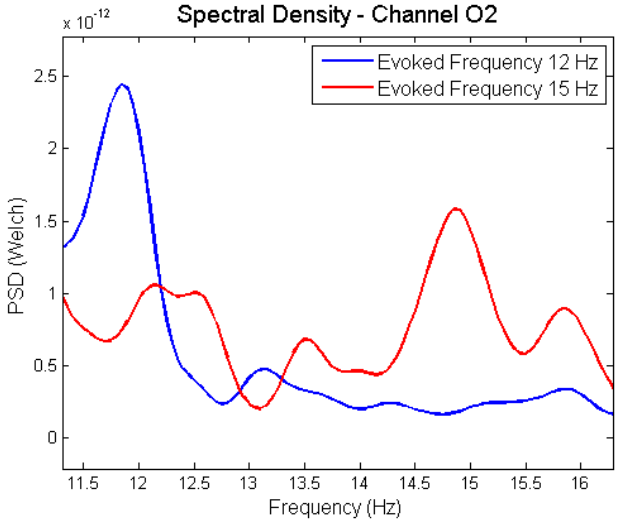

Figure 4.2 – SSVEP response for 12 Hz and 15 Hz stimulation – channel O2. Source: (CARVALHO *et al.*, 2015b)

For MI-BCI, a number of techniques have been employed in order to extract EEG features to discriminate the different motor-imagery tasks. As discussed in the previous chapter, most of them are defined in the frequency domain and in the spatial domain. In relation to the frequency domain analysis, the spectral power and phase synchrony

features can be used. For MI-BCI using phase synchronism, there have been works by the group of Pfurtscheller in Graz (SPIEGLER *et al.*, 2004) based on the computation of the phase-locking value (PLV). The PLV measures the degree of synchrony between couples of channels at different time windows. PLV revealed to be discriminative for motor-imagery, but the accuracies obtained with these features alone were inferior compared to band-power features. However, combining phase and amplitude information may improve the accuracy of teh system.

4.2.2 Spatial filters in BCI systems

In the best estimation of the signal and its features, it is expected that, in the classification step, the data will be separable and correctly represented for each of the projected classes. However, this is not entirely true for the case of BCIs. In these systems, it is known that the signal must be pre-processed for noise elimination: without appropiate noise removal, subsequent steps may lose their effectiveness. Thus, preprocessing techniques were often associated with the feature extraction and the classification stages to truly deal with the complexity of brain dynamics, by combining the information of temporal, frequency and spatial domains. In relation to this, reference models can be useful to define a pre-established response associated with the phenomenon, for example, information about the spatial region where the phenomenon is expected to happen, and its features.

One of the techniques that use information related to multiple domains are spatial filters. Spatial filtering consists of combining the original sensor signals, usually linearly, which can result in a signal with a higher signal-to-noise ratio than those of the individual sensors (LOTTE *et al.*, 2018). This type of method is oriented to process the signal in a way that pre-processing and feature extraction methods are considered together, oriented towards a simpler and more effective classification stage.

One perspective considered when working with spatial filters is oriented to the idea of converting the EEG signals obtained from each electrode location into source signals. This problem is an “inverse problem” and cannot be solved without a prior hypothesis. Despite this, when certain assumptions are made, spatial filters can be constructed with sources that significantly increase the signal-to-noise ratio in relation to the measured original signals (SEKIHARA, 2005). The weight matrix calculated by the spatial filter determines the degree of each EEG signal contribution to each source.

There are different methods to obtain the weight matrix. Beamforming methods use information available *a priori* about signal sources, electrode locations and properties in the environment that might affect transmission of the signal from a source to the sensors (e.g. density and composition of the head). Some examples include (BIEGER; MOLINA, 2010): linearly-constrained minimum variance (LCMV), low-resolution brain

electromagnetic tomography (LORETA) and Bayesian beamforming. On the other hand, independent component analysis (ICA) makes no assumptions about the source locations in the brain, or the effects from the environment, but instead assumes that the sources are all statistically independent, which is not entirely true (SHEN *et al.*, 2002). These methods do not include a direct relation with the extracted features, and knowledge about the BCI task is in general not necessary.

Differently, one of the most commonly used approaches of spatial filters in MI-BCI systems (PFURTSCHELLER; NEUPER, 2001) considers the properties of the MI phenomena from an EEG signal to obtain a covariance matrix that maximally discriminates two different classes. Common spatial patterns (CSP) aims to enhance the extracted information by maximizing the power of one ERP and minimizing the power of another ERP, taking into account the signal-to-interference (SIR) relationship. Since our proposal on functional connectivity is oriented to BCI systems with MI, in the next subsection, CSP will be explained in detail. Later, this method will be used for comparison purposes in the results sections.

4.2.3 Common Spatial Patterns (CSP)

The goal of Common Spatial Patterns (CSP) is to design spatial filters that lead to new time series whose variances are optimal for the discrimination of two classes of EEG (RAMOSER *et al.*, 2000). Given a single trial, an N-channel spatial-temporal EEG signal $\mathbf{E}$, where $\mathbf{E}$ is a $N \times T$ matrix and T denotes the number of samples in each channel, the normalized covariance matrix of the EEG can be obtained from:

$$\mathbf{C} = \frac{\mathbf{E}\mathbf{E}^T}{\text{trace}(\mathbf{E}\mathbf{E}^T)} \tag{4.1}$$

The operator trace(x) denotes the sum of the elements of (x). For two classes to be separated (i.e., left and right motor imagery), the spatial covariance $\mathbf{C_d}, \in [\mathbf{l}, \mathbf{r}]$ is calculated by averaging over the trials of each group. The composite covariance matrix its given by

$$\mathbf{C_c} = \bar{\mathbf{C}}_\mathbf{l} + \bar{\mathbf{C}}_\mathbf{r} \tag{4.2}$$

$\mathbf{C_c}$ can be factored using its eigenvalue decomposition as $\mathbf{C_c} = \mathbf{F_c}\Psi{\mathbf{F_c}}^T$. Where $\mathbf{F_c}$ is a matrix of normalized eigenvectors with corresponding matrix of eigenvalues, Ψ.

The whitening transformation in (4.3) equalizes the variances in the space spanned by the eigenvectors in $\mathbf{F_c}$, as will be used in the presented Equation 4.4.

$$\mathbf{P} = \Psi^{-1/2}{\mathbf{F_c}}^T \tag{4.3}$$

The CSP is extracted based on the simultaneous diagonalization of whitened covariance matrices,

$$\mathbf{S_l} = \mathbf{P}\bar{\mathbf{C}}_\mathbf{l}\mathbf{P}^T \text{ and } \mathbf{S_r} = \mathbf{P}\bar{\mathbf{C}}_\mathbf{r}\mathbf{P}^T \tag{4.4}$$

The resulting decomposition maximizes the differentiation between two groups of data. Then $\mathbf{S_l}$ and $\mathbf{S_r}$ share common eigenvectors.

$$\text{If } \mathbf{S_l} = \mathbf{U}\lambda_l\mathbf{U}^T \text{ then } \mathbf{S_r} = \mathbf{U}\lambda_r\mathbf{U}^T \text{ and } \lambda_l + \lambda_r = \mathbf{I} \tag{4.5}$$

Since the sum of the two corresponding eigenvalues is always one, the eigenvector with largest eigenvalue for $\mathbf{S_l}$ has the smallest eigenvalue for $\mathbf{S_r}$ and vice versa. This property makes the eigenvectors useful for classification of the two distributions. The projection of whitened EEG onto the first and last eigenvectors in $\mathbf{U}$ (i.e., the eigenvectors corresponding to the largest λ_l and λ_f) will yield feature vectors that are optimal for discriminating two populations of EEG in the least squares sense. The CSP projection matrix will be then $\mathbf{W_{CSP}} = (\mathbf{U}^T\mathbf{P})$, and the decomposition (mapping) of a trial $\mathbf{E}$ is given as $\mathbf{Z} = \mathbf{E}\mathbf{W}_{CSP}$ (NOVI *et al.*, 2007).

One practical issue to be considered with this technique of spatial filtering is that, in its original conception, it was intended to be used with a large number of electrodes. An additional problem associated with the supervised CSP algorithm in particular is its tendency to overfit, leading to poor generalisation (FARQUHAR *et al.*, 2006). This is a particular problem when the number of electrodes is large, and when the number of available trials is small.

4.3 Functional Connectivity

The study of BCIs brings together different areas of knowledge that explore the neurological phenomena associated with interesting brain responses. This has led to the exploration of other types of representations of the brain signal related to a deeper level (neuronal representation), for example, using methods for identification of sources (QIN *et al.*, 2004). Another approach associated to this type of work is to see the broader perspective, when it is observed the connectivity between neuronal regions. Related to this, recent BCI developments have used graph theory and functional connectivity (FC) to analyze the functional organization of the brain that underlies specific mental tasks (STEFANO FILHO *et al.*, 2018), (DALY *et al.*, 2012), (GHOSH *et al.*, 2015).

FC is defined as the temporal correlation among the activity of different neural assemblies (FINGELKURTS *et al.*, 2005). Because functional connectivity techniques are considerably dependent on calculating the correspondence of neural signals over time,

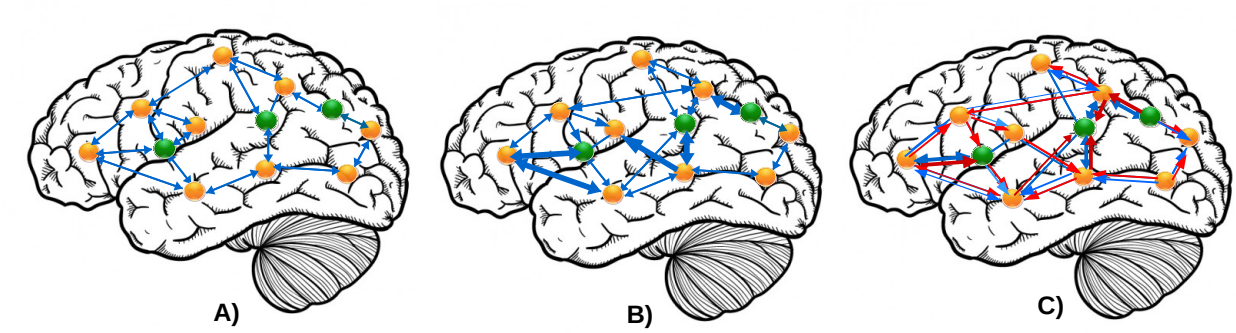

Figure 4.3 – A) Undirected and weighted Structural Connectivity (different number of connections). B) Undirected and weighted Functional Connectivity (different node strength connexion). C) Directed and weighted Effective Connectivity (different directionality connections). Source: Adapted from (RIBEIRO *et al.*, 2015).

.

EEG and MEG signals, which have excellent temporal resolution, are the most suitable option for calculating such connectivity (SAKKALIS, 2011). Figure 4.3 presents a comparison of the different types of connectivity used to understand the human brain function. The structural connectivity may be considered as close to a physical level, with the description of fiber pathways, tracked over extended regions of the brain, which are in accordance with general anatomical knowledge (KOCH *et al.*, 2002). Meanwhile, effective connectivity is a relatively new concept defined as the direct or indirect influence that one neural system exerts over another. It describes the dynamic directional interactions among brain regions (SAKKALIS, 2011).

In the next subsections, a brief explanation to introduce some concepts of graph theory will be included. Later, also some functional connectivity measures will be explained. Some of these methods will be used in the development of the proposal of functional connectivity and correntropy for a MI-BCI system.

4.3.1 Graph theory

In recent times, there has been a growing popularization of graph theory in the study of complex networks. This comes from the idea related to the fact that these methods can allow the simplified but efficient characterization of a network, which means that the analysis is not restricted only to the elements or relations of the individual items, but allows the understanding of the patterns of connection, or interaction, between the parts of the system as a whole (NEWMAN, 2010).

In graph theory, a network is a graph whose vertices, also known as nodes, represent the components of the system and the interaction between the elements is described by edges (or links). In this representation, illustrated in Figure 4.4, if there is an edge between

two vertices, it means that they are related in some way, and thus are considered neighbors.

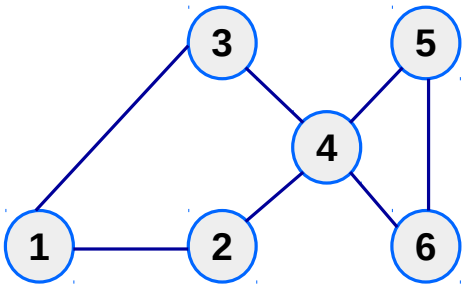

Figure 4.4 – Graph with 6 vertices and 7 edges.

One of the ways to represent a graph is by means of an adjacency matrix A, in which the matrix coefficients indicate whether or not there is a connection between vertices i and j. Graphs in which it is exclusively indicated if there is a connection between the nodes are known as unweighted and are represented by binary adjacency matrices in which $A_{ij} = 1$ if there is an edge between i and j, and $A_{ij} = 0$ otherwise (NEWMAN, 2010). Figure 4.5A presents an example of these graphs.

On the other hand, if it is necessary to show the intensity of the relationship between the different vertices, this can be done by using a weighted graph in which the edges can assume values other than 0 or 1, that express the strength of the connection (NEWMAN, 2010). It is worth noting that weighted graphs can be converted to non-weighted by the definition of a connection threshold, that is, the minimum/maximum value necessary to consider the existence of an edge between vertices of the graph. Figure 4.5B shows a weighted network with its adjacency matrix.

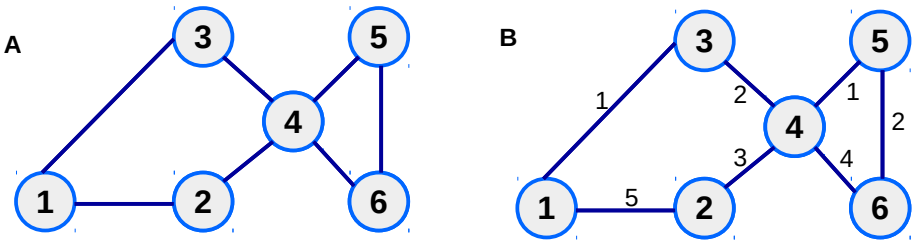

A=

v	1	2	3	4	5	6
1	0	1	1	0	0	0
2	1	0	0	1	0	0
3	1	1	0	1	0	0
4	0	1	1	0	1	1
5	0	0	0	1	0	1
6	0	0	0	1	1	0

A=

v	1	2	3	4	5	6
1	0	5	1	0	0	0
2	5	0	0	3	0	0
3	1	0	0	2	0	0
4	0	3	2	0	1	4
5	0	0	0	1	0	2
6	0	0	0	4	2	0

Figure 4.5 – Unweighted (A) and weighted graph (B) with their respective adjacency matrices below.

Other consideration has to be taken when a graph is defined. The form of connection between the nodes established a relationship between the vertices that can be mutual, or occur in only one direction. In the first case, the edges of the graph used to represent the network do not have direction (undirected graphs) (NEWMAN, 2010); such graphs were previously presented in the previous figures shown. Graphs that inform the direction of the information flow are usually known as directed graphs. Figure 4.6 presents a directed graph and its adjacency matrix.

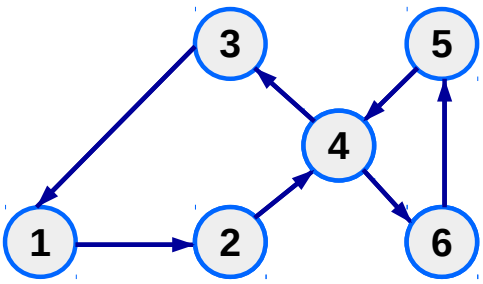

A=

v	1	2	3	4	5	6
1	0	1	0	0	0	0
2	0	0	0	1	0	0
3	1	0	0	0	0	0
4	0	0	1	0	0	1
5	0	0	0	1	0	0
6	0	0	0	0	1	0

Figure 4.6 – Directed graph and its adjacency matrix. It is possible to observe that the matrix A for directed graphs is not symmetric.

4.3.2 Graph measures

For a network that is modeled by a graph a next step executed in the analysis is to measure some statistics to characterize it. The information contained in a network can be summarized with graph measures. These have been applied to topological analysis of brain functional networks, and many of them have been used to study diseases and statistically significant differences between, for example, two different classes of brain states. This would be the case of the comparative study of healthy subjects against those affected by neuropathologies (SAKKALIS, 2011).

Thereby, it is necessary to use measures that quantify the structure of the network to analyze the relationship between the elements. Some of these measures are defined in Table 4.2, where some of their characteristics and their advantages are mentioned.

Graph measures can be classified within two broad categories (MIJALKOV *et al.*, 2017). Many measures can be implemented in both types of classes:

- global measures, that refer to global properties of a graph and, therefore, consist of a single number for each graph;
- nodal measures, that refer to properties of the nodes of a graph and, therefore, consist of a vector of numbers — one for each node of the graph.

Table 4.2 – Graph measures to quantify the network structure.

MEASURE	DEFINITION	ADVANTAGES	EXPRESSION
Degree	Number of edges, or neighbors, of a given vertex.	Valid to assume that highly connected vertices are more influential or give more access to information.	Undirected graph: $k_i = \sum_{j=1}^{n} A_{ij}$ Directed graph: $k_i^{in} = \sum_{j=1}^{n} A_{ji}$ $k_i^{out} = \sum_{i=1}^{n} A_{ij}$
Minimum path	Path that connects vertex i to j through as few edges as possible.	This index take into account spatial features (distance, surface) as well as the level of activity (traffic).	The distance l_{ij} between vertices, which is defined by the number of edges that form the minimum path between two vertices.
Clustering coefficient (Aggregation)	Measures the probability that two neighbors of a vertex are also neighbors, thus defining a measure of network transitivity.	Allows understanding of the topological structure of the neighborhood of a vertex (node).	The portion of the size 2 paths that are closed, i.e., the number of triangles of the network, filled is estimated. For the global coefficient: The clustering coefficient for a graph is given by (WATTS; STROGATZ, 1998).
Degree centrality	Centrality measures which are the most central elements, that are usually considered of great importance, since their removal from the network can impact on severe damages in the flow of information.	Takes into account the amount of edges of a vertex.	The definition will be included in the sections below.
Eigenvector centrality	Proportional to the sum of the centralities of the neighbors of that vertex.	Vertices connected to more connected neighbors are more important in the network than others with the same degree and neighbors less connected.	The definition will be included in the sections below.
Betweenness centrality	Or shortest-path betweenness; it is a measure of accessibility that is the number of times a node is crossed by shortest paths in the graph.	Allows identifying the vertices that control the flow (e.g. of information), which are those with higher values of centrality.	The definition will be included in the sections below.

On the other hand, it is possible to divide the graph metrics into other types of categories by their quantifying function (RUBINOV; SPORNS, 2010):

- Integration: these metrics are characterized by the ability to easily combine specialized information from different regions of the brain, estimating the communication efficiency. The most common integration measure is known as a characteristic path length and is the average distance from a node to all other nodes. The inverse of this metric is known as global efficiency. A network with high efficiency presents close vertices, which allows them a high functional integration (RUBINOV; SPORNS, 2010; SPORNS, 2011).

- Segregation: these metrics suggest that a graph can be divided into clearly separated communities (i.e. subgraphs or modules). Its calculation requires a previously deter-

mined community structure. Metrics as grouping coefficient or modularity subdivide the network into non-overlapping groups. Neuronal units that form dense groups or communication modules are expected to share information easily, and thus constitute a likely functionally coherent system (RUBINOV; SPORNS, 2010; SPORNS, 2011).

- Centrality: these measures characterize local properties of networks. This is valuable since at the local scale, it is possible to detect which vertices are the most relevant to the organization and functioning of a network. Identifying the elements that have the potential to participate in a large number of functional interactions and / or control the flow of information has great value for analyzing the role played by individuals in social networks and for identifying essential proteins, keystone species and functionally important brain regions (SAKKALIS, 2011).

- Resilience: these measures are related to identifying vulnerabilities in the network, since the removal of important components can affect the functionality of integration between the parties (RUBINOV; SPORNS, 2010). For this purpose, it is necessary to detect regions that are not connected by means of the network degree distribution, using the average neighbor degree and also by detect the overall vertices connected by the assortativity coefficient, in which high values indicate that the vertices tend to connect with others of similar degree, while negative values indicate the inverse.

4.3.3 Functional connectivity metrics

Before analyzing graph metrics, the graph itself has to be estimated from data acquired through techniques such as EEG, MEG, fMRI, among other techniques (SPORNS, 2011). In brain functional networks, each vertex is identified with a specific brain channel/region or electrode, and each edge corresponds to a measure of statistical dependence between the activities of different brain areas. It is assumed here that the activity of a brain area is represented as a scalar time series. Several synchronization techniques have been used/developed to estimate both the linear and nonlinear dynamic coupling between different brain regions. In this section, some of these methods will be presented.

Functional connections correspond to magnitudes of temporal correlations, coherence or mutual information and can occur between pairs of regions anatomically decorrelated. These connections are time dependent and are not able to explain explicit causal relationships. The vertices in these networks usually represent the sensors (e.g. electrodes) used in the data acquisition and can present a strong correlation, being necessary appropriate preprocessing steps depending on the type of analysis (BULLMORE; BASSETT, 2011).

Consider an undirected, connected, weighted graph $\mathbf{G} = \{V, E, \mathbf{A}\}$, where V is a finite set of vertices with $|V| = N$. E is a set of edges, and $\mathbf{A}$ is the adjacency matrix. A signal $f : V \rightarrow \mathbb{R}^N$ can be defined on the vertices of the graph represented as a vector $f \epsilon \mathbb{R}^N$, where the n^{th} component, f_n, represents the signal value at the n^{th} vertex of V.

To define the functional connections it its possible to use a similarity function $s(f_i, f_j)$ between all pairs of data points f_i and f_j to create the neighborhood relationships between the vertices. The graphs similarity was established for two vertices connected if similarity $s(f_i, f_j)$ between the corresponding data points is positive or larger than a certain threshold T. The corresponding edge is therefore weighted by $a_{i,j} = s(f_i, f_j)$, and the weighted adjacency matrix of $\mathbf{G}$ is defined as $\mathbf{A} = (a_{i,j})_{i,j=\{1,\cdots,n\}}$. If $a_{i,j} = 0$, the vertices v_i and v_j are not connected since either $s(f_i, f_j) = 0$ or $s(f_i, f_j) < T$. If $\mathbf{G}$ is an undirected graph, then $a_{i,j} = a_{j,i}$ and $\mathbf{A}$ is a symmetric matrix with a complete set of real eigenvalues and an orthogonal eigenvector basis.

In this type of graph, a measure widely used to estimate the connectivity between sensors is the Pearson correlation, which is a measure of the statistical linear dependence, that can be estimated for two random variables or processes. It can be obtained the expression (4.6).

$$Similarity_{Pearson}(i, j) = \frac{cov(i, j)}{\sqrt{var(i)var(j)}} \tag{4.6}$$

where $cov(i, j)$ is the covariance between vertices i and j, and $var(x)$ is the variance of vertex x. Another measure used for this purpose is the Spearman correlation. This type of correlation is a special case of Pearson's correlation in which ranked data are used (MYERS, 2003). It can be defined as:

$$Similarity_{Spearman}(i, j) = 1 - \frac{6 \sum (x_i - y_i)^2}{n^3 - n} \tag{4.7}$$

where x_i and y_i are positions after the ranking of the observations and n is the number of ranked elements. Spearman's correlation is less sensitive to outliers, but also allows the evaluation of two monotonically related variables without restriction of linear relationships (GÖTTLICH *et al.*, 2015).

4.3.4 Correntropy and Correlation

Correntropy is an information-theoretic learning (ITL) based measure that can be interpreted as a generalized correlation function (GCF), capable of measuring the similarity between random variables / stationary random processes (PRINCIPE, 2010; SANTAMARÍA *et al.*, 2006). The concept of correntropy may be extended to cross-correntropy when it expresses a degree of similarity between two arbitrary scalar random

variables X and Y, since it computes a similarity measure in a kernel feature space. The cross-correntropy is defined as (PRINCIPE, 2010):

$$\begin{aligned} V(X,Y) &= E_{XY}\left[\kappa(X,Y)\right] \\ &= \int\int \kappa(x,y)\, p_{X,Y}(x,y)dxdy, \end{aligned} \tag{4.8}$$

in which the expected value is over the joint space, $\kappa(\cdot,\cdot)$ denotes a positive-definite kernel function and $p_{X,Y}(x,y)$ represents the joint PDF between X and Y.

Equation 4.8 can be reduced to the standard cross-correlation if $\kappa(x,y)$ is replaced by xy. The most widely used definite kernel function is the translation-invariant Gaussian kernel, defined as:

$$\kappa(X,Y) = \frac{1}{\sqrt{2\pi}\sigma} exp\left(\frac{-(X-Y)^2}{2\sigma^2}\right), \tag{4.9}$$

in which σ, known as kernel size, represents an adjustable parameter which is responsible for controlling the "observation window" where similarity is computed. In practical applications, the statistical average required for computing the correntropy is replaced by a sample mean over a finite number of samples, resulting in the following estimator:

$$\hat{V}_{\sigma,N}(X,Y) = \frac{1}{N}\sum_{i=1}^{N} G_\sigma(x_i - y_i), \tag{4.10}$$

where $G_\sigma(\alpha) = \frac{1}{\sqrt{2\pi}\sigma}\exp\left(\frac{-|\alpha|^2}{2\sigma^2}\right)$.

Correntropy displays two key characteristics when used as a measure of similarity:

- Since inner products can be seen as a measure of similarity, the use of a GCF in terms of inner products of vectors in a kernel feature space is a manner of measuring the pairwise interaction of feature vectors and its temporal structure in the input space (POKHAREL *et al.*, 2010).
- From an ITL perspective, correntropy quantifies the shape and size of the group of points in the feature space, which gives information about the statistical distribution in the input space (LIU *et al.*, 2006).

When compared with conventional cross-correlation, the correntropy function also uses the second order moments of the data transformed by the eigenfunction of the Gaussian kernel to quantify similarities among pairs of lags of a random process. However, the correntropy function stands out because this similarity is not limited to second order moments. In fact for the Gaussian kernel all even moments of the random variable

contribute to the estimation of similarity due to the nonlinearity provided by the kernel (LIU *et al.*, 2006). This additional information may lead to a better notion of similarity - something essential in the FC graph-based methods - and yield more accurate analyses of the involved EEG random signals.

The nonlinearity introduced by the kernel has important implications in assessing the higher order moments of the joint PDF, but the Gaussian kernels also restricts the analysis to a local region of the joint space (LIU *et al.*, 2006). So correntropy is unable to assess similarity well in the entire joint space, but, for $X = Y$, it gives an estimate of probability density. Thereby, correntropy is directly related to the probability of how similar two random variables are in a neighborhood of the joint space controlled by the kernel bandwidth, then the use of higher-order moment information in correntropy is controlled smoothly by the kernel size (LIU *et al.*, 2007).

Despite this dependency, it has been proved experimentally that kernel size affects the performance of ITL algorithms much less than the case of density estimation (LIU *et al.*, 2007). In a practical context, when a limited number of data samples is available, the kernel width should be adjusted as a trade-off between estimation efficiency (small estimator variance) and outlier rejection (EMMERT-STREIB; DEHMER, 2009). Actually, a geometric analysis of correntropy shows that this function induces a new metric which is equivalent to using different norm distances in the sample space mapped by the kernel, according to how far apart the sample points are (LIU *et al.*, 2007). This geometric interpretation demonstrates the capacity of correntropy for outlier rejection.

The aforementioned tradeoff indicates a practical way to choose an appropriate kernel size, which should be selected according to the application. In this work, the performance sensitivity with respect to kernel size was quantified experimentally, something that has already been used in the literature (LIU *et al.*, 2007). It remains as a future perspective the use of other well-known methods for kernel size estimation, such as Silverman's rule (SILVERMAN, 1986), one of the most widely used kernel density estimation heuristics.

4.4 Experimental Setup and Pre-Processing

4.4.1 Data acquisition

EEG data from eight healthy MI-naive subjects (7 men, 1 woman, mean age 24 $\pm$ 4 years old) were recorded by a 64 Ag/AgCl channel BrainAmp amplifier (BrainProducts, Germany) at 5 kHz. The positions of the electrodes are shown in Figure 4.7. All subjects signed an informed consent term, and the procedure was approved by UNICAMP Ethics Committee (n. 791/2010). This data capture was made by one of the members associated

with our research group and was related to his master's work (STEFANO FILHO, 2016).

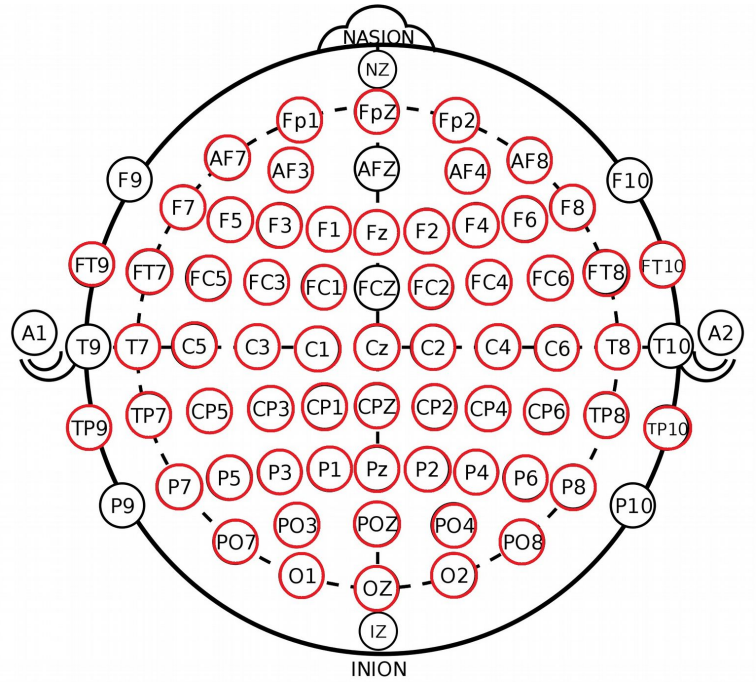

Figure 4.7 – Electrode recording positions for data acquisition are indicated in red circles, with remaining labels presented only for reference. One of the channels was used to record the electrocardiogram signal so only 63 of the 64 electrodes are shown.

Subjects were placed sitting comfortably on a chair, with a computer screen positioned in front of them, displaying a chronometer. They were instructed to imagine their right or left hand's grasping movements for 10 s, alternating each hand MI period with a 10 s resting block (Fig. 4.8). The hand MI to be performed (left or right) followed a pre-defined order: rest - right hand - rest - left hand - rest - right hand - etc, until the total recording time (170 s) was reached. Subjects should keep track of each block's duration using the displayed chronometer in front of them. To ensure that all participants understood the designed protocol, they were also asked to perform it using actual hand movements. Two MI runs were recorded for each subject.

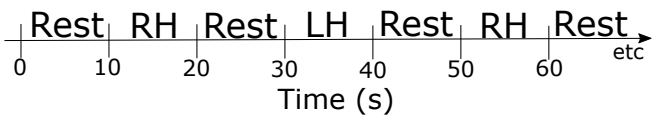

Figure 4.8 – Experimental protocol scheme consisting of alternating 10s blocks of rest and task periods. Either right hand (RH) or left hand (LH) MI were performed during the task blocks.

4.4.2 Data pre-processing

Data were downsampled to 256 Hz using EEGLab (DELORME; MAKEIG, 2004) and filtered in the mu (7 - 13 Hz) and beta (13 - 30 Hz) frequency bands.

A common average reference (CAR) spatial filter (GARCIA-MOLINA; ZHU, 2011) was used for minimizing simultaneous artifacts arising at multiple channels, as described in Equation (4.11) for 63 electrodes (the 64 channel was used to record the electrocardiogram signal):

$$V_i^{CAR} = V_i^{ER} - \frac{1}{63}\sum_{i=1}^{63} V_i^{ER}, \tag{4.11}$$

in which V_i^{ER} is the electric potential difference between electrode i and the system reference, and V_i^{CAR} represents the potential difference at i after the CAR filtering application.

In relation to the use of this pre-processing technique, there is a concern with respect of the effectiveness of this method to face the problem of volume conduction due to overlapping sensor lead fields, can cause spurious connectivity patterns that create high apparent correlations between sensor pairs (GREENBLATT *et al.*, 2012). The CAR filter is not exactly the most indicated technique to treat this kind of problem. However, it outperforms all the other types of reference methods, being one of the simplest filters that yields improved SNR (LAKSHMI *et al.*, 2014). Certainly, the finite sample density and incomplete head coverage could cause problems in calculating the average and can represent a disadvantage for this method.

This aspect be reviewed in the results section to confirm whether there was some spurious response, such as strong eye movement activity or other noise that may indicate an unexpected activity in some electrodes. It is left as a future perspective to continue the study of this aspect with pre-processing techniques that specifically target this phenomenon.

4.5 Feature generation

Feature extraction was performed to compare different similarity measures for graph-based modeling. The proposal of employing the information theoretical measure outlined by correntropy had special attention for this purpose, also its comparison to standard Pearson and Spearman correlations.

4.5.1 Graph adjacency matrix

The correntropy analysis is performed on the multi-variate time series$\{\mathbf{x}_t\}_{t=1}^{N} = \{x_{1,t}, x_{2,t}, ..., x_{n,t}\}_{t=1}^{N}$, an EEG segment of n channels and N samples. The observed vector

variable and its components at a time t can be denoted as $\mathbf{X}_t = \{X_{1,t}, X_{2,t}, ..., X_{n,t}\}$ or simply $\mathbf{X} = \{X_1, X_2, ..., X_n\}$. The correntropy matrix for the EEG signals may be defined as:

$$V[l] = E[k(\mathbf{X_t} - \mathbf{X_{t+l}})] \tag{4.12}$$

which can be estimated using the following unbiased and asymptotically consistent estimator:

$$\widehat{V}[l] = \frac{1}{N-l} \sum_{n=l+1}^{N} k(\mathbf{x_t} - \mathbf{x_{t+l}}) \text{ for } l \geq 0. \tag{4.13}$$

For lag l, the element $v_{ij}[l]$ of $\widehat{V}[l]$ denotes the correntropy of $X_{i,t}$, and $X_{j,t+l}$, denotes the cross-correntropy of X_i and X_j at lag l. When $l > 0$ or $l < 0$ the causality relationship between X_i and X_j is considered, for this reason in the current work we made $l = 0$ to restrict the analysis to the FC time domain. From Eq. 4.13 the following $\mathbf{V} = \widehat{V}[0]$ matrix can express the similarity between the EEG electrodes at $l = 0$.

$$\mathbf{V} = \begin{pmatrix} E[\kappa(X_1X_1)] & E[\kappa(X_1X_2)] & \dots & E[\kappa(X_1X_n)] \\ E[\kappa(X_2X_1)] & E[\kappa(X_2X_2)] & \dots & E[\kappa(X_2X_n)] \\ \vdots & \ddots & \ddots & \vdots \\ E[\kappa(X_nX_1)] & E[\kappa(X_nX_2)] & \dots & E[\kappa(X_nX_n)] \end{pmatrix} \tag{4.14}$$

$\mathbf{V}$ represents a graph adjacency matrix and its v_{ij} components represent the similarity strength between electrodes i and j. No threshold was defined for $\mathbf{V}$, to avoid the risk of losing relevant information and due to the lack of a definite criterion to do so (BORDIER *et al.*, 2017; TOPPI *et al.*, 2012). For comparison, a similar graph adjacency matrix was also calculated using the classical Pearson's and Spearman's approaches .

4.5.2 Graph analysis

In the present work, the nodes represent the electrodes and the links are defined by the similarity function between electrodes evaluated by Pearson's correlation, Spearman's correlation and correntropy. Stronger connections correspond to a larger similarity. These similarity calculations yielded connectivity matrices $\mathbf{V}$ with dimensions 63×63 (Eq. 4.14 for correntropy). From these matrices, three graph metrics were estimated: degree centrality (DC) or strength (for a weighted graph), betweenness centrality (BC) and eigenvector centrality (EC).

Each of these measures provides information regarding a node's importance within the network in terms of some criterion (NEWMAN, 2005). All metrics were calculated from a weighted, undirected graph.

For a node i in the matrix $\mathbf{V}$ the DC can be calculated through the sum of the edges' values (similarity measure) between i and all other nodes j it is connected to (ZHANG Z. ZHANG, 2012; BARRAT *et al.*, 2004):

$$DC_i = \sum_j v_{ij}. \tag{4.15}$$

The BC of a node i quantifies how many times the respective node acts as an intermediate between any other two nodes j and k. It consists in the ratio of shortest paths between this node pair (l_{jk}) and all other paths that pass through node i ($l(i)_{jk}$) (MONTEIRO, 2014):

$$BC_i = \frac{2}{(N-1)(N-2)} \sum_{j \neq k \neq i} \frac{l(i)_{jk}}{l_{jk}}. \tag{4.16}$$

N denotes the number of nodes and the multiplicative factor on the left is a normalization factor to yield BC values in the range [0,1].

It is important to note that a large node centrality value for one measure does not guarantee that the same node will display, also, a large value for another centrality measure. As an example, please refer to Fig. 4.9.

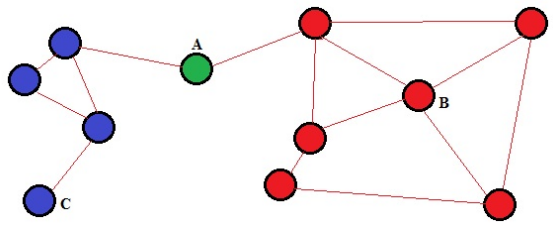

Figure 4.9 – Centrality values illustration. Node A has low DC, but possesses a fundamental role regarding communication between the red and blue nodes (high BC).

The EC for node i considers the importance of its neighbors; it is larger when the node is connected to high EC neighbors (MONTEIRO, 2014; NEWMAN, 2010). Assuming that the dependence of EC_i on all its neighbors j can be written as a linear combination, then:

$$EC_i = \frac{1}{\lambda} \sum_j v_{ij} EC_j. \tag{4.17}$$

Defining $\mathbf{EC} = (EC_1, EC_2, ..., EC_N)$ as the vector of ECs, then Eq. (4.17) can be written in the matrix form as

$$\lambda \mathbf{EC} = \mathbf{VEC}, \tag{4.18}$$

in which **V** is the graph's adjacency matrix, as explicitly displayed in Equation 4.14.

Each centrality measure provides insights regarding distinct interpretations within a network - hence our choice for studying these three measures.

4.6 Classification

The feature extraction stage generates a vector with 63 features for each evaluated centrality measure, i.e., one feature per electrode. Removing the information related to the 7 electrodes from the position of the middle line[1], 56 channels are obtained. From these new vectors, smaller 28-feature vectors were generated based on the difference of the graph measures concerning the symmetric electrode positions from the left and right hemispheres. Next, a selection algorithm was used to find the best combination of features.

4.6.1 Feature selection and classifier

The aim of the selection process is to test and determine the real relationship between the phenomena under study and the proposed signal processing methodology for each subject, considering that there is a limited number of electrodes - or parameters - to include as features for classification. There are three aspects that were defined in chapter 2, and that will also be used in this implementation of wrappers.

Search strategy. There are many ways to perform an efficient search over the feature space, such as genetic algorithms, simulated annealing or greedy heuristics. In this study, our search strategy consisted in wrappers operating through the greedy heuristic based on forward selection (GUYON; ELISSEEFF, 2003), in view of the trade-off between computational simplicity and achievable performance. It is known that this method is sub-optimal; however, it was able to provide us with the necessary computational complexity to address the comparison between the two classifier approaches, as well as the performance difference between the large group of subjects under study (This is the case of the BCI Competition IV database (TANGERMANN *et al.*, 2012)).

Stopping criteria. One of the simplest stopping criteria consists in the "if there was no improvement, then stop" rule; however, this approach can lead to poor local convergence. A more robust stopping criterion considers k consecutive steps without performance gain. In this study, $k = 2$ was adopted.

Classifier structure. Two types of classifiers were evaluated: a linear structure defined in the context of linear discriminant analysis (LDA) (BISHOP, 2006) and a

[1] The electrodes identified with a z at the end of their name in the denomination 10-20 for the location of electrodes for EEG recording were removed to study the laterality phenomenon when calculating only the difference between the activity of the electrodes of one hemisphere with respect to the other.

non-linear approach given by Extreme Learning Machine (ELM) (HUANG *et al.*, 2006; HUANG *et al.*, 2011).

Remembering that two data sets were used, two proposals were made to execute the training and validation stages of the classifier.

For the first data set used, the total session of each subject was divided into two sets of training and validation. Thus, using the k-fold method, different sets of sessions were used each time the classifier was trained (each time a new feature was chosen) and validated. 70% of the session were used for training and the remaining for validation. The final value for the classification performance, when a new feature included, was obtained from the average calculated after the execution of this procedure 10 times.

In the second set of data, that is, the set of BCI competition IV, this type of division already described was only carried out in the training stage. To obtain the final classification response, the data from the second data session available for each subject was used.

The selection of these two types of classifiers occurred due to the exploration, of differences between which a linear and non-linear model can offer to the separation of classes, for the specific case of this problem, but also in general for the use in BCI systems. LDA is one of the most used strategies in BCI systems (LOTTE *et al.*, 2007), due to its simplicity and low computational cost (THEODORIDIS; KOUTROUMBAS., 2008). ELMs, on the other hand, are universal approximators, they can approximate any continuous function in a defined region. Added to the fact that they can classify any number of classes, this makes them very flexible classifiers that can adapt to a great variety of problems (LOTTE *et al.*, 2007).

The activation function chosen for the ELM classifer was the hyperbolic tangent. Since the parameters of the hidden layer are randomly generated, some of their configurations might result in classifiers that do not satisfy a desired performance criterion. To overcome this difficulty, it was decided to generate ten sets of random parameters, thus yielding ten ELMs, which form a machine committee, responsible for the final decision according to the majority of outputs. This approach, based on a frequentist perspective concerning the balance between bias and variance, reduces the chances that a single inefficient ELM negatively affects the overall performance (HUANG *et al.*, 2006).

4.7 Results and Discussion

In the following, the results concerning of mu and beta bands were analyzed separately. Within each frequency band, the following topics were analyzed: (1) implications of using either the LDA or the ELM classifier in the correntropy case, by comparing

their performances and looking for possible differences between them. This discussion is threefold, involving: the LDA results, the ELM findings and a comparison between them (subsections 'LDA', 'ELM' and 'LDA and ELM comparisons'); (2) comparisons amongst the correntropy and the other similarity methods for constructing the graphs, studying whether they affect the classification outcome (subsection 'Correntropy and correlation comparison'); (3) review of the most recurrent electrodes selected by the wrapper for each classifier, associating them with the hand MI response location (subsection 'Electrode sites').

This section is concluded with a discussion of the findings when these methods are applied to the BCI competition IV 2a dataset. This comparison allows the association of the results of the proposed methodology with state-of-the-art techniques in these area.

4.7.1 Mu band

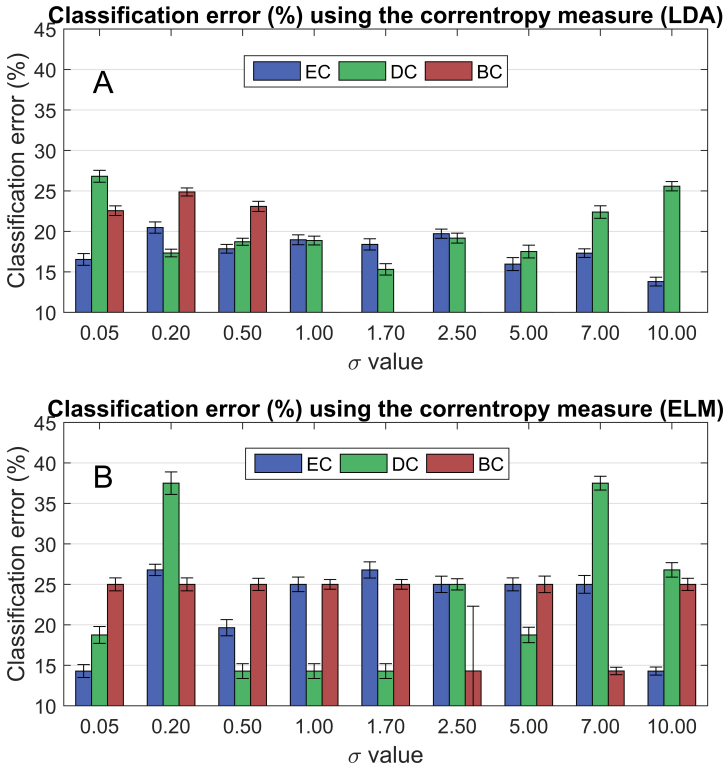

Figure 4.10 – Classification error for mu frequency band using the correntropy measure for building graph adjacency matrices. Each centrality measure is displayed as a distinct color: blue for EC, green for DC and red for BC.

LDA - Figure 4.10 shows the classification error using the correntropy measure according to its σ value, for each studied graph metric and classifier. From a specific σ onwards, BC yielded very sparse feature matrices, which were unfeasible for classification (Fig. 4.10A). Therefore, the bar representing BC is shown only when classification was possible. Even in these scenarios, however, BC did not provide the best performance.

Generally, either DC or EC performed better, depending on the value of σ. The smallest classification errors were reached for $\sigma = 1.70$ for the DC (around 15%), and for $\sigma = 10.00$, for the EC (around 13%).

ELM - For half the setups using the ELM (Figure 4.10B), DC was the metric that performed best. However, the same classification performance was achieved for EC for a σ of 0.05 and 10.00. Moreover, the ELM was able to map the data such that adequate classification was possible for BC, regardless of σ (differently from the LDA method, which could not cope with all classification scenarios for BC). Furthermore, BC was even the best for a few cases, such as $\sigma = 2.50$ and $\sigma = 7.00$.

LDA and ELM comparisons - For both classification methods, the resulting error was virtually insensitive to changes in σ within a specific range. For example, for BC in Figure 4.10A, for $\sigma \in \{0.50, 1.00, 2.50\}$. However, for some other ranges, there is a clear difference in classification performance that favored either one metric or another. For example, when using the LDA and ranging from $\sigma = 5.00$ to $\sigma = 10.00$, EC distinctly favors the classification scenario, whilst the contrary is true for DC (Fig. 4.10A).

Overall, there exists a variation in the classification results depending on the choice of the kernel size. Results for LDA seem to vary in a more strict range of values than for ELM. Moreover, regarding the classification error magnitude, both methods yielded similar results for the smallest errors, within the range of 10 to 15%. Nonetheless, the lowest error rates were observed more often for ELM, indicating that it is a more robust method for this problem. This is also supported by the fact that ELM was able to provide feasible classification scenarios for BC, regardless of σ, unlike the LDA approach.

Correntropy and correlation comparison - Figure 4.11 displays the classification error for each approach used for graph construction. All results were averaged across all subjects; however, for the correntropy, classification errors were taken as the ones corresponding to the optimum value of the kernel size for each subject, determined from the results of Figure 4.10. In this scenario, the correntropy method was the one that performed best for all cases, reaching error rates as low as 5% (see Figure 4.11B, DC feature). Finally, there is no noticeable preference for either of the correlation (Pearson and Spearman) methods, with both yielding similar performances.

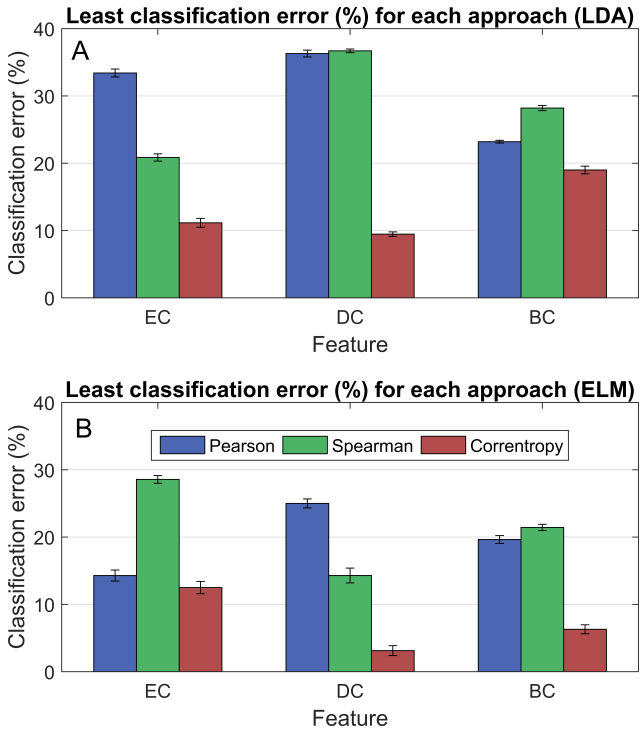

Figure 4.11 – Classification error when either Pearson (blue) or Spearman (green) correlation, or correntropy (red), were used to calculate the graphs' adjacency matrices for the LDA and ELM classifiers.

Electrode sites - Correntropy - Figure 4.12 shows scalp maps indicating the relative frequency with which each pair of electrodes was selected by the wrapper, across all subjects. Although relative frequencies were higher for LDA, this method also yielded a more spread pattern over the whole scalp, with a higher incidence of the electrode pairs C3/C4 and parietal areas. On the other hand, ELM was able to engender classification scenarios with comparable or better accuracy rates gathering a lower number of electrode pairs; besides, the recurrence pattern is not as marked as in the case of LDA and neither is consistent with areas commonly related to the hand MI task (SIVAKAMI; DEVI, 2015; HAUFE *et al.*, 2010; NEUPER *et al.*, 2005).

Finally, Figure 4.13 presents the contribution to feature selection for each type of graph methods with the LDA and ELM classifiers. This figure presents how feature selection was quite restricted to some specific electrodes in the ELM case, where there was not so much distribution and variety in the number of attributes chosen. This selection shows also some components that could be related to outliers of eye movement, when finding electrodes such as FP1 and FP2 selected.

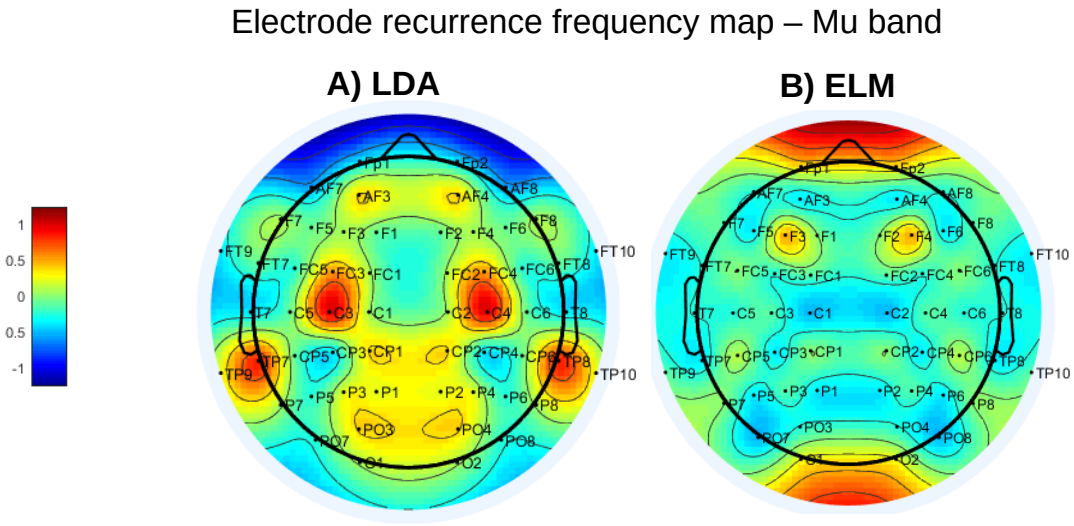

Figure 4.12 – Wrapper selected electrodes recurrence frequency map, accounted across all subjects. The magnitude of the colormap scale indicates a relative frequency.

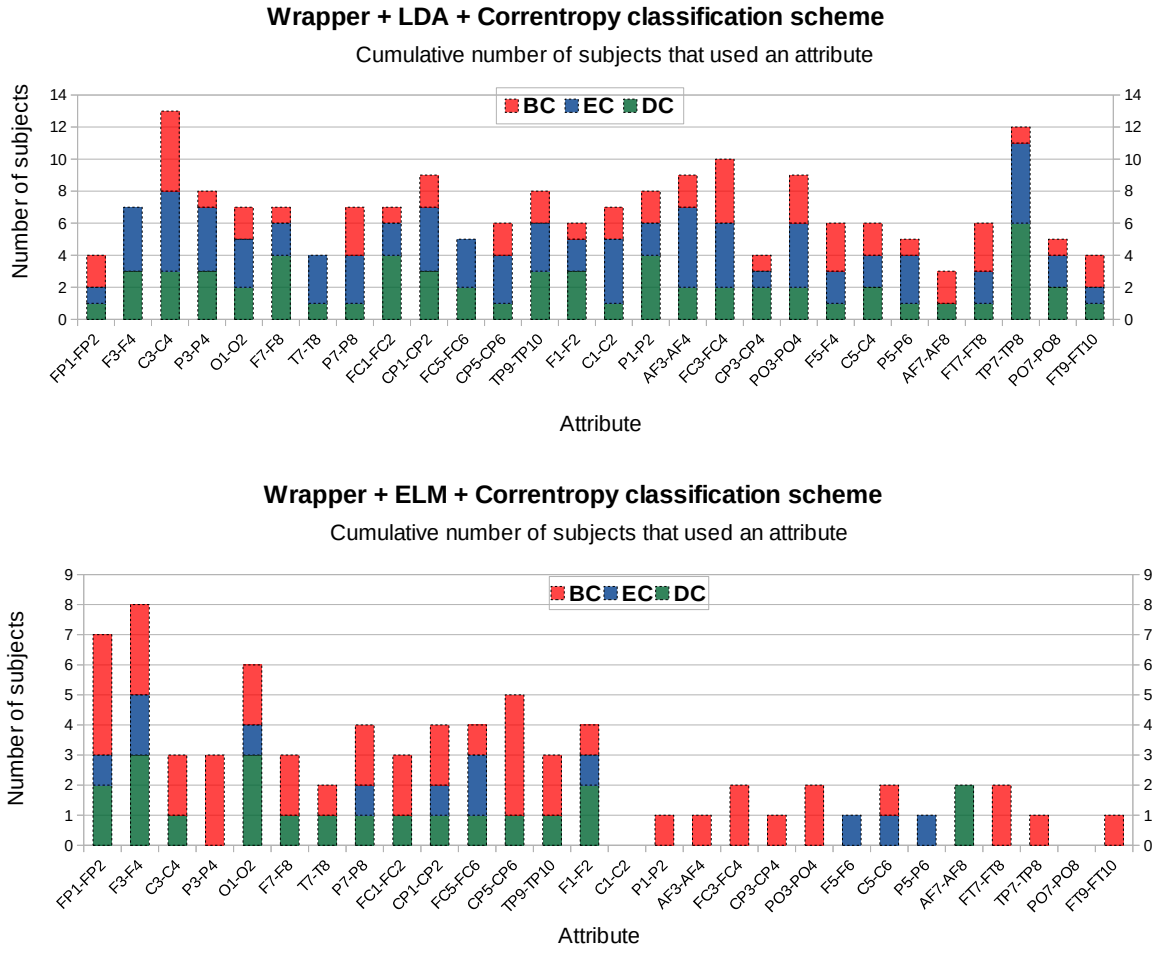

Figure 4.13 – Cumulative number of subjects that used each attribute for different combinations of wrapper selection + classifier + measure of centrality.

4.7.2 Beta band

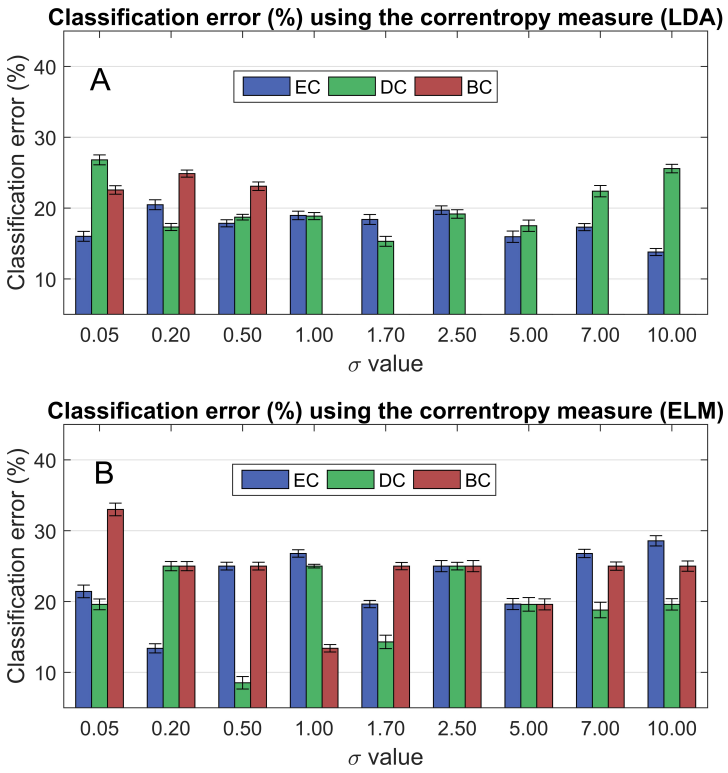

Figure 4.14 – Classification error for beta frequency band using the correntropy measure for building graphs adjacency matrices. Each centrality measure is displayed as a distinct color: blue for EC, green for DC and red for BC.

Figure 4.14 displays the classification error when using the correntropy for constructing the graph adjacency matrices for EEG beta frequency band.

LDA - Similarly to the mu band, BC also led to numerical computation problems and could not be obtained for tested σ values larger than 0.50 (Figure 4.14A). Moreover, either EC or DC could perform better depending on the σ choice, although the difference between them was very small for some cases (see, for example, $\sigma = 2.50$ and $\sigma = 5.00$). Overall, EC performed best, for $\sigma = 10.00$, yielding an average classification error slightly above 15% (yet still larger than the best result for the mu band; refer to Fig. 4.10A).

ELM - Again, the use of BC as a feature was possible with the ELM classifier (Figure 4.14B). In this case, classification performances were close to the values observed in the mu band condition, even though they did not necessarily occur for the same chosen features. Nevertheless, in general, classification errors for this method were larger in the beta band.

LDA and ELM comparisons - For some σ values, it is possible to identify scenarios where the LDA method performed better, such as for $\sigma = 0.05$ when using EC or BC. Nevertheless, no scenario for LDA was able to outperform the best ELM

result: using DC as a classification feature for $\sigma = 0.50$. This, together with the ELM's capability of always providing feasible classification scenarios for the BC usage, indicates its preference over the LDA method for the problem under consideration.

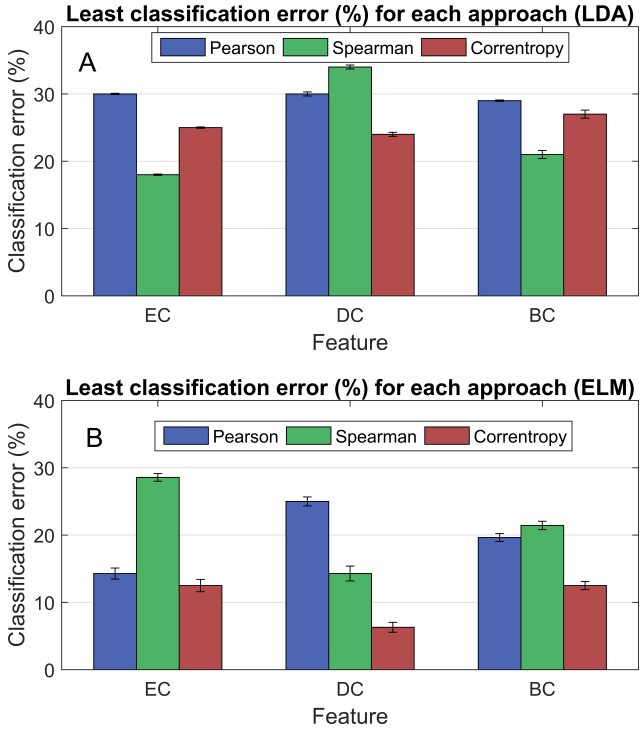

Figure 4.15 – Least classification error values for each one of the studied approaches and techniques for calculating the graphs adjacency matrices for the LDA and ELM classifiers.

Correntropy and correlation comparison - Figure 4.15 displays the smallest classification error for each approach. Overall, the correlation methods only provided the best classification scenario for the EC and DC features when using LDA, while correntropy performed best for all cases with the use of the ELM classifier (Figure 4.15B), and for the DC feature when using LDA (Figure 4.15A). Aditionally, classification errors were larger for this frequency band.

Electrode sites - Correntropy - For the best results in Figure 4.14 (that is, for $\sigma = 10.00$ using the DC feature for the LDA and for $\sigma = 0.20$ using EC for the ELM), we computed the most recurrent electrodes that were selected by the wrapper, across all subjects (Figure 4.16), which displayed maximum relative frequencies of about 30%. When comparing the electrode sites distribution over the scalp between the ELM and LDA approaches, findings are similar to the mu band: the overall pattern is more focused and specific in some area for the ELM usage.

Moreover, the comparison between both classifiers in this frequency shows that the recurrence pattern distribution suffers from the similar phenomenon of the extended inclusion of some new electrodes as significant. For the ELM method and beta band,

areas such as P3/P4, C3/C4 and the FC1/FC2, were more significant in relation to its equivalent case in the mu band. The electrode recurrence map for LDA included new electrodes, more spread over the scalp for the beta band than it was for the mu band, with the parietal area with important contributions, with the positions P3/P4, P5/P6 and P7/P8 being some of the most relevant ones.

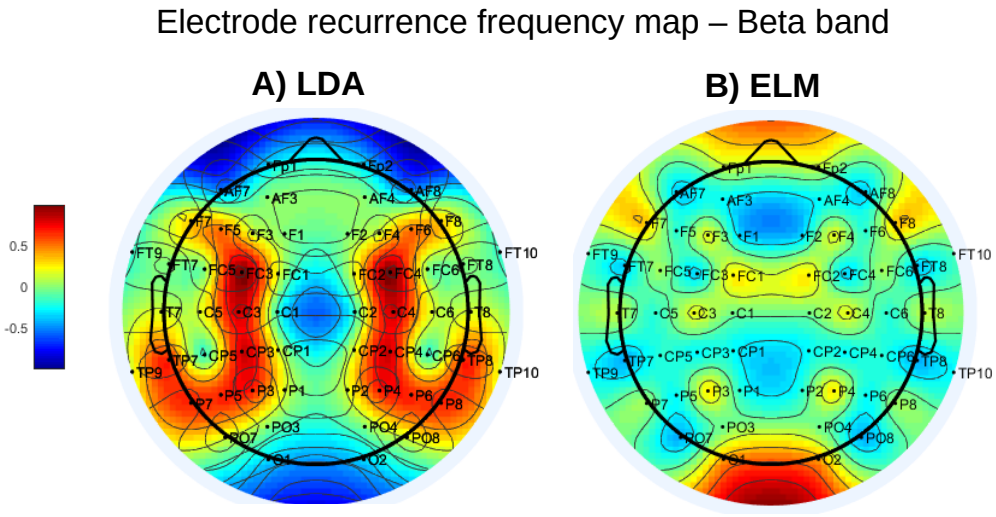

Figure 4.16 – Wrapper selected electrodes recurrence frequency map, accounted across all subjects. The magnitude of the colormap scale indicates a relative frequency.

To present the specific contribution in the selection of electrodes for the different techniques used, Figure 4.17 presents a comparison for the cases of ELM and LDA. One element to be considered in this figure is the appearance of more channels especially in the technique related to the use of ELM, where this time it is more marked the selection of the channels C3 / C4, which are highly associated with the motor imagination of left hand and right hand.

4.7.3 BCI Competition IV 2a database

The BCI competition IV dataset 2a was used to test how the response of our algorithm could compare to the results obtained by some of the state of the art methods. This database allows the separation of up to 4 classes of MI, with two sessions, recorded on different days, being available for each subject. As defined by the guidelines of the BCI competition, one of the available sessions should be used for training and, the other, for testing.

The performance measure (kappa index) associated with this database was also calculated. It represents a concordance coefficient in which the result is zero if the predicted value is the same as expected by chance, and 1, if the classification is perfect. Negative values suggest less than random concordance expectations (COHEN, 1960).

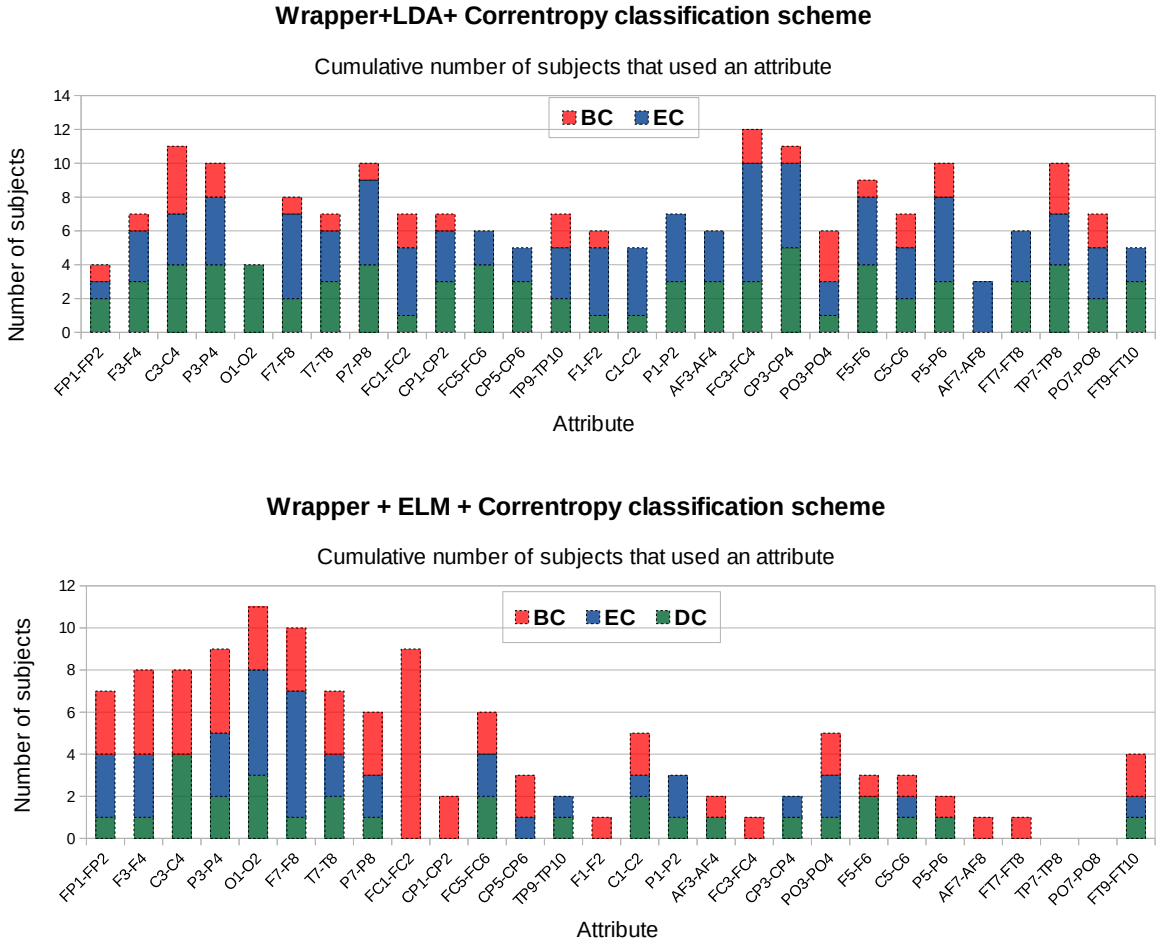

Figure 4.17 – Cumulative number of subjects that used each attribute for different combinations of wrapper selection + classifier + measure of centrality.

Table 4.3 presents the results of the first five places of the BCI competition set 2a and our correntropy method using LDA and ELM classifiers, as well as the three possible graph metrics as inputs.

The obtained performance was superior to that of the actual third place in this ranking. Regarding the graph metrics, EC and DC apparently better captured the importance of the graph nodes, at least if the MI class separability is considered. For the BC case, the worse results could indicate that the interpretation of a node's importance by information flow seems to not provide relevant features for distinguishing between the MI data classes. Moreover, the first three places in this ranking implemented modifications of classic algorithms, such as CSP; in this case, it is interesting to note how a connectivity measure (our proposal) can bring a different view to this type of problem. Even though our method could not reach the first place's kappa value, it is still promising, as it was able to yield better results that the third, fourth and fifth places. In the future, it its possible to study other graph metrics when constructing functional networks using the

Table 4.3 – Value of the kappa obtained by BCI Competition IV participants, including also the results here obtained using Correntropy with different graphs adjacency matrices for LDA and ELM

Sub	**1st place**	**2nd place**	**3rd place**	**4th place**	**5th place**	**Correntropy + LDA**			**Correntropy + ELM**		
						EC	**DC**	**BC**	**EC**	**DC**	**BC**
1	0.68	0.69	0.38	0.46	0.41	0.36	0.32	0.19	0.60	0.51	0.17
2	0.42	0.34	0.18	0.25	0.17	0.10	0.14	0.07	0.17	0.17	0.06
3	0.75	0.71	0.48	0.65	0.39	0.31	0.31	0.15	0.58	0.61	0.28
4	0.48	0.44	0.33	0.31	0.25	0.23	0.22	0.10	0.33	0.26	0.08
5	0,40	0,16	0,07	0,12	0,06	0,11	0,08	0,07	0,10	0,10	0,08
6	0,27	0,21	0,14	0,07	0,16	0,09	0,08	0,07	0,19	0,20	0,14
7	0,77	0,66	0,29	0,00	0,34	0,23	0,19	0,13	0,31	0,24	0,10
8	0,75	0,73	0,49	0,46	0,45	0,26	0,25	0,12	0,59	0,61	0,24
9	0,61	0,69	0,44	0,42	0,37	0,44	0,38	0,24	0,61	0,54	0,21
mean	**0,57**	**0,52**	**0,31**	**0,30**	**0,29**	**0,24**	**0,22**	**0,13**	**0,39**	**0,36**	**0,15**

correntropy, to investigate whether our results could improve and achieve the first place's performance.

4.8 Conclusion

In the work presented in this chapter, the use of correntropy as a measure (instead of classical correlation) to build graphs for studying FC in MI-BCIs was investigated. This investigation included two types of classification strategies - LDA and ELMs - and three graph metrics: DC, BC and EC. Our results included a number of representative combinations for distinct scenarios, using both the mu and beta EEG bands.

In summary, it was observed that the classification performance was slightly better for the mu band. Also, the ELM proved to be more adequate to the problem at hand, since it was able to perform the classification task for all σ values, even when the BC was used as a metric. Furthermore, for this classifier, a smaller number of features was necessary to achieve the same classification rates, as indicated by more concentrated patterns of the scalp maps, a result that occurred for both frequency bands. This finding suggests a better adaptability of this type of classifier over the linear approach, even though the classification error rates were similar in a few situations.

The fact that the use of correntropy led to better classification scenarios suggests that it was able to extract relevant higher-order statistical information from the electrode time series that could not be obtained by using either Pearson or Spearman correlations. Although the Spearman method could also, like the correntropy, gather information re-

garding the signal non-linearities, it was not part of the best classification scenarios, and its outcomes were even worse than those derived from Pearson correlation at specific situations (Figures 4.11 and 4.15).

For the most favorable scenarios for each subject, average classification errors across all subjects as low as 5% could be obtained. This indicates that correntropy is a very promising solution for generating adjacency matrices and their corresponding features for a MI-BCI. Correntropy could be used, for example, as an alternative or complementary tool with respect to the more traditional frequency domain analysis. However, for an online application, a training stage for optimizing σ and selecting the appropriate features for each subject would be necessary. Its optimization would give robustness to each subject's algorithm; however, its in-depth exploration is beyond the scope of this thesis. Instead, we restricted our work to test a few discrete σ values.

Finally, the comparison with the results obtained when using the BCI competition IV 2a database confirmed the use of the correntropy with an ELM classifier as the best option among the proposed algorithms.

5 Classification model based on Bayesian discrimination for a P300 speller with xDAWN algorithm

5.1 Introduction

There are basically two different methods to acquire conscious brain activity for users of a BCI system. In the first method, subjects perceive a set of stimuli displayed by the BCI system and can control their brain activity by focusing onto one specific stimulus. The changes in neurophysiologic signals resulting from perception and processing of stimuli are event-related potentials (ERPs). In the second method, users control their brain activity by concentrating on a specific mental task. For example, imagination of hand movement can be used to modify activity in the motor cortex. The following contribution will use one of the natural automatic responses of the brain to external stimuli, known as P300 response. This ERP is widely used as the basis of a paradigm of BCI systems, for their desirable properties as a typical application that gives stability to control several commands for a BCI.

Figure 5.1 shows the representation of some ERP responses. As defined in Chapter 1, the ERPs are associated with experiences that usually involve the presentation of several kinds of stimuli, under the assumption that there exists a typical spatio-temporal pattern which is time-locked to each kind of stimuli (also called events) (RIVET; SOULOUMIAC, 2013). ERPs can be categorized into two types (LI *et al.*, 2011).

- Exogenous potentials, corresponding to non-cognitive activity. They appear after luminous flash, a noise or a sudden action. Their location on the cortex depends on the type of stimulation. For example, a visual stimulation causes a decrease of electrical potential 100 ms after the stimulation (N100 response) in the occipital area.

- Endogenous potential corresponding to cognitive activity. For example, a subject is asked to differentiate two visual stimulations X and O. X is less common than the O. The patient has to count the number of appearing X. At each X, an endogenous ERP appears 300 ms after the stimulation on central and parietal area (P300 response).

The P300 wave is an ERP elicited by a salient or attended stimulus (KINDERMANS *et al.*, 2012) . It is a positive deflection which is typically detectable in the EEG

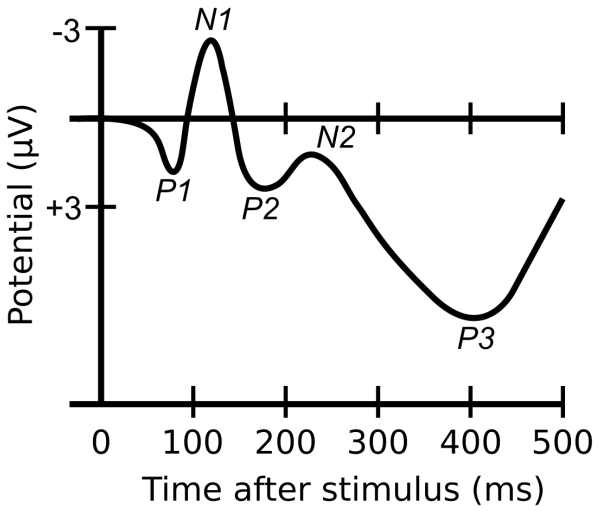

Figure 5.1 – A waveform showing several ERP components, including the N100 (labeled N1) and P300 (labeled P3). Note that the ERP is plotted with negative voltages upward, a common, but not universal, practice in ERP research.

measured near the parietal lobe, around 300 ms after the occurrence of the unexpected stimulus. Usually, to evoke the P300 response, subjects are asked to observe a random sequence of two types of stimuli. One stimulus type (the oddball or target stimulus) appears only rarely in the sequence, while the other stimulus type (the normal or non-target stimulus) appears more often. Whenever the target stimulus appears, a P300 can be observed in the EEG signal. This principle was exploited by Farwell and Donchin in a BCI system which allowed spelling words by sequentially selecting symbols from a matrix of symbols (FARWELL; DONCHIN, 1988).

5.1.1 The P300 Spelling Paradigm

The P300 speller was presented by Farwell et al. (FARWELL; DONCHIN, 1988) as an application of a BCI paradigm. This system allows a subject to spell words by looking at a desired character in a matrix shown on screen, thus enabling paralyzed patients to communicate with the outside world. A $6X6$ matrix that includes all the alphabet letters, as well as other symbols, was presented to the user on a computer screen. The subject had to focus on the symbol that he/she wanted to spell. The rows and columns of the grid are highlighted in random order. When the desired character is highlighted, the subject sees an unexpected stimulus and a P300 wave is generated. By correlating the detection of the P300 wave and the (known) sequence of row/column highlights, the character which the user has focused on can be inferred.

For a subject in the P300 experiment, the task includes an attentional focus enhanced by mental counting of the number of times that the row and the column containing

the symbol of interest were intensified. In a classical training or testing session, a single trial is defined as one of the random intensifications of each of the 6 rows and the 6 columns of the spelling matrix, hence, several repeated highlightings (12) occur in a sequence to complete an epoch. To build an accurate speller, it is necessary to use several epochs associated with the same character. Figure 5.2 presents the experimental paradigm used in the P300 speller, where the sequence of stimuli is shown in each of the epochs that divide the data capture for a letter as a symbol of interest.

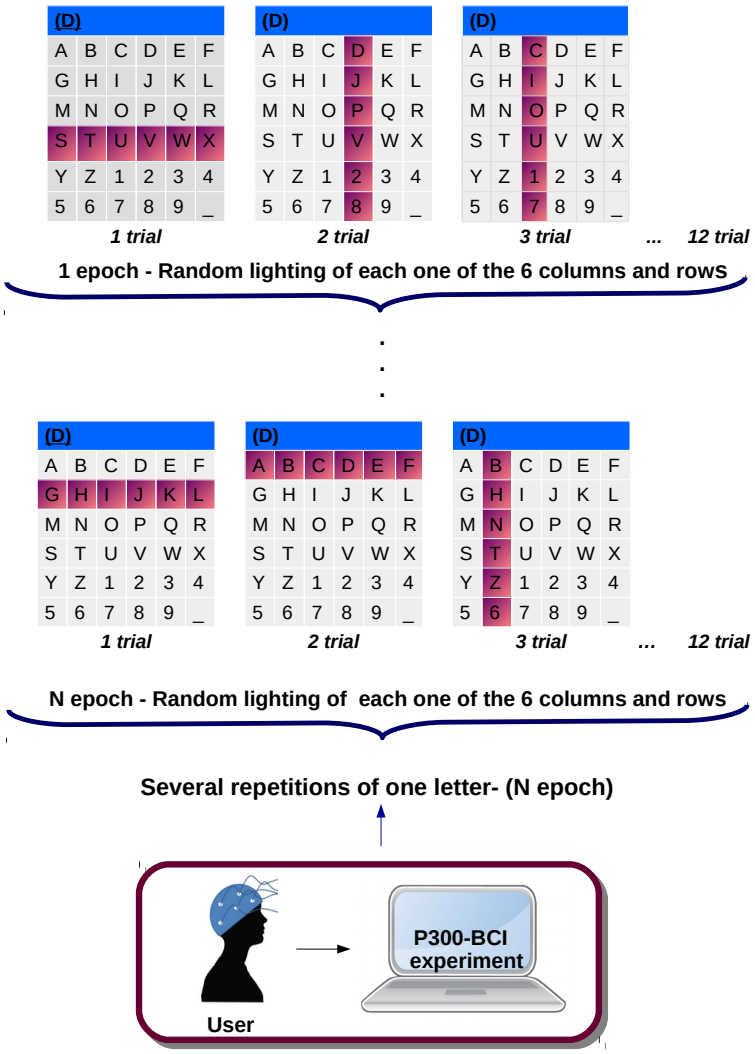

Figure 5.2 – Experimental paradigm used in the P300 speller.

Actually, the presence of some intrinsic and extrinsic phenomena such as attention, subject fatigue, electrode impedance, amplifier noise, and environmental noise lead to a very low signal-to-noise ratio (SNR) for P300 potential (LOTTE *et al.*, 2007). For that reason, the identification of a single trial may not be enough to give a reliable response of the character that the subject wants to select.

5.1.2 Signal processing on P300 speller

For the P300 speller, the number of repetitions (epochs) used to classify the detection of the P300 wave is an important characteristic. In this manner, the effective spelling rate and, by extension, the usability of the system are determined by this feature.

Several signal processing strategies have been considered for this problem, defining the necessary repetitions given for a high prediction accuracy. The most desirable would be to have the best classification performance, but, nevertheless, if this is achieved after many repetitions, the system would lose its facility of use.

Therefore, in the literature, some strategies for signal processing in the P300 speller were focused specifically on the classification stage, looking for the improvement and the adaptability of the classifier and the features used. It was a widely adopted strategy to include the time point features of the concatenation of EEG samples from all the channels or from those, where is expected the response of P300, to construct the feature vector. The size of this vector can be really large considering the different preprocessing methods used, the number of samples used, among other factors. Due to the complexity that can be found in the feature vector, the specificity of the classifier could be reflected in an increase of the number of classifiers, and in the structure used for their collaboration (KINDERMANS *et al.*, 2012), (BASHASHATI *et al.*, 2007). In general, linear classifiers, such as SVM or LDA, have been shown to solve this classification problem (RAKOTOMAMONJY; GUIGUE, 2008), but also the use of variations of these classifiers with regularization parameters has given considerably good results, as is the case of Bayesian linear discriminant analysis (BLDA) (MANYAKOV *et al.*, 2011).

In addition to the methods focused on classification, another approach to improve the symbol prediction accuracy is to enhance the P300 evoked potentials by spatial filtering of the channels. The use of spatial filters for automatically estimating the P300 subspace from raw EEG signals has already been proven relevant in previous contributions such as the xDAWN filter (RIVET; SOULOUMIAC, 2013). This filter estimates the jointly temporal signature and spatial distribution of the ERPs, as well as the spatial filters that provide the largest SNR, based only on the prior knowledge of the onsets of the stimuli used in the experiment, and without assumptions either on the temporal waveform or in the spatial distribution of the signal.

An advantage of using xDAWN as a spatial filter is its robustness in comparison with classical methods, such as ICA. The tests done with real EEG data confirm the good behavior of the xDAWN framework in the context of a P300 speller brain–computer interface (CECOTTI *et al.*, 2010). It should be understood that in the case of the use of this filter in the problem of the P300 speller, the classification is associated mainly to the separation of two classes, being one associated with all the P300 stimuli (ERP signal)

and the the other with responses to non-target stimuli. In (BARACHANT; CONGEDO, 2014), a proposal was made for a comparison using xDAWN, Stepwise Linear Discriminant Analysis (SWLDA) and a new proposal based on an information geometry framework, through a new estimation of covariance matrices. As compared to the state-of-the-art methods, this new strategy obtained a superior performance, reducing the number of data needed for the calibration with a good generalization across session and subjects.

5.1.3 Analysis of the performance of P300 speller and xDAWN algorithm

According to some reports studied in the literature, the problem of classification of the P300 response for the specific application of the P300 speller has been the object of important results through the years. As it is known, the problem of BCI addresses several types of approaches because of its variability. In the case of a speller, this variability has been worked upon with focus on the subject's response to the problem. However, it has not been analyzed how the structure of the speller could also define characteristics that can bring improvements in performance.

In order to analyze the actual effectiveness of classification on the $P300$ speller problem, the total value of classification could be associated directly with the 6x6 matrix where a character is being discriminated. By identifying a column and a row, two different classifications are made, where it is known beforehand that only a single row and a column must be associated with the P300 stimulus classes. Considering these ideas, it is proposed to directly model the total classification of the speller adopting a Bayesian linear classification model, where the classification of row and column will be considered separately. This means that the structure of rows and columns of the matrix will be taken into account. Besides, the idea behind this proposal is that the results of this model will serve as an estimation of the accuracy for the previously obtained classification performance with different number of repetitions.

The work that will be described in the next sections aims to apply the spatial-temporal filtering methodology of the spatial filter xDAWN to improve brain signal quality in P300-type BCIs, specifically in their union towards a classification model for a P300 speller. The starting point for this development will be the work that Prof. Bertrand Rivet has been developing on the subject (RIVET; SOULOUMIAC, 2013): this interest arose due to a collaboration developed through a period of internship carried out in 2017, in the laboratory GIPSA-Lab in Grenoble, France.

5.2 Proposal

To perform the proposed analysis of the P300 speller system using the xDAWN filter for the subsequent study of the total classification model, the proposed analysis will

be executed using a database, provided by Professor Bertrand Rivet. In this database, the spelled symbols are known as well as the order of rows/columns intensifications and the corresponding stimulus onsets (i.e. beginning time of illumination). To proceed the study the next steps were taken:

- Presentation of xDAWN filter (RIVET; SOULOUMIAC, 2013).
- Study and construction of the total classification model based on Bayesian discrimination for the P300 speller.
- Study of the possibility of optimizing the estimated values of the xDAWN filter and the classifier using the total classification model obtained in the last step.
- Analysis of comparison results of the values obtained for the total classification model studied.

According to the proposed work, to execute the performance analysis of the P300 speller and xDAWN algorithm to obtain a total classification model based on Bayesian discrimination, two stages will define the practical application of signal processing. Figure 5.3 shows, in general lines, some of the blocks used for signal processing in the training and testing stages. The idea behind this is to obtain two final performance classification results, one of theoretical prediction (training phase), and another calculated with validation data (testing phase). These results will be compared in order that their relationship be verified, as well as how they can be affected in a posterior optimization step.

5.3 xDAWN spatial filter

5.3.1 Model

The model of the EEG signals related to the ERP response studied in the problem of the P300 speller will be detailed in this section using the hypothesis of the original work of (RIVET; SOULOUMIAC, 2013). All the mathematical expression described in this Subsection come from this work. These concepts will be useful for our proposal based in the use of this filter.

It is assumed that there exists a typical spatio-temporal time-locked pattern associated with the stimuli, e.g., the P300 or non P300 response. Then, the signals $\mathbf{x}(k) \epsilon \mathbb{R}^{N_s}$ represent the signals recorded at the k instant from N_s sensors that can be modeled as the superposition of the N_e signals related to each of the N_e classes of events (i.e. kind of stimulations) plus the ongoing brain activity related to ocular and/or muscular artifacts $\mathbf{n}(k) \epsilon \mathbb{R}^{N_s}$.

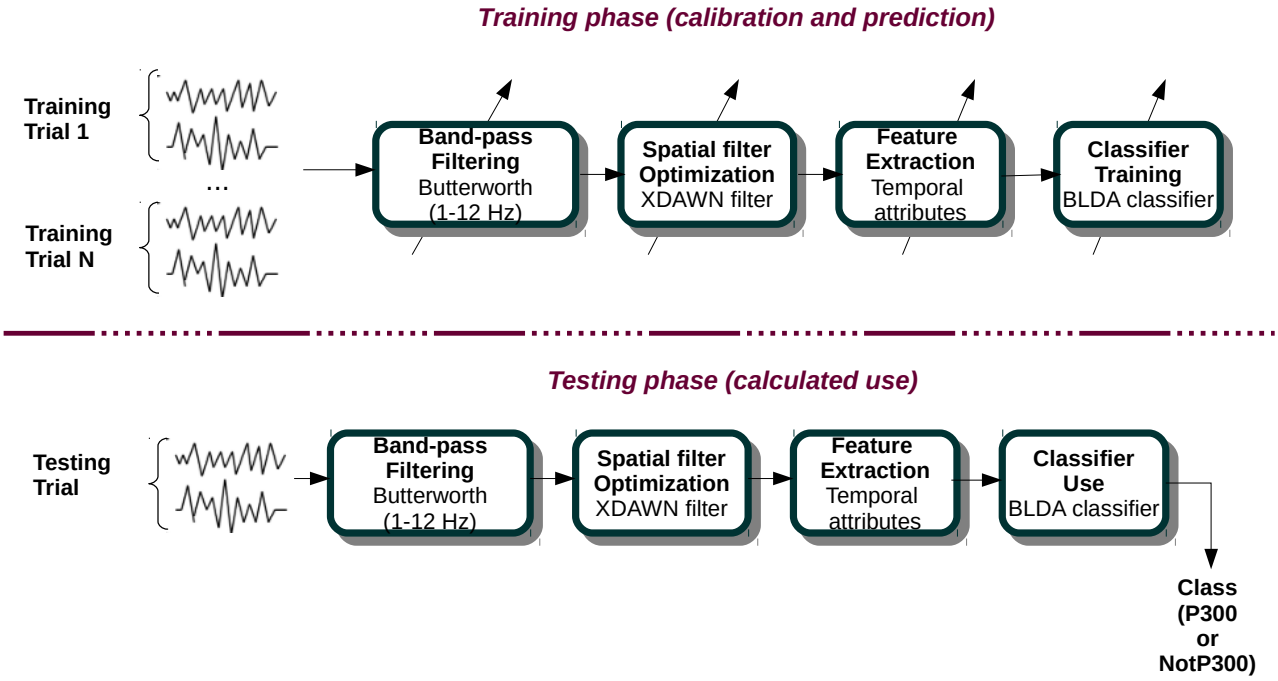

Figure 5.3 – Configuration used for the training and testing phases for P300 speller proposal.

If consider two classes for recognize the ERP responses studied, P300 and the absence of P300. It is necessary to take into account the variability of each ERP in a particular class that can appear during the experiment. For each time that a stimuli is pointed in the P300 speller, would be consider a new ERP response, that have to be included in the total response of one of the mentioned classes.

Thus, the j-th ERP of the i-th class is denoted as $\mathbf{p}_{ij}(k) \; \epsilon \; \mathbb{R}^{N_s}$. This spatio-temporal pattern is composed of $\mathbf{p}_i^{(c)}(k) \; \epsilon \; \mathbb{R}^{Ns}$, common to all ERPs of the i-th class and a random spatio-temporal pattern $\mathbf{p}_{ij}^{(r)}(k) \; \epsilon \; \mathbb{R}^{N_s}$ that is different for all the ERPs of the i-th class: $\mathbf{p}_{ij}(k) = \mathbf{p}_i^{(c)}(k) + \mathbf{p}_{ij}^{(r)}(k)$

The raw EEG $\mathbf{x}(\mathbf{k})$ can be modeled as:

$$\mathbf{x}(k) = \sum_{i=1}^{N_e} \sum_{j=1}^{K_i} \mathbf{p}_{ij}(k - \tau_i(j)) + \mathbf{n}(k), \tag{5.1}$$

where $\tau_i(j)$ is the index time of the j-th stimulus of the i-th ERP class and K_i is the number of stimuli of the i-th ERP class. The convolutional model 5.1 can be expressed in matrix notation as:

$$\mathbf{X} = \sum_{i=1}^{N_e} \sum_{j=1}^{K_i} \mathbf{D_{ij}} \mathbf{P_{ij}} + \mathbf{N}, \tag{5.2}$$

where the k-th row of $\mathbf{X} \epsilon \mathbb{R}^{N_t \times N_s}$ is $\mathbf{x}(k)^T$ and N_t is the total number of time samples. $\mathbf{P_{ij}} \epsilon \mathbb{R}^{M_i \times N_s}$ is the j-th ERP spatio-temporal pattern of the i-th class of stimuli whose k-th row is $\mathbf{p}_{ij}^T$. $\mathbf{D_{ij}} \epsilon \mathbb{R}^{N_t \times M_i}$ is a Toeplitz matrix whose first column entries are null but $\mathbf{D_{ij}}(\tau_i(j), 1) = 1$, M_i is the number of time samples of the temporal pattern of the i-th class of ERPs. This matrix contains the time signature, that is expressed in the number of positions that have value equal to 1, indicating where the stimulus is begin.

In (5.2), $\sum_j \mathbf{D_{ij}}\mathbf{P_{ij}}$ models the signals related to the i-th class of events. Since $\mathbf{P_{ij}}$ is often a singular matrix (i.e. of reduced rank), spatio-temporal patterns can be factorized as $\mathbf{P_{ij}} = \mathbf{A_{ij}}\mathbf{W}_{ij}^T$, where $\mathbf{A_{ij}} \epsilon \mathbb{R}^{M_i \times N_{s_i}}$ is the temporal pattern of reduced dimensions and $\mathbf{W_{ij}} \epsilon \mathbb{R}^{N_s \times N_{s_i}}$ is its spatial distribution over sensors, with $N_{s_i} < N_s$.

In this model (RIVET; SOULOUMIAC, 2013) is considered that each ERPs have a strong temporal signature that differenciates the spatio-temporal patterns $\mathbf{P_{ij}}$ for each class.

$$\mathbf{P_{ij}} = (\mathbf{A_i}^{(c)} + \mathbf{A_{ij}}^{(r)})\mathbf{W}_i^T \tag{5.3}$$

where $\mathbf{A_i^{(c)}} \epsilon \mathbb{R}^{M_i \times Ns_i}$ denotes the common temporal pattern and $\mathbf{A_{ij}}^{(r)} \epsilon \mathbb{R}^{M_i \times Ns_i}$ models the random temporal pattern. The model (5.2) can be expressed as:

$$\mathbf{X} = \sum_{i=1}^{N_e} (\mathbf{D_i}^{(c)}\mathbf{A_i}^{(c)} + \mathbf{D_i}^{(r)}\mathbf{A_i}^{(r)})\mathbf{W}_i^T + \mathbf{N} \tag{5.4}$$

where $\mathbf{D_i}^{(c)} = \sum_{j=1}^{K_i} \mathbf{D_{ij}}$, $\mathbf{D_i^{(r)}} = [\mathbf{D_{i,1}}, ..., \mathbf{D_{i,K_i}}]$ and $\mathbf{A_i}^{(r)} = \left[\mathbf{A_{i,1}}^{(r)^T}, ..., \mathbf{A_{i,K_i}}^{(r)^T}\right]^T \in \mathbb{R}^{(M_i K_i) \times Ns_i}$ are white centered Gaussian random variables. For ERP analysis the interest is related to the common (averaged) temporal patterns $\mathbf{A_i^{(c)}}$, that represent the common signature of an ERP for a class, e.g., the P300 response class.

5.3.2 xDAWN framework

The estimation of the N_{f_i} spatial filters for xDAWN framework, $\mathbf{U_i} \in \mathbb{R}^{N_s \times N_{f_i}}$, is based on the maximization of the SNR. The expression is

$$\widetilde{\mathbf{U}}_i = arg \max_U \widetilde{\rho}_i(\mathbf{U}) \tag{5.5}$$

The SNR is defined by

$$\widetilde{\rho}_i(\mathbf{U}) = \frac{Tr(\mathbf{U}^T \widetilde{\mathbf{\Sigma}}_\mathbf{i} \mathbf{U})}{Tr(\mathbf{U}^T \widetilde{\mathbf{\Sigma}}_\mathbf{X} \mathbf{U})} \tag{5.6}$$

with the estimation of the covariance of the signal $\mathbf{X}$ in Eq.(5.7), and the estimation of the covariance of the common temporal pattern defined by the Eq.(5.8).

$$\widetilde{\mathbf{\Sigma}}_{\mathbf{X}} \frac{E[\mathbf{X}^T\mathbf{X}]}{N_t} \tag{5.7}$$

$$\widetilde{\mathbf{\Sigma}}_{\mathbf{i}} = \frac{E[\mathbf{P_i^{(c)^T}} \mathbf{D_i^{(c)^T}} \mathbf{D_i^{(c)}} \mathbf{P_i^{(c)}}]}{N_t} \tag{5.8}$$

where $\mathbf{P_i}^{(c)} = \mathbf{A_i^{(c)}} \mathbf{W_i^T}$. In practice since neither the actual spatio-temporal patterns $\mathbf{P_i^{(c)}}$ and nor the actual durations of these patterns M_i are known, xDAWN algorithm maximizes the estimated SNR $\widehat{\rho}_i(\mathbf{U})$:

$$\widehat{\mathbf{U}}_{\mathbf{i}} = arg \max_{U} \widehat{\rho}_i(\mathbf{U}) \tag{5.9}$$

with

$$\widehat{\rho}_i(\mathbf{U}) = \frac{Tr(\mathbf{U^T} \widehat{\mathbf{\Sigma}}_{\mathbf{i}} \mathbf{U})}{Tr(\mathbf{U^T} \widehat{\mathbf{\Sigma}}_{\mathbf{X}} \mathbf{U})} \tag{5.10}$$

The expectations in 5.7 and 5.8 are replaced by their stochastic estimates

$$\widehat{\mathbf{\Sigma}}_{\mathbf{X}} = \frac{\mathbf{X^T X}}{N_t} \tag{5.11}$$

$$\widehat{\mathbf{\Sigma}}_{\mathbf{i}} = \frac{\widehat{\mathbf{P}}_{\mathbf{i}}^{\mathbf{(c)^T}} \widehat{\mathbf{D}}_{\mathbf{i}}^{\mathbf{(c)^T}} \widehat{\mathbf{D}}_{\mathbf{i}}^{\mathbf{(c)}} \widehat{\mathbf{P}}_{\mathbf{i}}^{\mathbf{(c)}}}{N_t} \tag{5.12}$$

The expressions $\widehat{\mathbf{D}}_{\mathbf{i}}^{\mathbf{(c)}}$ and $\widehat{\mathbf{P}}_{\mathbf{i}}^{\mathbf{(c)}}$ are estimates of these actual values. $\widehat{\mathbf{D}}_{\mathbf{i}}^{\mathbf{(c)}}$ is a Toeplitz matrix defined from the set of stimuli onsets $\tau_i(j)$ and the estimated durations of the ERP $\widehat{M}_i$. $\widehat{\mathbf{P}}_{\mathbf{i}}^{\mathbf{(c)}}$ is estimated in the least mean square (LMS) sense by

$$\widehat{\mathbf{P}}^{\mathbf{(c)}} \triangleq arg \min_{P} \|\mathbf{X} - \widehat{\mathbf{D}}^{\mathbf{(c)}} \mathbf{P}\|_F^2 = \left(\widehat{\mathbf{D}}^{\mathbf{(c)^T}} \widehat{\mathbf{D}}^{\mathbf{(c)}}\right)^{-1} \widehat{\mathbf{D}}^{\mathbf{(c)^T}} \mathbf{X} \tag{5.13}$$

where $\widehat{\mathbf{D}}^{\mathbf{(c)}} = [\widehat{\mathbf{D}}_{\mathbf{1}}^{\mathbf{(c)}}, ..., \widehat{\mathbf{D}}_{\mathbf{N_e}}^{\mathbf{(c)}}]$ and $\widehat{\mathbf{P}}^{\mathbf{(c)}} = \left[\widehat{\mathbf{P}}_{\mathbf{1}}^{\mathbf{(c)^T}}, ..., \widehat{\mathbf{P}}_{\mathbf{N_e}}^{\mathbf{(c)^T}}\right]^{\mathbf{T}}$. Consequently,

$$\widehat{\mathbf{P}}_{\mathbf{i}}^{\mathbf{(c)}} = \widehat{\mathbf{B}}_{\mathbf{i}}^{\mathbf{T}} \mathbf{X} \tag{5.14}$$

with $\widehat{\mathbf{B}}_{\mathbf{i}}^{\mathbf{T}}$ the matrix of corresponding rows in $(\widehat{\mathbf{D}}^{\mathbf{(c)^T}} \widehat{\mathbf{D}}^{\mathbf{(c)}})^{-\mathbf{1}} \widehat{\mathbf{D}}^{\mathbf{(c)^T}}$. Because the decomposition $(\mathbf{A_i^{(c)}}, \mathbf{W_i})$ of the spatio-temporal pattern $\mathbf{P_i^{(c)}}$ is associated to the spatial filters which maximize the SNR, it is possible to use the generalized eigenvalue decomposition (GEVD) (GOLUB; LOAN, 1996) of the pair $(\widehat{\mathbf{\Sigma}}_{\mathbf{i}}, \widehat{\mathbf{\Sigma}}_{\mathbf{X}})$ by: $\widehat{\mathbf{\Sigma}}_{\mathbf{i}} \mathbf{\Theta_i} = \widehat{\mathbf{\Sigma}}_{\mathbf{X}} \mathbf{\Theta_i} \mathbf{\Lambda_i}$.

Where $\mathbf{\Lambda_i}$ is the diagonal matrix of the eigenvalues sorted in the descending order $\lambda_i^{(i)} > ... > \lambda_{N_s}^{(i)}$ and related eigenvectors $\Theta_i = [\theta_{\mathbf{1}}^{(\mathbf{i})}, ..., \theta_{\mathbf{N_s}}^{(\mathbf{i})}]$ with $\Theta_i^T \widehat{\mathbf{\Sigma_X}} \Theta_i = \mathbf{I}$; where $\mathbf{I}$ is the identity matrix. The N_f spatial filters $\widehat{\mathbf{U}}_\mathbf{i}$ which satisfy (5.9) are given through the GEVD of the pair $(\widehat{\mathbf{\Sigma}}_\mathbf{i}, \widehat{\mathbf{\Sigma_X}})$ by the N_f eigenvectors associated with the N_f largest eigenvalues (RIVET; SOULOUMIAC, 2013): $\widehat{U}_i = \left[\theta_1^{(i)}, ..., \theta_{N_f}^{(i)}\right]$

The spatial distribution will be defined by

$$\widehat{\mathbf{W}}_\mathbf{i} = \widehat{\mathbf{\Sigma}}_\mathbf{X} \left[\theta_1^{(i)}, ..., \theta_{N_f}^{(i)}\right] \tag{5.15}$$

The temporal pattern is obtained from

$$\widehat{\mathbf{A}}_\mathbf{i}^{(\mathbf{c})} = \widehat{\mathbf{B}}_\mathbf{i}^\mathbf{T} \mathbf{X} \left[\theta_1^{(i)}, ..., \theta_{N_f}^{(i)}\right] \tag{5.16}$$

Finally, the enhanced signals are given by

$$\widehat{\mathbf{F}}_\mathbf{i} = \mathbf{X}\widehat{U}_i \tag{5.17}$$

The GEVD of the pair of (spatial) covariance matrices $(\widehat{\mathbf{\Sigma}}_\mathbf{i}, \widehat{\mathbf{\Sigma}}_\mathbf{X})$ allows to estimate the spatial pattern $\widehat{\mathbf{W}}_\mathbf{i}$ but also the temporal pattern $\widehat{\mathbf{A}}_\mathbf{i}^{(\mathbf{c})}$. The matrix $\widehat{\mathbf{\Sigma}}_\mathbf{i}$ not only summarizes the spatial information about the ERP, but also all temporal model information about the shape of ERPs.

Algorithm 1 (RIVET; SOULOUMIAC, 2013)

1. Compute matrices $\widehat{\mathbf{B}}_\mathbf{i}^\mathbf{T}$ (5.14), $\widehat{\mathbf{\Sigma}}_\mathbf{X}$ (5.11) and $\widehat{\mathbf{\Sigma}}_\mathbf{i}$ (5.12)
2. Compute GEVD of $(\widehat{\mathbf{\Sigma}}_\mathbf{i}, \widehat{\mathbf{\Sigma}}_\mathbf{X}) \Rightarrow (\mathbf{\Lambda_i}, \Theta_i)$
3. Select the N_{f_i} largest generalized eigenvalues $\Lambda_i^{(s)}$
4. Estimate enhanced signals (5.17): $\widehat{\mathbf{F}}_\mathbf{i} = \mathbf{X}\widehat{U}_i$
5. Finally $(\widehat{\mathbf{U}}_\mathbf{i}, \widehat{\mathbf{A}}_\mathbf{i}^{(\mathbf{c})}, \widehat{\mathbf{W}}_\mathbf{i}) = (\Theta_i^{(s)}, \widehat{\mathbf{B}}_\mathbf{i}^\mathbf{T} \mathbf{X} \Theta_i^{(s)}, \widehat{\mathbf{\Sigma}}_\mathbf{X} \Theta_i^{(s)})$

5.4 Study and construction of the total classification model based on Bayesian discrimination for a P300 speller

5.4.1 Experimental basis and setup of the P300 speller

First, to consider the classification problem in a P300 speller, it is necessary to remember that the oddball paradigms are used in BCI to generate event-related potentials

(ERPs), like the P300 wave, on targets selected by a user (FARWELL; DONCHIN, 1988). A $6X6$ matrix containing all the available characters is presented to the user on a computer screen. To spell a character, the user has to focus on the character s/he wants to spell. When the user focuses on a cell of the matrix, it is possible to detect a P300 after the cell has been intensified.

On a general experimental setup for a training phase to generate ERPs, the row and columns are randomly intensified. Row/column intensifications are randomized in blocks of 12 (6 rows and 6 columns). The sets of 12 intensifications is repeated N_{epoch} times for each character. Therefore, $2N_{epoch}$ possible P300 responses should be detected for the recognition of one character.

After obtaining the EEG data, the classification problem of the P300 speller could be decomposed in two steps:

- The first classification step is to detect the presence of a P300 in the electroencephalogram (EEG).
- The second one corresponds to the combination of a minimum of two P300 responses for determining the right character to spell (one row and one column).

Generally, these two steps are sequential. The detection of P300 responses amounts to a binary classification: one class represents signals that correspond to a P300 wave, the second class is the opposite. The general analysis of the P300 wave is made on the time domain: the synchronization of the stimulus (timing of the flashing lights) provides the triggers for the P300, which depends on the user. Although a P300 response can be expected at one particular latency, it is possible that the user does not produce a P300 response at the right moment, as many artifacts can occur. This first part of the problem generally is related with different signal processing methods that give an accurate detection of the P300 wave: this was also treated briefly in Section 5.1.2.

In the second step, related to character recognition, the outputs of the P300 classification are combined to discriminate the main classes of the application (characters). In the oddball paradigm, a character is defined by the selection of a couple (row,column). The flashing lights are on each row and column and not on each character. As a character was repeated several N_{epoch} times its detection is supposed to correspond to the intersection of the accumulation of several P300 waves.

For the matrix $\boldsymbol{V} \in \mathbb{R}^{12\times N_{epoch}}$ containing the cumulative probabilities of the P300 detection for each of the 12 flashes and for each epoch (CECOTTI *et al.*, 2010) .

$$V(i,j) = \sum_{k=1}^{j} E_{P300Detec}(P(i,k)) \tag{5.18}$$

where $P(i,j) \in \mathbb{R}^{N_f \times N_e}$ is the pattern at the epoch j corresponding to the subject response for the flash i, (i $(1,\cdots,12)$; j $(1,\cdots,Nepoch)$). N_e and N_f are the number of sensors and the number of sampling points representing the signal, respectively. $E_{P300Detec}$ is a classifier that returns a confidence value $v \in [1;0]$: 1 (resp. 0) denotes a perfect confidence that P300 response is detected (resp. not detected).

$$\mathbf{V} = \begin{pmatrix} \sum_{k=1}^{1} E_{P300Detec}(P(1,k)) & \sum_{k=1}^{2} E_{P300Detec}(P(1,k)) & \dots & \sum_{k=1}^{j} E_{P300Detec}(P(1,k)) \\ \sum_{k=1}^{1} E_{P300Detec}(P(2,k)) & \sum_{k=1}^{2} E_{P300Detec}(P(2,k)) & \dots & \sum_{k=1}^{j} E_{P300Detec}(P(2,k)) \\ \vdots & \ddots & \ddots & \vdots \\ \sum_{k=1}^{1} E_{P300Detec}(P(i,k)) & \sum_{k=1}^{2} E_{P300Detec}(P(i,k)) & \dots & \sum_{k=1}^{j} E_{P300Detec}(P(i,k)) \end{pmatrix} \tag{5.19}$$

The accumulation of P300 waves for the horizontal (resp. vertical) flashing lights determines the row (resp. the column) of the desired character. From the expression (5.19), the two expressions that relate this accumulated value for row and column detection are defined:

$$x_j = \underset{1 \le i \le 6}{argmax}\, V(i.j) \tag{5.20}$$

$$y_j = \underset{7 \le i \le 12}{argmax}\, V(i.j) \tag{5.21}$$

At each epoch j, it is possible to evaluate the coordinate (x_j, y_j) of the selected character. The final value of classification is defined by the selected character $E_{Speller}(x_{N_{Epoch}}, y_{N_{Epoch}}) = (row, column)$.

Having the above in consideration, on the next section, it will be discussed how to define a model based on Bayesian discrimination for the problem of prediction of the column and the row for the P300 speller. This model could help in the study of the performance of the final value of classification in this problem, and indirectly impacts the first classification problem that was already defined, that is, the detection of the P300 wave.

5.4.2 Classification model based on Bayesian discrimination

In a model of Bayesian discrimination, it is possible to describe the problem of class separation assuming the separation of two classes that are defined by a normal multivariate distribution. It is known that the total output of classification is composed of the separate row and column identification where the P300 wave is located. Thus, S_i is defined as the output of the classifier that detects separately columns ($N_{columns} = 1, ..., 6$)

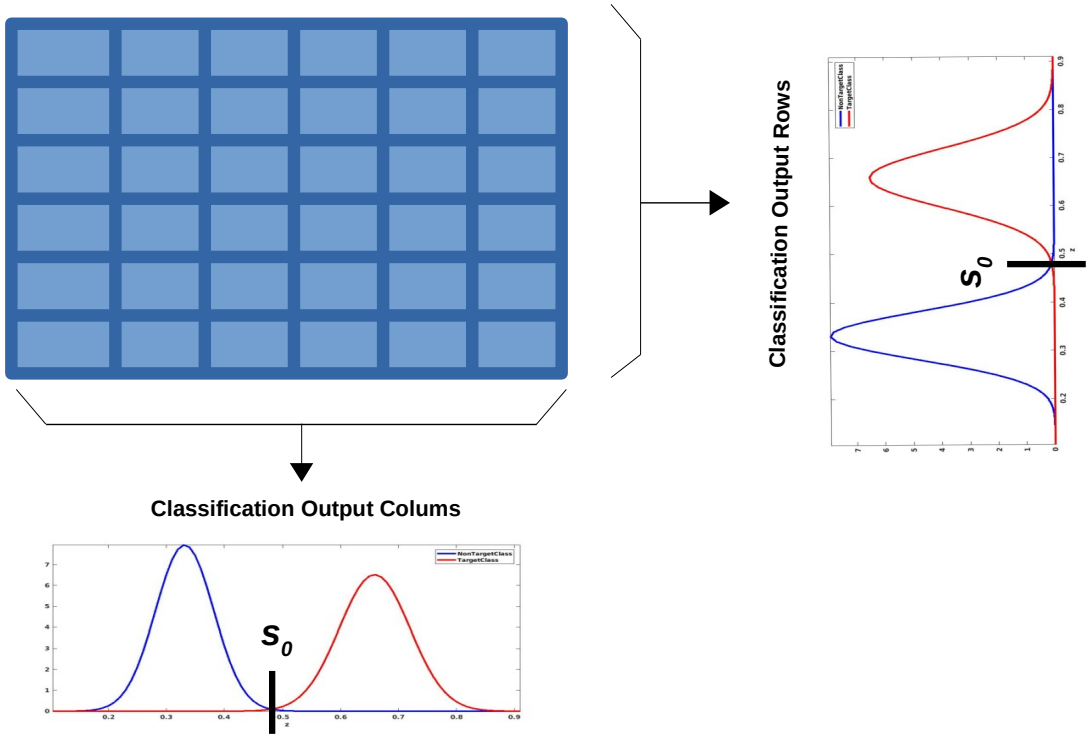

Figure 5.4 – Representation of the Normal multivariate distribution for the output S_i of the classifier of columns/rows separately.

or rows ($N_{rows} = 1, ..., 6$). Figure 5.4 represents the output classification for row and column using these model.

The cumulative score of the i_{th} row/column after j repetitions is defined in the expression $S_i^{(j)}$, Eq. (5.22):

$$S_i^{(j)} = \frac{1}{j} \sum_{k=1}^{j} s_i(k) \tag{5.22}$$

where $(i\ (1, \cdots, N_{Row/Column}); j\ (1, \cdots, N_{rep}))$ and $s_i(k)$ is the score of the i_{th} row/column at k repetition that is the same expression $E_{P300Detect}$.

$$\text{If } i \text{ is Target } \Rightarrow s_i(k) \sim N(\mu_T, \sigma_T^2),\ \forall\, k$$
$$\text{If } i \text{ is Non Target} \Rightarrow s_i(k) \sim N(\mu_{NT}, \sigma_{NT}^2),\ \forall\, k$$

To define a general expression of classification output (with $j = 1$) for row/column i separately, $E_{P300-COLROW}$:

$$E_{P300-COLROW} = \underset{i}{argmax}\ (S_i)\ \ i\,\epsilon\,\{1, \cdots, 6\} \tag{5.23}$$

Considering for example if S_1 is the correct row/column:

$$\{S_i\}_i \quad \begin{cases} S_1 : Target\ (T) \\ \{S_i\}_{i \neq 1} : Non\ Target\ (NT) \end{cases} \tag{5.24}$$

As already described, there is a problem of separation of two classes Target and Non-target; for the case of Equation (5.24) there is S_i, $i-1$ outputs for the Non-target case, expressing this as an event A which has a probability that could be expressed as:

$$\begin{aligned} A &= (S_2 < s_1)\,\&\,(S_3 < s_1)\,\&\ \cdots (S_i < s_1) \\ Pr(A \mid S_1 = s_1) &= Pr((S_2 < s_1)\,\&\,Pr(S_3 < s_1)\,\&\ \cdots Pr(S_i < s_1)) \\ &= Pr(S_2 < s_1)\ Pr(S_3 < s_1) \cdots Pr(S_i < s_1) \\ &= F_{NT}(s_1)^{i-1} \end{aligned}$$

where $F_{NT}(s_1)$ is the cumulative density function (cdf) of Non-target class. Then the corresponding mean of $Pr(A \mid S_1 = s_1)$, which would indicate the prediction value of the detection of a row / column correctly, is:

$$\mathbb{E}\left[Pr(A \mid S_1 = s_1)\right] = \int_{-\infty}^{\infty} (F_{NT}(s_1))^{(i-1)} p_T(s_1) ds_1 \tag{5.25}$$

The cdf of a continuous random variable (F_{NT}) can be expressed as the integral of its probability density function (pdf) p_{NT} as follows:

$$F_{NT}(s_1) = \int_{-\infty}^{s_1} p_{NT}(z) dz \tag{5.26}$$

Thus, the Eq. (5.25) will be expressed as:

$$\mathbb{E}\left[Pr(A \mid S_1 = s_1)\right] = \int_{-\infty}^{\infty} \int_{-\infty}^{s_1} \cdots \int_{-\infty}^{s_1} p_{NT}(z_1) p_{NT}(z_2) ... p_{NT}(z_{i-1}) p_T(s_1) dz_1 ... dz_{i-1} ds_1 \tag{5.27}$$

The product of the internal factors of Equation (5.25) :
$\underline{p_{NT}(z_1) p_{NT}(z_2) ... p_{NT}(z_{i-1}) p_T(s_1)}$ described the transformation that can be done on the product of the i normal univariate distribution, which can be joined in a single new

multivariate distribution that is defined by:

$$N(\mu^*, \mathbf{\Sigma}^*) \Rightarrow \quad \mu^* = \begin{pmatrix} \mu_T \\ \mu_{NT\ (1)} \\ \vdots \\ \mu_{NT\ (i-1)} \end{pmatrix} \quad \mathbf{\Sigma}^* = \begin{bmatrix} \sigma_T^2 & 0 & \cdots & \\ 0 & \sigma_{NT\ (1)}^2 & & \\ \vdots & & \ddots & \\ & & & \sigma_{NT\ (i-1)}^2 \end{bmatrix} \tag{5.28}$$

The new normal multivariate pdf could be expressed for a new variable $z^* = (s_1, z_1, ..., z_{i-1})$.

$$\mathbb{E}\left[Pr(A \mid S_1 = s_1)\right] = \int_{-\infty}^{\infty} \int_{-\infty}^{s_1} \cdots \int_{-\infty}^{s_1} p_G(z^* \mid \mu^*, \mathbf{\Sigma}^*) dz^* \tag{5.29}$$

To change the limits of the integrals we use the variable $v^* = Az^*$, $dv^* = |A|\, dz^*$

$$v^* = \mathbf{A}z^* = \begin{pmatrix} s_1 \\ z_1 - s_{1\ (1)} \\ \vdots \\ z_{i-1} - s_{1\ (i-1)} \end{pmatrix} = v' \tag{5.30}$$

$$\mathbf{A} = \begin{bmatrix} 1 & 0 & \cdots & & 0 \\ -1\,|_{(1)} & 0 & 1 & \cdots & 0 \\ \vdots\,| & 0 & 0 & \ddots & 0 \\ -1\,|_{(i-1)} & 0 & 0 & & 1 \end{bmatrix} \tag{5.31}$$

With $v^* \in \mathbb{R}^i$ and $\mathbf{A} \in \mathbb{R}^{i \times i}$. Then Equation (5.29) turns out:

$$\mathbb{E}\left[Pr(\mathbf{A} \mid S_1 = s_1)\right] = \int_{-\infty}^{\infty} \int_{-\infty}^{0} \cdots \int_{-\infty}^{0} p_G(v^* \mid \mathbf{A}\mu^*, \mathbf{A}\mathbf{\Sigma}^*\mathbf{A^T}) dv^* \tag{5.32}$$

Over all the limits of integration, the first one is different of all the $i-1$ following, but, if we marginalize the pdf, we can only leave all the equal $i-1$ limits. Marginalizing, we obtain $v^* \to v'$ and $\mathbf{A} \to \mathbf{A}'$:

$$\mathbf{A}' = \begin{bmatrix} -1\,|_{(1)} & 0 & 1 & \cdots & 0 \\ \vdots\,| & 0 & 0 & \ddots & 0 \\ -1\,|_{(i-1)} & 0 & 0 & & 1 \end{bmatrix} \tag{5.33}$$

$$\mathbb{E}\left[Pr(\mathbf{A} \mid S_1 = s_1)\right] = \int_{-\infty}^{0} \cdots \int_{-\infty}^{0} p_G(v' \mid \mathbf{A}'\mu^*, \mathbf{A}'\mathbf{\Sigma}^*\mathbf{A'^T}) dv' \tag{5.34}$$

With $v' \in \mathbb{R}^{i-1}$ and $\mathbf{A'} \in \mathbb{R}^{i-1 \times i}$. Then, Equation (5.34) expresses the cumulative function distribution (cdf), evaluated in $-\infty < v' < 0$:

$$\mathbb{E}\left[Pr(\mathbf{A} \mid S_1 = s_1)\right] = F_G(0 \mid \mathbf{A}^{'}\mu^*, \mathbf{A}^{'}\mathbf{\Sigma}^*\mathbf{A}^{'\mathbf{T}}) \tag{5.35}$$

for a normal multivariate distribution defined by: $N(\mathbf{A}^{'}\mu^*, \mathbf{A}^{'}\mathbf{\Sigma}^*\mathbf{A}^{'\mathbf{T}})$. Then, the final mean and variance of this distribution are directly affected by matrix A':

$$\mu_G = \mathbf{A}^{'}\mu^* \tag{5.36}$$

$$\mathbf{\Sigma_G} = \mathbf{A}^{'}\mathbf{\Sigma}^*\mathbf{A}^{'\mathbf{T}} \tag{5.37}$$

Turning again to the idea of the cumulative score, Eq.(5.22), we can go back to the concept of distribution of the Target and Non-target classes, and how it is affected by the number of repetitions j

$$\text{If } i \text{ is Target } \Rightarrow S_i^{(j)} \sim N(\mu_T, \frac{1}{j}\sigma_T^2),\ \forall\, k$$

$$\text{If } i \text{ is Non Target} \Rightarrow S_i^{(j)} \sim N(\mu_{NT}, \frac{1}{j}\sigma_{NT}^2),\ \forall\, k$$

According to the objectives of this work, for the analysis of the classification prediction, a comparison can be made between the practical and theoretical/prediction, Eq. (5.35), reached when the xDAWN filter is used for the P300 speller problem. The following steps were carried out for the execution of this task:

1. Split the data on training and testing. A higher percentage of characters will be used for the training set.
2. On training:
   - Learn the spatial filter $\hat{\mathbf{U}}$.
   - Train the classifier $\underline{c}$, obtain the $\mathbf{w}$ parameters of the classifier. $s_i = \mathbf{w}(\mathbf{X}\hat{\mathbf{U}})$
   - Obtain the $\mathbf{V}$ matrix of Eq.(5.19). $E_{P300Detect} = s_i$
   - Calculate (μ_T, σ_T^2) and $(\mu_{NT}, \sigma_{NT}^2)$, with $\mu_T = \mathbb{E}[s_T]$, $\mu_{NT} = \mathbb{E}[s_{NT}]$ and $\sigma_T^2 = var[s_T]$, $\sigma_{NT}^2 = var[s_{NT}]$, where s_T and s_{NT} are all the output of the matrix Eq.(5.19) which correspond respectively to the Target and Non-target classes.
   - Obtain μ^* and $\mathbf{\Sigma}^*$ from Eq.(5.28). Obtain also v' (5.30) and $\mathbf{A'}$ (5.33).
   - Calculate the theoretical predicted accuracy $F_G(0 \mid \mathbf{A}^{'}\mu^*, \mathbf{A}^{'}\mathbf{\Sigma}^*\mathbf{A}^{'\mathbf{T}})$.

3. On testing:

   - Apply the spatial filter $\mathbf{X}\hat{\mathbf{U}}$.
   - Apply the classifier and obtain $(s_i)_i$.
   - For 1 symbol and a k given repetition determine if a correct detection occurred (1: Good detection, 0: else), e.g. analyze the 6 scores related to the 6 rows $s_1, s_2, ..., s_6$, do the same for the columns, and determine the response.
   - For the k repetitions [1 0 1 ... 0], calculate the mean value of practical accuracy (for rows and columns).

4. Repeat the process from step 1, doing it several times, for example 10, to obtain a total average of the theoretical performance (step 2) versus the practical performance (step 3).

5.5 Optimization of the practical detection on the P300 speller based on the theoretical predictive model F_G

For the problem that was studied in the previous section, on how to correctly detect the P300 response in rows and columns of the P300 speller in a theoretical form, the focus will be directed now on how the output of the score of classification s_i is determined (the binary classification of P300 and no P300 responses). This output had also been previously called by the name of $E_{P300Detect}$ (Eq. 5.18). In the case of the use of the xDAWN filter, this output is related to the parameters $\hat{\mathbf{U}}$, which would be the coefficients of the filter obtained when using xDAWN and also the parameters of the classifier $\mathbf{w}$. Equation (5.38) shows the expression that relate the coefficients of the classifier($\mathbf{w}$) and the spatial filter ($\hat{\mathbf{U}}$) in the classification output.

$$s_i = \mathbf{w}(f_i) = \mathbf{w}(\mathbf{X}\hat{\mathbf{U}}) \tag{5.38}$$

The used classifier was based on Bayesian linear discriminant analysis (BLDA) (MACKAY, 1992). This classifier finds a discriminant vector $\mathbf{w}$ such that the distance between the associated vector of a class c and $\mathbf{w}^T\mathbf{p}$ is minimized when the input vector p belongs to the class c. The vector $\mathbf{p}$ is obtained by the concatenation of the different time-course signals. For the classification, only the four first components of the enhanced signal are considered ($N_{OUTfilters} = 4$).

When separating the detection output s_i for the Target and Non-target classes, it is possible to define an expression to find the mean value (μ_T, μ_{NT}) and the variance (σ_T, σ_{NT}).

$$\mathbb{E}[s_T] = \mathbf{w}^T\mathbb{E}[f_T] = \mathbf{w}^T\mathbb{E}[X_T]\hat{\mathbf{U}} \tag{5.39}$$

$$\mathbb{E}[s_{NT}] = \mathbf{w}^T\mathbb{E}[f_{NT}] = \mathbf{w}^T\mathbb{E}[X_{NT}]\hat{\mathbf{U}} \tag{5.40}$$

From Equation (5.40), it can be observed that the mean, and variance equally, can be expressed as functions of the parameters $\hat{\mathbf{U}}$ and $\mathbf{w}$. Then $\mu_T(\mathbf{w}, \hat{\mathbf{U}})$, $\sigma_T(\mathbf{w}, \hat{\mathbf{U}})$; these expressions are equivalent for the Non-target class. From Equations (5.28) and (5.35), it is seen that there is a direct relation also between the cdf that describes the theoretical prediction model defined in the previous section and these same parameters:

$$F_G(0 \mid \mathbf{A}^{'}\mu^*, \mathbf{A}^{'}\mathbf{\Sigma}^*\mathbf{A}^{'\mathbf{T}}) = f(\mathbf{w}, \hat{\mathbf{U}}) \tag{5.41}$$

If Equation (5.41) is considered the cost function over which an optimization process can be performed to find the maximum value of the function f, it is possible to find the maximum value of classification prediction with respect to the parameters $(\mathbf{w}, \hat{\mathbf{U}})$. In this way, it could be possible to find an optimal value of the coefficients of the spatial filter and the classifier. In the optimization process, our proposal suggests that using the initially calculated values of these parameters as a basis, the optimization of one of the parameters could be done (the order of optimization of the parameters should not have any influence on the final result). Then, a successive optimization looking for the next parameter is executed. These optimizations can be carried out in a continuous cycle (e.g, first $\hat{\mathbf{U}}$, then $\mathbf{w}$) until a certain number of repetitions have been completed.

$$\hat{\mathbf{U}}_{opt} = arg\ \max_{\hat{\mathbf{U}}}\ f(\hat{\mathbf{U}}, \mathbf{w}) \tag{5.42}$$

$$\mathbf{w}_{opt} = arg\ \max_{\mathbf{w}}\ f(\hat{\mathbf{U}}, \mathbf{w}) \tag{5.43}$$

To solve this optimization problem, there are several techniques that can be used, such as classical approaches with search methods incorporating the gradient. Currently, there are plenty of options for choosing an algorithm to use. Thus, the constraints of the problem to be solved and the type of cost function must be considered as well, so that the optimization algorithm can be correctly determined. In the case of the cost function $f(\mathbf{w}, \hat{\mathbf{U}})$ (Eq. 5.41) of our problem, the cdf is an expression of a set of multi-variable evaluated integrals of normal distributions. These integrals do not have a closed form in which an expression can be determined - they can be numerically evaluated. For this reason, there is a difficulty in expressing the gradient and using a more classic strategy.

The two methods we decided to test for optimization were:

- A method for direct search - this kind of algorithm searches for an optimal point, analysing a set of points around a current point, looking for one where the value of the objective function is lower than the value at the current point. Direct search solves problems for which the objective function is not differentiable, or even continuous (BJÖRKMAN; HOLMSTRÖM, 1999).

- A method based on optimizations in manifolds (VANDEREYCKEN, 2012). The reason for the inclusion of this method was based on the type of definition set for constrain $\hat{U}$ and $\mathbf{w}$ parameters. In particular, optimization on manifolds is well-suited to deal with rank and orthogonality constraints. The constraints defined in these case are related to search for matrix/vectors with unit-norm.

In the next section, the results obtained by using the prediction function F_G to perform the optimization of the spatial filter and the classifier parameters, using different algorithms within the manifolds optimization package, called manopt (BOUMAL *et al.*, 2014), will be presented.

5.6 Results and discussion

5.6.1 Prediction accuracy model

First, the result obtained for the calculated value of classification through the use of the predictive model will be presented. This task was carried out following the steps mentioned at the end of Subsection 5.4.2, where it was described that, according to the division of the data into training and test sets, it would be possible to obtain a calculated theoretical prediction value (training data) and a value of practical prediction (test data).

These obtained values were compared evaluating different cases of configuration of input and output channels for the employed spatial filter. Generally, the use of the spatial filter will always consider a reduction of the output channels. These channels specifically refer to the inputs/outputs of the spatial filter. For example, for the main case of study, $NumberInputCh = 32$, $NumberOutputCh = 4$. Other cases were also analyzed starting with a smaller number of both input and output channels. Figure 5.5 presents two of the classic cases to compare the results of the theoretical and practical prediction of classification.

As mentioned in previous sections, the number of repetitions affects the obtained classification output. This is the reason why these comparisons were also made to see the impact of this parameter on the value of the total classification. This classification value is the average over 10 different sets of test and training data on which the executions were carried out. Figures 5.6, 5.7, 5.8, presents other cases studied by varying the number of

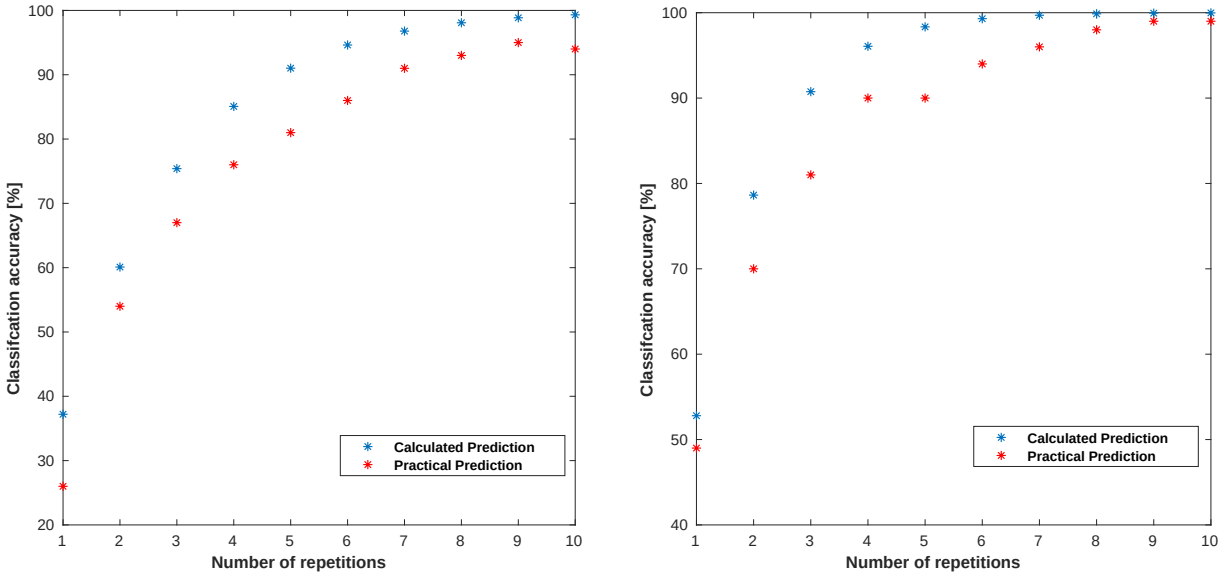

(a) Case 16-2 (b) Case 32-4

Figure 5.5 – Comparison of two classical cases of channels configuration for the spatial filter, practical and calculated accuracy.

channels of the spatial filter used. It can be seen, in general, that, for all the cases presented in Figure 5.5 and in the Figures 5.6, 5.7, 5.8, the calculated value of the classification prediction model is in most of the cases above the practical values obtained.

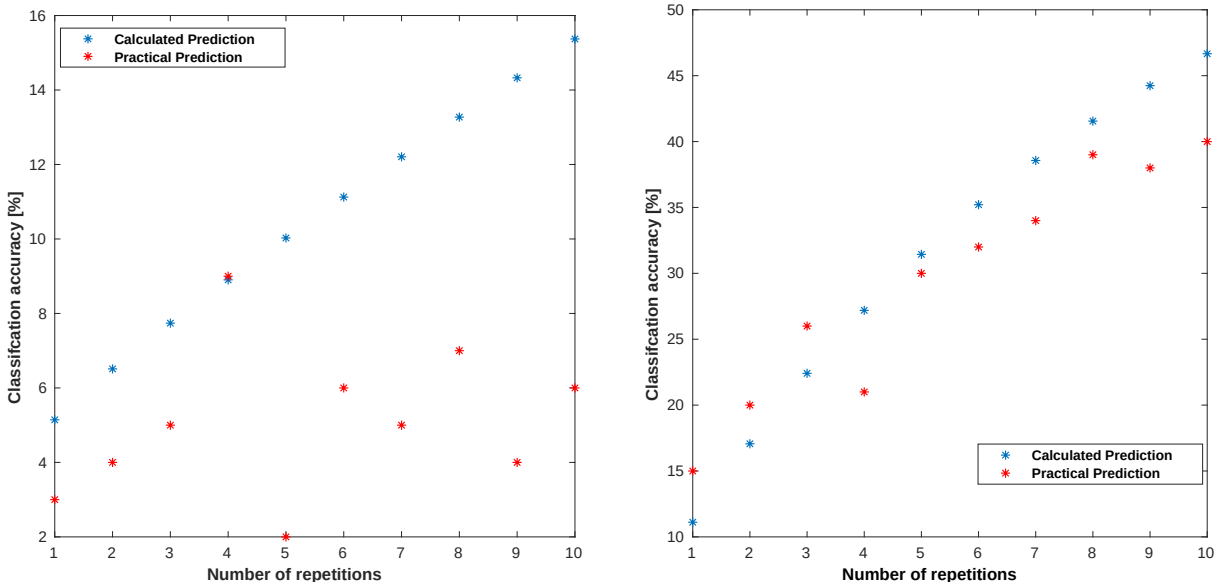

(a) Case 2-1 (b) Case 3-1

Figure 5.6 – Comparison of the cases 2-1 and 3-1 of channels configuration for the spatial filter, practical and calculated accuracy.

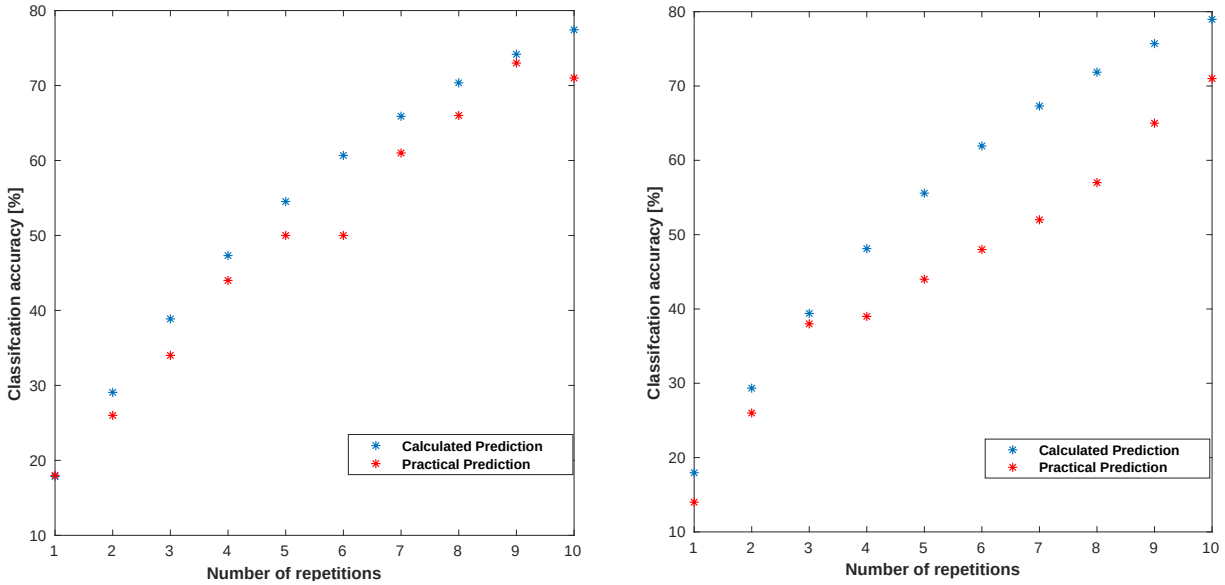

(a) Case 4-1 (b) Case 5-1

Figure 5.7 – Comparison of the cases 4-1 and 5-1 of channels configuration for the spatial filter, practical and calculated accuracy.

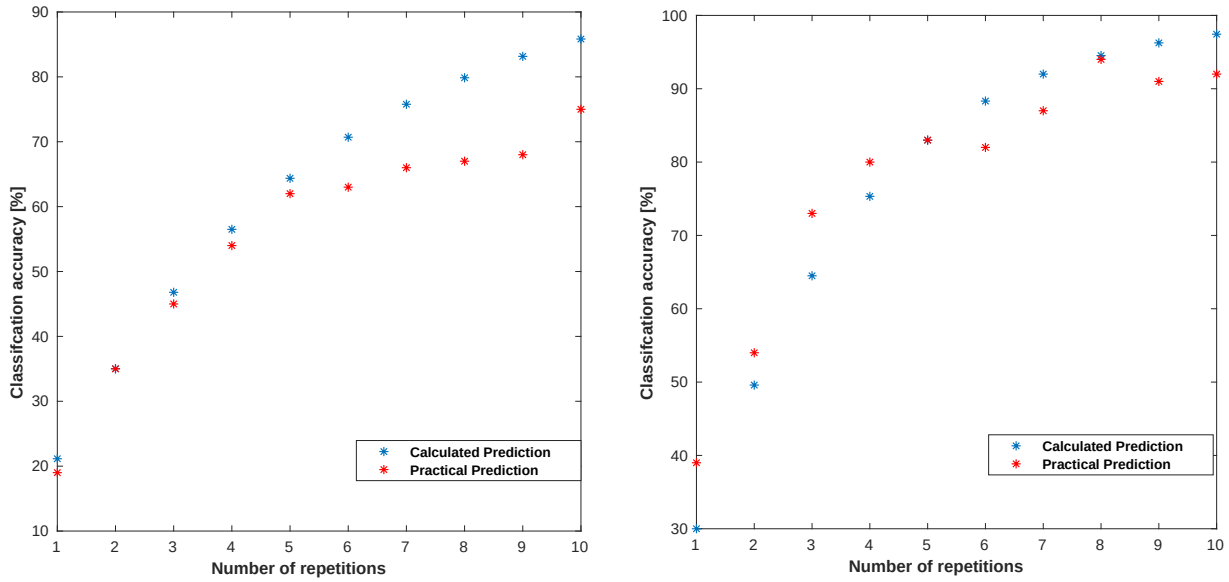

(a) Case 6-1 (b) Case 16-1

Figure 5.8 – Comparison of the cases 6-1 and 16-1 of channels configuration for the spatial filter, practical and calculated accuracy.

The adjustment of the separation between the two curves (calculated vs. practical) becomes close as the number of input channels increases. This would indicate that the theoretical model serves to give an idea of the practical value of classification output. It could be considered that for the case of Figure 5.6, the practical values of output

classification are quite low and continuously varying no matter how many repetitions are made. This makes quite good sense if it is thought that very little information is obtained by using two random channels that may not capture any relevant information from the P300 phenomenon.

According to the results of Figure 5.7A, it can be seen that from the use of 4 input channels the approximate value of classification for the calculated model is near 70%. In the practical case it is seen that similar results are obtained for 5 input channels (Figure 5.7B). For this very small number of input channels, it is possible to see that, with a low number of repetitions, it would take possibly more than 6 repetitions to obtain acceptable classification values. The analysis of how effective the use of six input channels and 1 output channel would be is quite surprising: this effectively registers the potential associated with the use of the spatial filter.

It is important to highlight that, from the first two cases presented (Figure 5.5), these cases contemplate the use of half and the total of the input channels. With these configurations, one of the best classification values are obtained. So, the impact of the number of repetitions for the classification values in this case is strong when viewed and verified the results of classification around 80% (using approximately 4-5 repetitions) for both calculated and practical values.

5.6.2 Optimization based on prediction accuracy model

The second part of the analysis consisted in a comparison between the values obtained for classification accuracy with the original parameters of the filter and classifier and the values from the optimized search. To execute this process using the function of prediction accuracy model, it was mentioned that manifold optimization was used through the manopt toolbox. This tool gives us different options to choose several search algorithms: since there is no gradient function, it was decided to choose two types of algorithm that are not based on gradient; the first used was particle filter and the second Nelder-Mead.

Figure 5.9A presents the values of classification obtained for the calculated prediction value when was considered a single repetition (j = 1). As already seen, the regular values of classification are between 10% and 50%. There is a small superiority of the optimized values, but these decrease when considering cases with 16 or more electrodes in the input. These values are considered the theoretical basis on which the practical values of classification will be expected.

In relation to the practical prediction values (Figure 5.9B), it can be said that in general these values were higher in relation to the calculated results. This time, the classification success was in the range of 10% to 60%. These results do not show that there

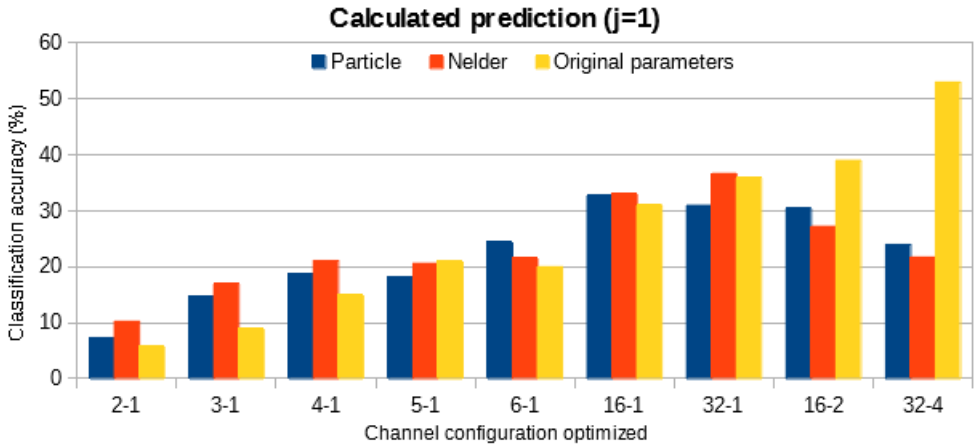

(a) Calculated prediction for j=1 repetitions.

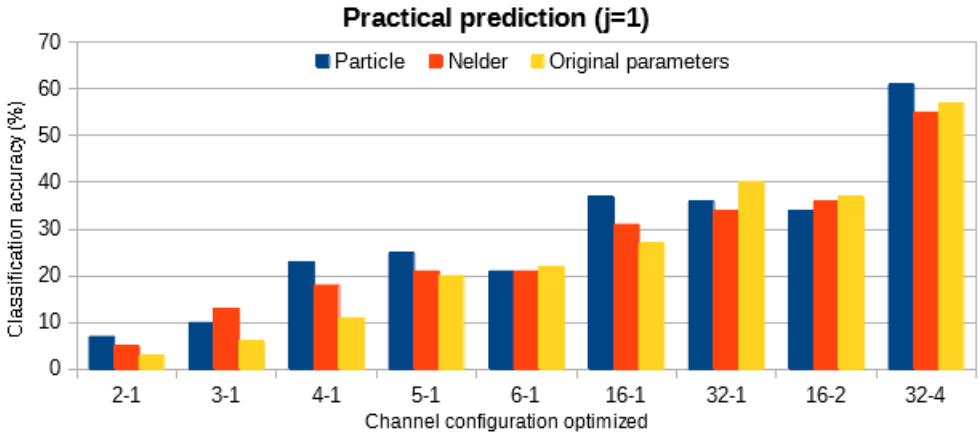

(b) Practical prediction for j=1 repetitions.

Figure 5.9 – Classification accuracy obtained with two strategies of optimization compared to when the original parameters were used. Considering also different channel configurations for the spatial filter $\hat{U}$.

was only one case in which the values obtained when the optimized process was made were inferior in relation to the use of the original parameters (16-2 channel configuration). For the channel configuration 32-4, the results obtained with particle filtering were superior with 61%, compared to 57% obtained when using the original parameters.

One more comparative analysis was considered for the classification values (Figure 5.10), taking into account the average value after 10 repetitions (j = 10). The practical value obtained when using optimization was compared with the use of the original parameters- practical value and calculated value. It can be observed that a superiority of the classification performance is seen for cases where the number of input channels is less than 4. For the other cases, there is a proximity in the performance, in which the use of the original parameters did not always show superior values. The best performances were found for the last 4 cases of Figure 5.10 where performances achieved were between 90% and 100%, case 16-1, 32-1, 16-2, 32-4.

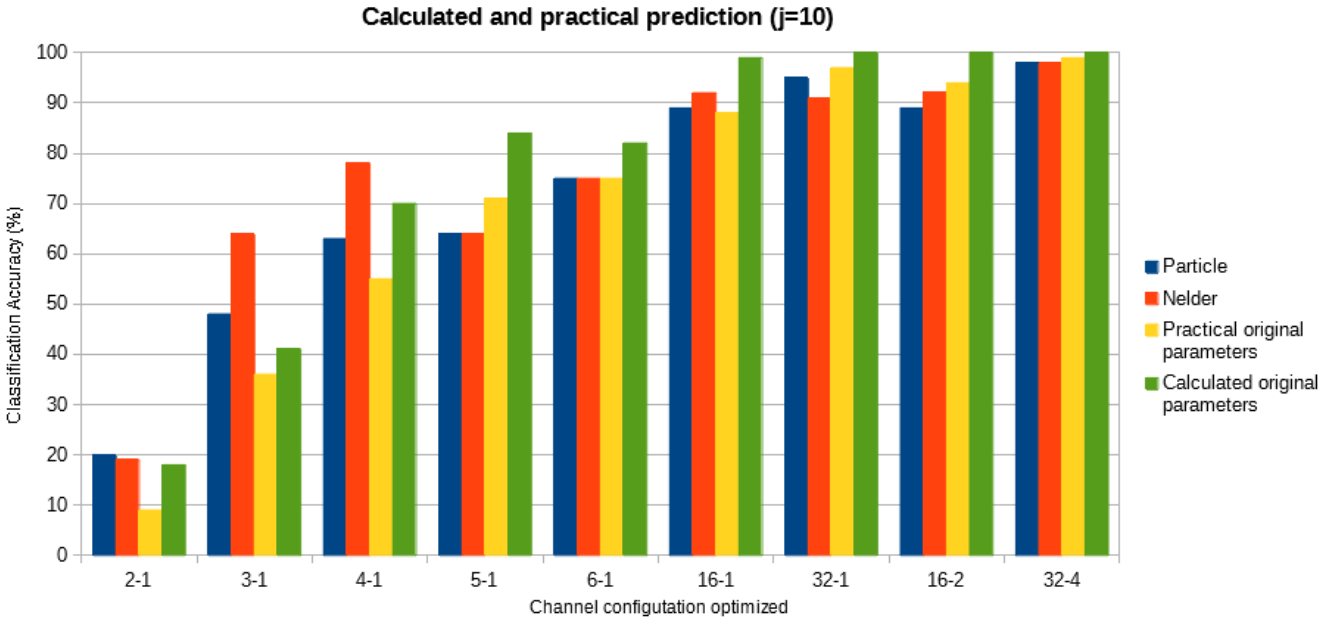

Figure 5.10 – Comparison of the performance of practical prediction when 10 repetitions were executed for the cases in which optimization was used and when the original parameters were used. For this last case the calculated value is also presented. Different cases of channel configurations for the spatial filter $\hat{U}$ were considered.

5.7 Conclusion

According to the study carried out in this chapter on the use of the spatial filter xDAWN for the classification problem of the P300 speller, the results show that the prediction model based on a Bayesian model gave a general idea of the response of the system. This response, considered to be the ideal case, was that the greater the number of channels used in the input, the greater the similarity found in the theoretical and practical response.

The importance of this model can also be highlighted in the sense that, in some way, it is implicitly including restrictions and characteristics of the P300 speller problem, which can still be studied in greater depth, for example, the probability of one letter being more expected than another.

Also with respect to the idea of using the prediction model to execute an optimization of the parameters of the classifier and the spatial filter, it was important because it was possible to see that the values of the optimization in the practical classification became higher for some cases. Particularly, it was impressive to see how using only 4 input channels and one output channel, the values of classification accuracy were near 80%. On the other hand, for cases with a greater number of input channels, the results of the optimization were very close to those originally obtained by the spatial filter. In this way, it remains open to explore if there is any other way to execute the optimization

using some other type of restriction or model, trying to express the gradient function in some way that can give more tools to include other types of search algorithms.

Summary and Future Directions

In this thesis, the development of practical Brain-Computer Interfacing communication was addressed by studying different components and stages that are involved in the BCI closed-loop, i.e., the pre-processing, the feature extraction, the classifier. The objective was to improve the speed and the reliability of non-invasive BCI systems that acquire brain signals via EEG. In order to reach this main goal, this work focused on two BCI paradigms: the event-related (de-)synchronization (ERD/ERS) based on Motor Imagery and the event related potential (ERP) associated to the P300 response. The former is the amplitude increase or decrease of the brain waves during performed or imagined movement (e.g., hands, tongue or feet movement), and the latter reflects attention to unexpected stimuli. Whereas the ERD/ERS constitutes an endogenous BCI (respond to internally generated signal), the P300 signal constitutes an exogenous BCI (responds to an automatic response to a given stimulus).

Concerning ERD/ERS communication, crucial parameters for the detection of ERD/ERS brain patterns were identified and the relevance of the use of the spatial filters was investigated in Chapter 3. Consistent with other studies, the results of the explorative analysis showed that the ERD/ERS patterns were subject- dependent and varied in frequency (around mu and beta bands) and space (electrode location). These results were very helpful for the analysis of the two classes of MI studied in this chapter. The search for the signal sources, in order to reduce the artifacts such as eye blinking, or the involuntary movement of the subject, led to the use of techniques such as ICA, for the identification of the components where the ERS/ERD activity would be found. Finally, the exploration of the prominent differences between the independent components recovery from the ICA analysis was implemented when the feature selection was applied together to identify the most relevant features at the classification standpoint for the recognition of the two types of MI studied.

In Chapter 3, together with the study of the ERD/ERS phenomenon, the analysis of the pattern regularity and its behavior during a period of several days was also considered. This aspect was analyzed by the comparison of the results obtained using the filter parameters of one day, on the data of other days. In the preliminary results obtained using ICA, it was seen that this filter could reduce the time of training of a subject before using a BCI system. In relation to the data acquisition performed, the experience with this paradigm showed that the execution of the activity of ERD/ERS requires significant commitment and a lot of concentration from the user. The reduction of calibration times would be vital for any further implementation that focuses on online ERD/ERS communication.

Chapter 4 described a proposal for feature analysis of MI. The techniques that explore functional connectivity appeared within the study of this brain phenomenon, and comprehend an interpretation of the activities in different brain regions during the execution of motor imagination task. In this contribution the interactions between electrodes were modeled using graphs, each node being associated to a single electrode. The edges of this graph represent interactions between these nodes, which were estimated by three methods - Pearson's correlation, Spearman correlation and correntropy. From the constructed graphs, centrality measures were obtained, and later they were used as classification attributes. For each type of constructed graph the corresponding classification performances were compared. The purpose of this comparison is basically to verify if the higher order information brought by the correntropy has an effective role in improving the classification performance.

The results obtained showed hat the FC analysis completed an effective extraction of the relevant information that is associated with the phenomenon studied. It should be noted that the union of several factors was analyzed, such as the use of two types of classifiers in conjunction with feature selection, in addition to the three types of graph centrality measures.

The classification performance obtained for this variety of techniques was compared to the results obtained by the best algorithms that were applied to the BCI competition IV database. The comparison showed that among all the proposals tested, the nonlinear structure in the classification, in conjunction with the measure of eigenvector centrality, gave the best results when used with correntropy. It remains as a perspective to investigate the other different options to use corrrentropy, e.g. considering delays over time. This measure is rich to explore the statistical behavior of the data, so it must also be evaluated as this could be interpreted later by other measures of graph connectivity. In this way, several cases will have to be considered to arrive at results considering the aspect of classification.

Finally, Chapter 5 described a proposal to model the total classification response obtained by using the spatial filter xDAWN in the P300 speller. This issue was proposed considering how a model of the predictive response could be discovered, given the specific characteristics of the application. In this case it was considered that only one row and column must contain the response of class P300 (target class). It is known that spatial filters include information in several domains, generally the first being spatial information. The xDAWN filter has been one of the spatial filters that has been shown to be among the most outstanding options to be used in the P300 phenomenon classification problem (BARACHANT; CONGEDO, 2014). The xDAWN filter leads to an unbiased and consistent estimator of optimal spatial filters and stands out because in its model it only requires knowledge of the start of each stimulus.

The results from the model of prediction were obtained in relation to a practical and a theoretical value. The theoretical analysis yielded a perspective of that in some cases this model fits to the values obtained in the practical way. It was possible to observe the dependence on the selection of the number of input and output channels on the filter response, as well as on the number of repetitions executed for the classification of a symbol. In this case it was observed that by increasing the number of channels used in the input there is a tendency towards a proximity between the practical and theoretical values. Also, based on the prediction model, an optimization of the system parameters was carried out, which led to obtaining new values for the coefficients of the filter and the classifier. This new way of adjusting the parameters system allowed to bring a gain over the value of the classification performance when using a small number of input channels. However, this perspective must be further studied, considering also the use of other methods for spatial filtering and the process of tuning the parameters of the experiments, e.g., the number of target stimulus repetitions needed to obtain a desired SINR.

Future perspectives

A number of possible future works can be developed from the one presented here; below we list some of them:

- As mentioned previously, the BCI problem requires a process of adaptation and learning from the subject that is using the system. This adaptation is strongly related to the type of feedback that he/she receives. In our work, only one feedback method was used to execute MI experiments, but it would be interesting to further explore in how this task should be executed, in order to keep the subject's attention for longer periods, or perhaps facilitate this task, considering the aspect of concentration is key and was somewhat difficult to maintain for some subjects during the experiments performed. It is worth mentioning that this type of feedback studies also deserve a real quantification of what the subject is going through as s/he performs this activity.

- From the results obtained during the work in this thesis an interest arose in the study and definition of methods to make a temporary fusion of patterns. Due to the instability during several days of execution of experiments in the response of the studied phenomena, aspects related to this problem should be further investigated. This point could be explored in relation to the algorithms that facilitates the training of the system and that allows the interpretation of the response evolution.

- The exploration of methods related to the definition of statistical prediction models for the classification response of BCI systems. In this case it is clear that a proposal

was made in relation to this point when using the xDAWN filter for the case of the P300 speller, but other cases of different paradigms can be studied, considering specific practical aspects of each problem. A model like this allows the adjustment of several types of practical parameters of a BCI system, such as the number of repetitions necessary for a specific value of classification performance, which is an important aspect for the operation of these systems. From these models, different optimization methods can be explored that can generate better classification responses.

Bibliography

ACQUALAGNA, L.; BOTREL, L.; VIDAURRE, C.; KÜBLER, A.; BLANKERTZ, B. Large-scale assessment of a fully automatic co-adaptive motor imagery-based brain computer interface. *PLoS ONE*, v. 11, n. 2, p. 1–19, 2016. ISSN 19326203. Citado na página 44.

AHN, M.; JUN, S. C. Performance variation in motor imagery brain-computer interface: A brief review. *Journal of Neuroscience Methods*, Elsevier B.V., v. 243, p. 103–110, 2015. ISSN 1872678X. Citado na página 52.

AMIRI, S.; FAZEL-REZAI, R.; ASADPOUR, V. A review of hybrid brain-computer interface systems. *Advances in Human-Computer Interaction*, Hindawi Limited, v. 2013, p. 1–8, 2013. Citado na página 26.

ANG, K. K.; CHIN, Z. Y.; WANG, C.; GUAN, C.; ZHANG, H. Filter bank common spatial pattern algorithm on BCI competition IV datasets 2a and 2b. *Frontiers in Neuroscience*, Frontiers Media SA, v. 6, 2012. Citado na página 42.

ANG, K. K.; GUAN, C. EEG-Based Strategies to Detect Motor Imagery for Control and Rehabilitation. *IEEE Transactions on Neural Systems and Rehabilitation Engineering*, v. 25, n. 4, p. 392–401, 2017. ISSN 15344320. Citado na página 52.

BAMDAD, M.; ZARSHENAS, H.; AUAIS, M. A. Application of BCI systems in neurorehabilitation: A scoping review. *Disability and Rehabilitation: Assistive Technology*, v. 10, n. 5, p. 355–364, 2015. Citado 2 vezes nas páginas 30 and 34.

BARACHANT, A.; CONGEDO, M. A plug&play P300 BCI using information geometry. *CoRR*, abs/1409.0107, 2014. Citado 2 vezes nas páginas 115 and 137.

BARRAT, A.; BARTHELEMY, M.; PASTOR-SATORRAS, R.; VESPIGNANI, A. The architecture of complex weighted networks. *Proceedings of the National Academy of Sciences*, Proceedings of the National Academy of Sciences, v. 101, n. 11, p. 3747–3752, mar 2004. Citado na página 98.

BASHASHATI, A.; FATOURECHI, M.; WARD, R. K.; BIRCH, G. E. A survey of signal processing algorithms in brain–computer interfaces based on electrical brain signals. *Journal of Neural Engineering*, IOP Publishing, v. 4, n. 2, p. R32–R57, mar 2007. Citado 2 vezes nas páginas 43 and 114.

BELL, A.; SEJNOWSKI, T. J. Fast blind separation based on information theory. v. 1, p. 43–47, 1995. Citado na página 59.

BELOUCHRANI, A.; ABED-MERAIM, K.; CARDOSO, J.-F.; MOULINES, E. A blind source separation technique using second-order statistics. *IEEE Transactions on Signal Processing*, Institute of Electrical and Electronics Engineers (IEEE), v. 45, n. 2, p. 434–444, 1997. Citado na página 59.

BIEGER, J.; MOLINA, G. G. Technical note TN-2010-00315 Light Stimulation Properties to Influence Brain Activity. 2010. Citado na página 84.

BILLINGER, M.; BRUNNER, C.; MÜLLER-PUTZ, G. R. Single-trial connectivity estimation for classification of motor imagery data. *Journal of Neural Engineering*, v. 10, n. 4, 2013. ISSN 17412560. Citado na página 79.

BIN, G.; GAO, X.; WANG, Y. VEP-based brain-computer interfaces: time, frequency, and code modulations. *Computational Intelligence Magazine, IEEE*, v. 4 , Issue:, n. November, p. 22–26, 2009. Citado na página 37.

BIRBAUMER, N.; ELBERT, T.; CANAVAN, A. G.; ROCKSTROH, B. Slow potentials of the cerebral cortex and behavior. *Physiological Reviews*, American Physiological Society, v. 70, n. 1, p. 1–41, jan 1990. Citado na página 26.

BISHOP, C. *Pattern Recognition and Machine Learning*. [S.l.]: Springer-Verlag New York, 2006. Citado 2 vezes nas páginas 65 and 99.

BJÖRKMAN, M.; HOLMSTRÖM, K. *Global optimization using DIRECT algorithm in matlab*. 1999. Citado na página 129.

BLANKERTZ, B.; TANGERMANN, M.; VIDAURRE, C.; FAZLI, S.; SANNELLI, C.; HAUFE, S.; MAEDER, C.; RAMSEY, L.; STURM, I.; CURIO, G.; MÜLLER, K. R. The Berlin brain-computer interface: Non-medical uses of BCI technology. *Frontiers in Neuroscience*, v. 4, n. DEC, p. 1–17, 2010. ISSN 16624548. Citado 3 vezes nas páginas 25, 26, and 51.

BLANKERTZ, B.; TOMIOKA, R.; LEMM, S.; KAWANABE, M.; MÜLLER, K.-R. Optimizing spatial filters for robust EEG single-trial analysis [revealing tricks of the trade]. n. January 2008, p. 41–56, 2008. Citado 2 vezes nas páginas 42 and 51.

BORDIER, C.; NICOLINI, C.; BIFONE, A. Graph analysis and modularity of brain functional connectivity networks: Searching for the optimal threshold. *Frontiers in Neuroscience*, Frontiers Media SA, v. 11, aug 2017. Citado na página 97.

BOUMAL, N.; MISHRA, B.; ABSIL, P.-A.; SEPULCHRE, R. Manopt, a matlab toolbox for optimization on manifolds. *Journal of Machine Learning Research*, v. 15, p. 1455–1459, 2014. Citado na página 129.

BULLMORE, E. T.; BASSETT, D. S. Brain graphs: Graphical models of the human brain connectome. *Annual Review of Clinical Psychology*, Annual Reviews, v. 7, n. 1, p. 113–140, apr 2011. Citado na página 91.

BURGES, C. J. A tutorial on support vector machines for pattern recognition. *Data Mining and Knowledge Discovery*, v. 2, n. 2, p. 121–167, Jun 1998. ISSN 1573-756X. Citado na página 68.

CARDOSO, J. F. High-order contrasts for independent component analysis. *Neural computation*, v. 11, p. 157–192, 1999. ISSN 0899-7667. Citado 2 vezes nas páginas 59 and 60.

CARVALHO, S. N.; COSTA, T. B.; URIBE, L. F.; SORIANO, D. C.; ALMEIDA, S. R.; MIN, L. L.; CASTELLANO, G.; ATTUX, R. Effect of the combination of different numbers of flickering frequencies in an ssvep-bci for healthy volunteers and stroke patients. *International IEEE/EMBS Conference on Neural Engineering, NER*, v. 2015-July, p. 78–81, 2015. Citado na página 26.

CARVALHO, S. N.; COSTA, T. B. S.; URIBE, L. F. S.; SORIANO, D. C.; YARED, G. F. G.; CORADINE, L. C.; ATTUX, R. Comparative analysis of strategies for feature extraction and classification in ssvep bcis. *Biomedical Signal Processing and Control*, Elsevier Ltd, v. 21, p. 34–42, 2015. Citado 3 vezes nas páginas 11, 26, and 83.

CECOTTI, H.; RIVET, B.; CONGEDO, M.; JUTTEN, C.; BERTRAND, O.; MABY, E.; MATTOUT, J. Suboptimal sensor subset evaluation in a P300 brain-computer interface. *European Signal Processing Conference*, v. 12, p. 924–928, 2010. Citado 5 vezes nas páginas 10, 26, 38, 114, and 121.

CHAUDHARY, U.; BIRBAUMER, N.; RAMOS-MURGUIALDAY, A. Brain-computer interfaces for communication and rehabilitation. *Nature Reviews Neurology*, v. 12, n. 9, p. 513–525, 2016. ISSN 17594766. Citado 4 vezes nas páginas 24, 25, 30, and 35.

CHENG, M.; JIA, W.; GAO, X.; GAO, S.; YANG, F. Mu rhythm-based cursor control: an offline analysis. *Clinical Neurophysiology*, Elsevier BV, v. 115, n. 4, p. 745–751, apr 2004. Citado na página 39.

CINCOTTI, F.; BIANCHI, L.; MILLAN, J. del R.; MOURINO, J.; SALINARI, S.; MARCIANI, M.; BABILONI, F. Brain computer interface: the use of low resolution surface laplacian and linear classifiers for the recognition of imagined hand movements. In: *2001 Conference Proceedings of the 23rd Annual International Conference of the IEEE Engineering in Medicine and Biology Society*. [S.l.: s.n.], 2001. Citado na página 39.

COHEN, D.; CUFFIN, B. Demonstration of useful differences between magnetoencephalogram and electroencephalogram. *Electroencephalography and Clinical Neurophysiology*, Elsevier BV, v. 56, n. 1, p. 38–51, jul 1983. Citado na página 33.

COHEN, J. A coefficient of agreement for nominal scales. *Educational and Psychological Measurement*, SAGE Publications, v. 20, n. 1, p. 37–46, apr 1960. Citado na página 107.

COMON, P. Independent component analysis, a new concept? *Signal Processing*, Elsevier BV, v. 36, n. 3, p. 287–314, apr 1994. Citado na página 57.

CRISTIANINI, N.; SHAWE-TAYLOR, J. *An Introduction to Support Vector Machines: And Other Kernel-based Learning Methods*. New York, NY, USA: Cambridge University Press, 2000. ISBN 0-521-78019-5. Citado na página 68.

DALY, I.; NASUTO, S. J.; WARWICK, K. Brain computer interface control via functional connectivity dynamics. *Pattern Recognition*, Elsevier, v. 45, n. 6, p. 2123–2136, 2012. Citado na página 86.

DAVIES, D. L.; BOULDIN, D. W. A cluster separation measure. *IEEE Transactions on Pattern Analysis and Machine Intelligence*, Institute of Electrical and Electronics Engineers (IEEE), PAMI-1, n. 2, p. 224–227, apr 1979. Citado na página 62.

DELORME, A.; MAKEIG, S. EEGLAB: an open source toolbox for analysis of single-trial EEG dynamics including independent component analysis. *Journal of Neuroscience Methods*, Elsevier BV, v. 134, n. 1, p. 9–21, mar 2004. Citado na página 96.

DIEDRICHSEN, J.; YOKOI, A.; ARBUCKLE, S. A. Pattern component modeling: A flexible approach for understanding the representational structure of brain activity patterns. *NeuroImage*, n. March, p. 1–15, 2017. Citado na página 34.

DORNHEGE G., K. M. M. K.-R. . B. B. General signal processing and machine learning tools for bci analysis. In: *Toward Brain-Computer Interfacing.* Cambridge, MA, US: The MIT Press, 2007. p. 207–233. ISBN 9780262042444. Citado 2 vezes nas páginas 40 and 43.

DOUD, A. J.; LUCAS, J. P.; PISANSKY, M. T.; HE, B. Continuous three-dimensional control of a virtual helicopter using a motor imagery based brain-computer interface. *PloS one*, v. 6, n. 10, p. e26322, jan 2011. Citado na página 25.

DUNCAN-JOHNSON, C. C.; DONCHIN, E. The p300 component of the event-related brain potential as an index of information processing. *Biological Psychology*, v. 14, n. 1, p. 1 – 52, 1982. ISSN 0301-0511. Citado na página 83.

EMMERT-STREIB, F.; DEHMER, M. (Ed.). *Information Theory and Statistical Learning*. Springer US, 2009. Disponível em: <https://doi.org/10.1007/978-0-387-84816-7>. Citado na página 94.

ERP, J. B. F. van; LOTTE, F.; TANGERMANN, M. Brain-Computer Interfaces: Beyond Medical Applications. *Computer*, v. 45, n. 4, p. 26–34, 2012. Citado na página 25.

FABIANI, G.; MCFARLAND, D.; WOLPAW, J.; PFURTSCHELLER, G. Conversion of EEG activity into cursor movement by a brain–computer interface (BCI). *IEEE Transactions on Neural Systems and Rehabilitation Engineering*, Institute of Electrical and Electronics Engineers (IEEE), v. 12, n. 3, p. 331–338, sep 2004. Citado 2 vezes nas páginas 40 and 42.

FARQUHAR, J.; HILL, N.; LAL, T.; SCHÖLKOPF, B. Regularised CSP for sensor selection in BCI. In: MAX-PLANCK-GESELLSCHAFT. *Proceedings of the 3rd International Brain-Computer Interface Workshop and Training Course 2006*. Graz, Austria: Verlag der Technischen Universität Graz, 2006. p. 14–15. Citado na página 86.

FARWELL, L. A.; DONCHIN, E. Talking off the top of your head: toward a mental prosthesis utilizing event-related brain potentials. *Electroencephalography and Clinical Neurophysiology*, v. 70, n. 6, p. 510–523, 1988. Citado 3 vezes nas páginas 27, 112, and 121.

FINGELKURTS, A. A.; FINGELKURTS, A. A.; KäHKöNEN, S. Functional connectivity in the brain—is it an elusive concept? *Neuroscience & Biobehavioral Reviews*, Elsevier BV, v. 28, n. 8, p. 827–836, jan 2005. Citado na página 86.

FRIMAN, O.; VOLOSYAK, I.; GRASER, A. Multiple channel detection of steady-state visual evoked potentials for brain-computer interfaces. *IEEE Transactions on Biomedical Engineering*, Institute of Electrical and Electronics Engineers (IEEE), v. 54, n. 4, p. 742–750, apr 2007. Citado na página 83.

GARCIA-MOLINA, G.; ZHU, D. Optimal spatial filtering for the steady state visual evoked potential: BCI application. In: *2011 5th International IEEE/EMBS Conference on Neural Engineering*. [S.l.]: IEEE, 2011. Citado na página 96.

GENÇER, N. G.; ACAR, C. E.; TANZER, I. O. Forward Problem Solution of Magnetic Source Imaging. In: *Magnetic source imaging of the human brain.* Mahwah, NJ, US: Lawrence Erlbaum Associates Publishers, 2003. p. 77–100. ISBN 0-8058-4511-9 (Hardcover); 0-8058-4512-7 (Paperback). Citado na página 33.

GHOSH, P.; MAZUMDER, A.; BHATTACHARYYA, S.; TIBAREWALA, D.; HAYASHIBE, M. Functional connectivity analysis of motor imagery EEG signal for brain-computer interfacing application. In: *2015 7th International IEEE/EMBS Conference on Neural Engineering (NER).* [S.l.]: IEEE, 2015. Citado na página 86.

GILJA, V.; PANDARINATH, C.; BLABE, C. H.; NUYUJUKIAN, P.; SIMERAL, J. D.; SARMA, A. A.; SORICE, B. L.; PERGE, J. A.; JAROSIEWICZ, B.; HOCHBERG, L. R.; SHENOY, K. V.; HENDERSON, J. M. Clinical translation of a high-performance neural prosthesis. *Nature Medicine*, Springer Nature, v. 21, n. 10, p. 1142–1145, sep 2015. Citado na página 35.

GOLUB, G. H.; LOAN, C. F. V. *Matrix Computations (3rd Ed.).* Baltimore, MD, USA: Johns Hopkins University Press, 1996. ISBN 0-8018-5414-8. Citado na página 119.

GÖTTLICH, M.; BEYER, F.; KRÄMER, U. M. BASCO: a toolbox for task-related functional connectivity. *Frontiers in Systems Neuroscience*, Frontiers Media SA, v. 9, sep 2015. Citado na página 92.

GRAIMANN, B.; ALLISON, B.; PFURTSCHELLER, G. Brain–Computer Interfaces: A Gentle Introduction. In: GRAIMANN, B.; PFURTSCHELLER, G.; ALLISON, B. (Ed.). *Brain-Computer Interfaces: Revolutionizing Human-Computer Interaction.* Berlin, Heidelberg: Springer Berlin Heidelberg, 2010. p. 1–27. Citado 2 vezes nas páginas 26 and 56.

GREENBLATT, R. E.; PFLIEGER, M. E.; OSSADTCHI, A. E. Connectivity measures applied to human brain electrophysiological data. *Journal of Neuroscience Methods*, Elsevier B.V., v. 207, n. 1, p. 1–16, 2012. ISSN 01650270. Citado na página 96.

GROSSE-WENTRUP, M.; BUSS, M. Multiclass common spatial patterns and information theoretic feature extraction. *IEEE transactions on bio-medical engineering*, v. 55, n. 8, p. 1991–2000, 2008. Citado na página 42.

GUGER, C.; RAMOSER, H.; PFURTSCHELLER, G. Real-Time EEG Analysis with Subject-Specific Spatial Patterns for a Brain – Computer Interface (BCI). *IEEE transactions on rehabilitation engineering : a publication of the IEEE Engineering in Medicine and Biology Society*, v. 8, n. 4, p. 447–456, 2000. Citado 2 vezes nas páginas 41 and 50.

GUGER, C.; SCHLOGL, A.; NEUPER, C.; WALTERSPACHER, D.; STREIN, T.; PFURTSCHELLER, G. Rapid prototyping of an EEG-based brain-computer interface (BCI). *IEEE Transactions on Neural Systems and Rehabilitation Engineering*, Institute of Electrical and Electronics Engineers (IEEE), v. 9, n. 1, p. 49–58, mar 2001. Citado 2 vezes nas páginas 44 and 50.

GUYON, I.; ELISSEEFF, A. Special issue on variable and feature selection. *An Introduction to Variable and Feature Selection*, v. 3, p. 1157–1182, 2003. Citado 3 vezes nas páginas 43, 62, and 99.

HALDER, S.; AGORASTOS, D.; VEIT, R.; HAMMER, E.; LEE, S.; VARKUTI, B.; BOGDAN, M.; ROSENSTIEL, W.; BIRBAUMER, N.; KüBLER, A. Neural mechanisms of brain–computer interface control. *NeuroImage*, Elsevier BV, v. 55, n. 4, p. 1779–1790, apr 2011. Citado na página 39.

HAUFE, S.; TOMIOKA, R.; DICKHAUS, T.; SANNELLI, C.; BLANKERTZ, B.; NOLTE, G.; MULLER, K.-R. Localization of class-related mu-rhythm desynchronization in motor imagery based brain-computer interface sessions. In: *2010 Annual International Conference of the IEEE Engineering in Medicine and Biology*. [S.l.]: IEEE, 2010. Citado na página 103.

HAYKIN, S. *Adaptive Filter Theory (5th Ed.)*. Upper Saddle River, NJ, USA: Prentice-Hall, Inc., 2008. ISBN 0-13-322760-X. Citado na página 60.

HAYNES, J. D. A Primer on Pattern-Based Approaches to fMRI: Principles, Pitfalls, and Perspectives. *Neuron*, Elsevier Inc., v. 87, n. 2, p. 257–270, 2015. Citado na página 34.

HAYNES, J.-D.; REES, G. Decoding mental states from brain activity in humans. v. 7, n. July, p. 523–534, 2006. Citado na página 34.

HUANG, G.-B.; CHEN, L.; SIEW, C.-K. Universal approximation using incremental feedforward networks with arbitrary input weights. *Technical Report ICIS/46/2003*, Nayang Technological University, Oct 2003. Citado 3 vezes nas páginas 65, 66, and 67.

HUANG, G.-B.; WANG, D. H.; LAN, Y. Extreme learning machines: a survey. *International Journal of Machine Learning and Cybernetics*, Springer Nature, v. 2, n. 2, p. 107–122, may 2011. Citado 2 vezes nas páginas 65 and 100.

HUANG, G.-B.; ZHU, Q.-Y.; SIEW, C.-K. Extreme learning machine: Theory and applications. *Neurocomputing*, Elsevier BV, v. 70, n. 1-3, p. 489–501, dec 2006. Citado 2 vezes nas páginas 65 and 100.

HUEBNER, D.; VERHOEVEN, T.; MUELLER, K.-R.; KINDERMANS, P.-J.; TANGERMANN, M. Unsupervised learning for brain-computer interfaces based on event-related potentials: Review and online comparison [research frontier]. *IEEE Computational Intelligence Magazine*, v. 13, n. 2, p. 66–67, 2018. ISSN 1556-603X. Citado 3 vezes nas páginas 26, 28, and 44.

KA XIONG CHARAND. *Action Potentials*. 2002. <http://hyperphysics.phy-astr.gsu.edu/hbase/Biology/actpot.html>. Access on 28 jul. 2018. Citado na página 32.

KANOH, S.; MURAYAMA, Y. m.; MIYAMOTO, K. i.; YOSHINOBU, T.; KAWASHIMA, R. A NIRS-based brain-computer interface system during motor imagery: System development and online feedback training. In: *2009 Annual International Conference of the IEEE Engineering in Medicine and Biology Society*. [S.l.]: IEEE, 2009. Citado na página 35.

KENNEDY, P. R.; BAKAY, R. A. Restoration of neural output from a paralyzed patient by a direct brain connection. *NeuroReport*, v. 9, n. 8, p. 1707–1711, 1998. Citado na página 35.

KINDERMANS, P.-J.; VERSTRAETEN, D.; SCHRAUWEN, B. A bayesian model for exploiting application constraints to enable unsupervised training of a P300-based BCI. *PLoS ONE*, Public Library of Science (PLoS), v. 7, n. 4, p. e33758, apr 2012. Citado 3 vezes nas páginas 37, 111, and 114.

KLUGE, T.; HARTMANN, M. Phase coherent detection of steady-state evoked potentials: Experimental results and application to brain-computer interfaces. In: *2007 3rd International IEEE/EMBS Conference on Neural Engineering*. [S.l.: s.n.], 2007. p. 425–429. ISSN 1948-3546. Citado na página 83.

KOCH, M. A.; NORRIS, D. G.; HUND-GEORGIADIS, M. An investigation of functional and anatomical connectivity using magnetic resonance imaging. *NeuroImage*, Elsevier BV, v. 16, n. 1, p. 241–250, may 2002. Citado na página 87.

KOHAVI, R.; JOHN, G. H. Wrappers for feature subset selection. *Artificial Intelligence*, Elsevier BV, v. 97, n. 1-2, p. 273–324, dec 1997. Citado 3 vezes nas páginas 43, 62, and 63.

LAKSHMI, M. R.; PRASAD, T. V.; CHANDRA, P. V. Survey on EEG Signal Processing Methods. *International Journal of Advanced Research in Computer Science and Software Engineering*, v. 4, n. 1, p. 2277–128, 2014. Citado 2 vezes nas páginas 79 and 96.

LARSON, E.; LEE, A. K. C. Potential use of MEG to understand abnormalities in auditory function in clinical populations. *Frontiers in Human Neuroscience*, Frontiers Media SA, v. 8, mar 2014. Citado na página 33.

LI, K.; RAJU, V. N.; SANKAR, R.; ARBEL, Y.; DONCHIN, E. Advances and challenges in signal analysis for single trial p300-BCI. In: *Foundations of Augmented Cognition. Directing the Future of Adaptive Systems*. [S.l.]: Springer Berlin Heidelberg, 2011. p. 87–94. Citado na página 111.

LIU, W.; POKHAREL, P.; PRINCIPE, J. Correntropy: A Localized Similarity Measure. *The 2006 IEEE International Joint Conference on Neural Network Proceedings*, n. 5, p. 4919–4924, 2006. ISSN 10987576. Citado 2 vezes nas páginas 93 and 94.

LIU, W.; POKHAREL, P. P.; PRINCIPE, J. C. Correntropy: Properties and applications in non-Gaussian signal processing. *IEEE Transactions on Signal Processing*, v. 55, n. 11, p. 5286–5298, 2007. Citado na página 94.

LIYANAGE, S. R.; GUAN, C.; ZHANG, H.; ANG, K. K.; XU, J.; LEE, T. H. Dynamically weighted ensemble classification for non-stationary EEG processing. *Journal of Neural Engineering*, IOP Publishing, v. 10, n. 3, p. 036007, apr 2013. Citado na página 52.

LOTTE, F. Signal processing approaches to minimize or suppress calibration time in oscillatory activity-based Brain-Computer Interfaces. *Proceedings of the IEEE, Institute of Electrical and Electronics Engineers*, 2015. ISSN 00189219. Citado 4 vezes nas páginas 10, 25, 48, and 80.

LOTTE, F.; BOUGRAIN, L.; CICHOCKI, A.; CLERC, M.; CONGEDO, M.; RAKOTOMAMONJY, A.; YGER, F. A review of classification algorithms for EEG-based brain–computer interfaces: a 10 year update. *Journal of Neural Engineering*, IOP Publishing, v. 15, n. 3, p. 031005, 2018. Citado na página 84.

LOTTE, F.; CONGEDO, M.; LÉCUYER, a.; LAMARCHE, F.; ARNALDI, B. A review of classification algorithms for EEG-based brain-computer interfaces. *Journal of neural engineering*, v. 4, n. 2, p. R1–R13, jun 2007. Citado 6 vezes nas páginas 26, 27, 28, 46, 100, and 113.

LUMEN. *The Nervous System: Biology for majors II*. 2018. <https://courses.lumenlearning.com/wm-biology2/chapter/brain/>. Access on 30 jul. 2018. Citado 2 vezes nas páginas 10 and 36.

MACKAY, D. J. C. Bayesian interpolation. *Neural Computation*, MIT Press - Journals, v. 4, n. 3, p. 415–447, may 1992. Citado na página 127.

MAHAJAN, R.; BANSAL, D.; KHATTER, A. EEG based cognitive brain mapping in time domain to analyze EM radiation effect on human brain. In: *Communications in Computer and Information Science*. [S.l.]: Springer Singapore, 2018. p. 308–319. Citado na página 59.

MALMIVUO, J.; PLONSEY, R. Bioelectromagnetism. In: *Bioelectromagnetism - Principles and Applications of Bioelectric and Biomagnetis Fields*. Oxford. New York: Oxford University Press, 2017. cap. 13. Citado 2 vezes nas páginas 10 and 34.

MANYAKOV, N. V.; CHUMERIN, N.; COMBAZ, A.; Van Hulle, M. M. Comparison of classification methods for P300 brain-computer interface on disabled subjects. *Computational Intelligence and Neuroscience*, v. 2011, 2011. ISSN 16875265. Citado na página 114.

MASON, S. G.; BASHASHATI, A.; FATOURECHI, M.; NAVARRO, K. F.; BIRCH, G. E. A comprehensive survey of brain interface technology designs. *Annals of Biomedical Engineering*, Springer Nature, v. 35, n. 2, p. 137–169, nov 2006. Citado na página 33.

MAYO CLINIC. *Spinal Cord Injury*. 2017. <https://www.mayoclinic.org/diseases-conditions/spinal-cord-injury/symptoms-causes/syc-20377890>. Access on 19 jul. 2018. Citado na página 24.

MCFARLAND, D. J.; MCCANE, L. M.; DAVID, S. V.; WOLPAW, J. R. Spatial filter selection for EEG-based communication. *Electroencephalography and clinical neurophysiology*, v. 103, n. 3, p. 386–94, sep 1997. ISSN 0013-4694. Citado 4 vezes nas páginas 11, 40, 56, and 57.

MCFARLAND, D. J.; NEAT, G. W.; READ, R. F.; WOLPAW, J. R. An EEG-based method for graded cursor control. *Psychobiol.*, v. 21, p. 77–81, 1993. Citado na página 49.

MERCK MANUALS. *Homunculus*. 2018. <https://www.merckmanuals.com/professional/multimedia/figure/neu_homunculus.> Access on 17 sep. 2018. Citado 2 vezes nas páginas 10 and 40.

MIJALKOV, M.; KAKAEI, E.; PEREIRA, J. B.; WESTMAN, E.; AND, G. V. BRAPH: A graph theory software for the analysis of brain connectivity. *PLOS ONE*, Public Library of Science (PLoS), v. 12, n. 8, p. e0178798, aug 2017. Citado na página 89.

MILLÁN, J. D. R.; RUPP, R.; MÜLLER-PUTZ, G. R.; MURRAY-SMITH, R.; GIUGLIEMMA, C.; TANGERMANN, M.; VIDAURRE, C.; CINCOTTI, F.; KÜBLER, a.; LEEB, R.; NEUPER, C.; MÜLLER, K.-R.; MATTIA, D. Combining Brain-Computer Interfaces and Assistive Technologies: State-of-the-Art and Challenges. *Frontiers in neuroscience*, v. 4, n. September, p. 1–15, jan 2010. ISSN 1662-453X. Citado 3 vezes nas páginas 23, 24, and 25.

MONTEIRO, L. H. A. *Sistemas Dinâmicos Complexos*. [S.l.]: LF editorial, 2014. Citado na página 98.

MULLER-PUTZ, G.; PFURTSCHELLER, G. Control of an electrical prosthesis with an SSVEP-based BCI. *Biomedical Engineering, IEEE Transactions on*, v. 55, n. 1, p. 361–364, 2008. Citado na página 25.

MYERS, A. D. W. J. L. *Research Design and Statistical Analysis, Third Edition*. [S.l.]: London: Lawrence Erlbaum Associates, 2003. Citado na página 92.

NAIK, G. R. Measure of Quality of Source Separation for Sub- and Super-Gaussian Audio Mixtures. v. 23, n. 4, p. 581–599, 2012. Citado 3 vezes nas páginas 11, 58, and 60.

NEUPER, C.; SCHERER, R.; REINER, M.; PFURTSCHELLER, G. Imagery of motor actions: Differential effects of kinesthetic and visual–motor mode of imagery in single-trial EEG. *Cognitive Brain Research*, Elsevier BV, v. 25, n. 3, p. 668–677, dec 2005. Citado na página 103.

NEWMAN, M. E. J. Mathematics of networks. In: *Networks: An Introduction*. [S.l.]: Oxford University Press, 2010. p. 109–167. Citado na página 98.

NEWMAN, M. J. A measure of betweenness centrality based on random walks. *Social Networks*, Elsevier BV, v. 27, n. 1, p. 39–54, jan 2005. Citado na página 97.

NEWMAN, M. J. *Networks: An Introduction*. [S.l.]: Oxford University Press, 2010. Citado 3 vezes nas páginas 87, 88, and 89.

NG, K. B.; BRADLEY, A. P.; CUNNINGTON, R. Stimulus specificity of a steady-state visual-evoked potential-based brain-computer interface. *Journal of neural engineering*, v. 9, n. 3, p. 036008, jun 2012. Citado 2 vezes nas páginas 10 and 37.

NOVI, Q.; GUAN, C.; DAT, T. H.; XUE, P. Sub-band Common Spatial Pattern (SBCSP) for Brain-Computer Interface. *2007 3rd International IEEE/EMBS Conference on Neural Engineering*, Ieee, p. 204–207, may 2007. Citado 2 vezes nas páginas 51 and 86.

OOSTENVELD, R.; PRAAMSTRA, P. The five percent electrode system for high-resolution EEG and ERP measurements. *Clinical Neurophysiology*, Elsevier BV, v. 112, n. 4, p. 713–719, apr 2001. Citado na página 54.

ORTNER, R.; ALLISON, B. Z.; KORISEK, G.; GAGGL, H.; PFURTSCHELLER, G. An SSVEP BCI to control a hand orthosis for persons with tetraplegia. *IEEE transactions on neural systems and rehabilitation engineering*, v. 19, n. 1, p. 1–5, feb 2011. ISSN 1558-0210. Citado na página 25.

PERRIN, X.; CHAVARRIAGA, R.; COLAS, F.; SIEGWART, R.; MILLÁN, J. del R. Brain-coupled interaction for semi-autonomous navigation of an assistive robot. *Robotics and Autonomous Systems*, Elsevier BV, v. 58, n. 12, p. 1246–1255, dec 2010. Citado na página 44.

PFURTSCHELLER, G.; ARANIBAR, A. Event-related cortical desynchronization detected by power measurements of scalp EEG. *Electroencephalography and Clinical Neurophysiology*, Elsevier BV, v. 42, n. 6, p. 817–826, jun 1977. Citado na página 39.

PFURTSCHELLER, G.; FLOTZINGER, D.; KALCHER, J. Brain-Computer Interface—a new communication device for handicapped persons. *Journal of Microcomputer Applications*, v. 16, n. 3, p. 293–299, 1993. Citado 2 vezes nas páginas 47 and 49.

PFURTSCHELLER, G.; NEUPER, C. Motor imagery and direct brain-computer communication. *Proceedings of the IEEE*, v. 89, n. 7, p. 1123–1134, jul 2001. Citado 6 vezes nas páginas 26, 38, 46, 47, 70, and 85.

PFURTSCHELLER, G.; NEUPER, C.; FLOTZINGER, D.; PREGENZER, M. EEG-based discrimination between imagination of right and left hand movement. *Electroencephalography and Clinical Neurophysiology*, v. 103, n. 6, p. 642–651, 1997. Citado 2 vezes nas páginas 39 and 49.

PINEGGER, A.; WRIESSNEGGER, S. C.; FALLER, J.; MüLLER-PUTZ, G. R. Evaluation of different EEG acquisition systems concerning their suitability for building a brain–computer interface: Case studies. *Frontiers in Neuroscience*, Frontiers Media SA, v. 10, sep 2016. Citado na página 33.

POKHAREL, P.; SANTAMARIA, I.; XU, J.; JEONG, K. hwa; LIU, W. Correntropy for random processes: Properties and applications in signal processing. In: *Information Theoretic Learning*. [S.l.]: Springer New York, 2010. p. 415–455. Citado na página 93.

PRINCIPE, J. C. *Information Theoretic Learning*. [S.l.: s.n.], 2010. ISSN 1613-9011. ISBN 978-1-4419-1569-6. Citado 2 vezes nas páginas 92 and 93.

QI, H.; ZHU, Y.; MING, D.; WAN, B. Independent Component Analysis using clustering on motor imagery EEG. *Conference proceedings : ... Annual International Conference of the IEEE Engineering in Medicine and Biology Society. IEEE Engineering in Medicine and Biology Society. Conference*, v. 2009, p. 4735–4738, jan 2009. ISSN 1557-170X. Citado na página 51.

QIN, L.; DING, L.; HE, B. Motor imagery classification by means of source analysis for brain-computer interface applications. *Journal of neural engineering*, v. 1, n. 3, p. 135–141, sep 2004. ISSN 1741-2560. Citado 2 vezes nas páginas 50 and 86.

RAKOTOMAMONJY, A.; GUIGUE, V. BCI competition III: Dataset II- ensemble of SVMs for BCI P300 speller. *IEEE Transactions on Biomedical Engineering*, v. 55, n. 3, p. 1147–1154, 2008. ISSN 00189294. Citado 2 vezes nas páginas 83 and 114.

RAMOSER, H.; MULLER-GERKING, J.; PFURTSCHELLER, G. Optimal spatial filtering of single trial EEG during imagined hand movement. *IEEE Transactions on Rehabilitation Engineering*, Institute of Electrical and Electronics Engineers (IEEE), v. 8, n. 4, p. 441–446, 2000. Citado 4 vezes nas páginas 42, 46, 49, and 85.

RAO, R. P. N. *Brain-Computer Interfacing*. [S.l.]: Cambridge University Press, 2013. Citado na página 56.

RIBEIRO, A. S.; LACERDA, L. M.; FERREIRA, H. A. Multimodal imaging brain connectivity analysis (MIBCA) toolbox. *PeerJ*, PeerJ, v. 3, p. e1078, jul 2015. Citado 2 vezes nas páginas 11 and 87.

RIVET, B.; SOULOUMIAC, A. Optimal linear spatial filters for event-related potentials based on a spatio-temporal model: Asymptotical performance analysis. *Signal Processing*, Elsevier, v. 93, n. 2, p. 387–398, 2013. Citado 7 vezes nas páginas 36, 111, 114, 115, 116, 118, and 120.

RIVET, B.; SOULOUMIAC, A.; GIBERT, G.; ATTINA, V.; BERTRAND, O. Sensor selection for P300 speller brain computer interface. In: *17th European Symposium on Artificial Neural Networks (ESANN 2009)*. Bruges, Belgium: [s.n.], 2009. p. –. Citado na página 37.

RODRIGUES, P. G.; STEFANO, F. C. A.; ATTUX, R.; CASTELLANO, G.; SORIANO, D. C. Performance comparison of functional connectivity evaluation for graph-based classification in brain-computer interface. In: *VIII Simpósio de Instrumentação e Imagens Médicas & VII Simpósio de Processamento de Sinais, São Bernardo do Campo, São Paulo, Brasil*. [S.l.: s.n.], 2017. Citado na página 80.

RUBINOV, M.; SPORNS, O. Complex network measures of brain connectivity: Uses and interpretations. *NeuroImage*, Elsevier BV, v. 52, n. 3, p. 1059–1069, sep 2010. Citado 2 vezes nas páginas 90 and 91.

SAEEDI, S.; CHAVARRIAGA, R.; MILLAN, J. D. R. Long-term stable control of motor-imagery BCI by a locked-in user through adaptive assistance. *IEEE Transactions on Neural Systems and Rehabilitation Engineering*, v. 25, n. 4, p. 380–391, 2017. Citado na página 25.

SAKKALIS, V. Review of advanced techniques for the estimation of brain connectivity measured with EEG/MEG. *Computers in Biology and Medicine*, Elsevier, v. 41, n. 12, p. 1110–1117, 2011. ISSN 00104825. Citado 3 vezes nas páginas 87, 89, and 91.

SANEI, S.; CHAMBERS, J. Introduction to EEG. In: *EEG Signal Processing*. [S.l.]: John Wiley & Sons Ltd,, 2013. p. 1–34. Citado 5 vezes nas páginas 10, 30, 31, 32, and 33.

SANTAMARÍA, I.; MEMBER, S.; POKHAREL, P. P.; MEMBER, S.; PRINCIPE, J. C. Generalized Correlation Function : Definition , Properties , and Application to Blind Equalization. v. 54, n. 6, p. 2187–2197, 2006. Citado na página 92.

SCHIRRMEISTER, R. T.; SPRINGENBERG, J. T.; FIEDERER, L. D. J.; GLASSTETTER, M.; EGGENSPERGER, K.; TANGERMANN, M.; HUTTER, F.; BURGARD, W.; BALL, T. Deep learning with convolutional neural networks for EEG decoding and visualization. *Human Brain Mapping*, Wiley, v. 38, n. 11, p. 5391–5420, aug 2017. Citado na página 28.

SCHLINDWEIN, F. S.; EVANS, D. H. Autoregressive spectral analysis as an alternative to fast fourier transform analysis of doppler ultrasound signals. In: *Diagnostic Vascular Ultrasound*. [S.l.]: Edward Arnold, 1992. cap. 8. Citado na página 61.

SCHLÖGL, A.; KEINRATH, C.; ZIMMERMANN, D.; SCHERER, R.; LEEB, R.; PFURTSCHELLER, G. A fully automated correction method of EOG artifacts in EEG recordings. *Clinical Neurophysiology*, Elsevier BV, v. 118, n. 1, p. 98–104, jan 2007. Citado na página 40.

SCHLÖGL, A.; LEE, F.; BISCHOF, H.; PFURTSCHELLER, G. Characterization of four-class motor imagery EEG data for the BCI-competition 2005. *Journal of neural engineering*, v. 2, n. 4, p. L14–22, dec 2005. ISSN 1741-2560. Citado na página 50.

SEKIHARA, S. S. N. K. Neuromagnetic source reconstruction and inverse modeling. In: *Modeling and Imaging of Bioelectrical Activity*. [S.l.]: Springer US, 2005. Citado na página 84.

SERENCES, J. T.; SAPROO, S. Computational advances towards linking BOLD and behavior. *Neuropsychologia*, Elsevier BV, v. 50, n. 4, p. 435–446, mar 2012. Citado na página 35.

SHAN, H.; XU, H.; ZHU, S.; HE, B. A novel channel selection method for optimal classification in different motor imagery BCI paradigms. *Biomedical engineering online*, BioMed Central, v. 14, n. 1, p. 93, 2015. Citado 2 vezes nas páginas 26 and 52.

SHEN, M. S. M.; ZHANG, X. Z. X.; LI, X. L. X. Independent component analysis of electroencephalographic signals. *6th International Conference on Signal Processing, 2002.*, v. 2, n. 3, 2002. Citado na página 85.

SHENOY, P.; KRAULEDAT, M.; BLANKERTZ, B.; RAO, R. P. N.; MüLLER, K.-R. Towards adaptive classification for BCI. *Journal of Neural Engineering*, IOP Publishing, v. 3, n. 1, p. R13–R23, mar 2006. Citado na página 52.

SHIN, J.; MÜLLER, K.-R.; HWANG, H.-J. Near-infrared spectroscopy (NIRS)-based eyes-closed brain-computer interface (BCI) using prefrontal cortex activation due to mental arithmetic. *Scientific Reports*, Springer Nature, v. 6, n. 1, nov 2016. Citado na página 35.

SHOICHET, M. S.; TATE, C. C.; BAUMANN, M. D.; LAPLACA, M. C. Regeneration and repair in the injured central nervous system. In: REICHERT, W. M. (Ed.). *Indwelling Neural Implants: Strategies for Contending with the In Vivo Environment.* Boca Raton (FL): CRC Press/Taylor & Francis, 2008. cap. 8. Citado na página 24.

SILVERMAN, B. W. *Density Estimation for Statistics and Data Analysis*. [S.l.]: Springer US, 1986. Citado na página 94.

SIVAKAMI, A.; DEVI, S. S. Analysis of eeg for motor imagery based classification of hand activities. In: . [S.l.: s.n.], 2015. Citado na página 103.

SPIEGLER, A.; GRAIMANN, B.; PFURTSCHELLER, G. Phase coupling between different motor areas during tongue-movement imagery. *Neuroscience Letters*, v. 369, n. 1, p. 50 – 54, 2004. ISSN 0304-3940. Citado na página 84.

SPORNS, O. *Networks of the Brain*. [S.l.]: The MIT Press, 2011. Citado 2 vezes nas páginas 90 and 91.

STEFANO FILHO, C. A. *Performance analysis of graph metrics for assessing hand motor imagery tasks from electroencephalography data*. Dissertação (Mestrado), 2016. Citado na página 95.

STEFANO FILHO, C. A.; ATTUX, R.; CASTELLANO, G. Can graph metrics be used for EEG-BCIs based on hand motor imagery? *Biomedical Signal Processing and Control*, Elsevier Ltd, v. 40, p. 359–365, 2018. ISSN 17468108. Citado 2 vezes nas páginas 80 and 86.

STIPPICH, C.; OCHMANN, H.; SARTOR, K. Somatotopic mapping of the human primary sensorimotor cortex during motor imagery and motor execution by functional magnetic resonance imaging. *Neuroscience Letters*, Elsevier BV, v. 331, n. 1, p. 50–54, oct 2002. Citado na página 39.

STÖGBAUER, H.; KRASKOV, a.; ASTAKHOV, S.; GRASSBERGER, P. Least-dependent-component analysis based on mutual information. *Phys. Rev. E*, v. 70, n. Mic, p. 66123, 2004. ISSN 1539-3755. Citado 2 vezes nas páginas 58 and 59.

STOICA, P.; MOSES, R. *Spectral analysis of signals*. Upper Saddle River, NJ, USA: Prentice-Hall, Inc., 2005. ISBN 0-13-322760-X. Citado na página 62.

TANG, Z.; LI, C.; SUN, S. Single-trial EEG classification of motor imagery using deep convolutional neural networks. *Optik - International Journal for Light and Electron Optics*, Elsevier BV, v. 130, p. 11–18, feb 2017. Citado 2 vezes nas páginas 10 and 40.

TANGERMANN, M.; MüLLER, K.-R.; AERTSEN, A.; BIRBAUMER, N.; BRAUN, C.; BRUNNER, C.; LEEB, R.; MEHRING, C.; MILLER, K. J.; MüLLER-PUTZ, G. R.; NOLTE, G.; PFURTSCHELLER, G.; PREISSL, H.; SCHALK, G.; SCHLöGL, A.; VIDAURRE, C.; WALDERT, S.; BLANKERTZ, B. Review of the BCI competition IV. *Frontiers in Neuroscience*, Frontiers Media SA, v. 6, 2012. Citado 2 vezes nas páginas 80 and 99.

TEPLAN, M. Fundamentals of EEG measurement. *Measurement Science Review*, v. 2, p. 1–11, 2002. Citado 4 vezes nas páginas 26, 33, 47, and 55.

THE NATIONAL INSTITUTE OF NEUROLOGICAL DISORDERS AND STROKE, NIH. *Brain Basics: The Life and Death of a Neuron*. 2018. <https://www.ninds.nih.gov/Disorders/Patient-Caregiver-Education/Life-and-Death-Neuron>. Access on 27 jul. 2018. Citado 2 vezes nas páginas 10 and 31.

THEODORIDIS, S. Optimal margin classification: support vector machines. In: *Machine Learning: A Bayesian and Optimization Perspective, 1st Edition*. Orlando, FL, USA: Academic Press, 2015. p. 539–551. Citado na página 69.

THEODORIDIS, S.; KOUTROUMBAS., K. Feature selection. In: *Pattern Recognition, Second Edition*. Orlando, FL, USA: Academic Press, 2003. Citado na página 63.

THEODORIDIS, S.; KOUTROUMBAS., K. Feature selection. In: *Pattern Recognition, Fourth Edition*. Orlando, FL, USA: Academic Press, 2008. p. 261–322. Citado 9 vezes nas páginas 11, 42, 43, 62, 63, 65, 67, 70, and 100.

THEODORIDIS, S.; PIKRAKIS, A.; KOUTROUMBAS, K.; CAVOURAS, D. *Introduction to Pattern Recognition: A Matlab Approach*. Orlando, FL, USA: Academic Press, Inc., 2010. ISBN 0123744865, 9780123744869. Citado 3 vezes nas páginas 11, 64, and 68.

THULASIDAS, M.; GUAN, C. Optimization of BCI Speller Based on P300 Potential. In: *2005 IEEE Engineering in Medicine and Biology 27th Annual Conference*. [S.l.: s.n.], 2005. p. 5396–5399. ISBN 0780387406. Citado na página 83.

THULASIDAS, M.; GUAN, C.; WU, J. Robust classification of EEG signal for brain-computer interface. *IEEE transactions on neural systems and rehabilitation engineering : a publication of the IEEE Engineering in Medicine and Biology Society*, v. 14, n. 1, p. 24–29, 2006. ISSN 1534-4320. Citado na página 83.

TOPPI, J.; FALLANI, F. D. V.; VECCHIATO, G.; MAGLIONE, A. G.; CINCOTTI, F.; MATTIA, D.; SALINARI, S.; BABILONI, F.; ASTOLFI, L. How the statistical validation of functional connectivity patterns can prevent erroneous definition of small-world properties of a brain connectivity network. *Computational and Mathematical Methods in Medicine*, Hindawi Limited, v. 2012, p. 1–13, 2012. Citado na página 97.

URIBE, L. F. S.; FAZANARO, F. I.; CASTELLANO, G.; SUYAMA, R.; ATTUX, R.; CARDOZO, E.; SORIANO, D. C. A recurrence-based approach for feature extraction in brain-computer interface systems. In: *Springer Proceedings in Mathematics & Statistics*. [S.l.]: Springer International Publishing, 2014. p. 95–107. Citado na página 82.

URIBE, L. F. S.; STEFANO FILHO, C. A.; OLIVATTO, V.; OLIVEIRA, V.; SORIANO, D. C.; BOCCATO, L.; CASTELLANO, G.; ATTUX, R. A comparative analysis of correlation and correntropy in graph-based brain computer interfaces. In: *XXXV Simpósio Brasileiro de Telecomunicações, São Pedro, Brasil*. [S.l.]: Sociedade Brasileira de Telecomunicações, 2017. Citado na página 80.

VAID, S.; SINGH, P.; KAUR, C. EEG signal analysis for BCI interface: A review. *International Conference on Advanced Computing and Communication Technologies, ACCT*, v. 2015-April, p. 143–147, 2015. ISSN 23270659. Citado 2 vezes nas páginas 79 and 82.

VANDEREYCKEN, B. Low-rank matrix completion by Riemannian optimization—extended version. *ArXiv e-prints*, set. 2012. Citado na página 129.

VIDAL, J. Real-time detection of brain events in EEG. *Proceedings of the IEEE*, Institute of Electrical and Electronics Engineers (IEEE), v. 65, n. 5, p. 633–641, 1977. Citado 2 vezes nas páginas 30 and 69.

VIDAURRE, C.; BLANKERTZ, B. Towards a cure for BCI illiteracy. *Brain Topography*, Springer Nature, v. 23, n. 2, p. 194–198, nov 2009. Citado na página 39.

WANG, Y.; WANG, Y.-T.; JUNG, T.-P. Translation of EEG spatial filters from resting to motor imagery using independent component analysis. *PloS one*, v. 7, n. 5, p. e37665, jan 2012. ISSN 1932-6203. Citado 4 vezes nas páginas 42, 51, 57, and 58.

WATTS, D. J.; STROGATZ, S. H. Collective dynamics of 'small-world' networks. *Nature*, Springer Nature, v. 393, n. 6684, p. 440–442, jun 1998. Citado na página 90.

WELCH, P. The use of fast fourier transform for the estimation of power spectra: A method based on time averaging over short, modified periodograms. *IEEE Transactions on Audio and Electroacoustics*, Institute of Electrical and Electronics Engineers (IEEE), v. 15, n. 2, p. 70–73, jun 1967. Citado na página 60.

WOLPAW, J.; BIRBAUMER, N.; HEETDERKS, W.; MCFARLAND, D.; PECKHAM, P.; SCHALK, G.; DONCHIN, E.; QUATRANO, L.; ROBINSON, C.; VAUGHAN, T. Brain-computer interface technology: a review of the first international meeting. *IEEE Transactions on Rehabilitation Engineering*, Institute of Electrical and Electronics Engineers (IEEE), v. 8, n. 2, p. 164–173, jun 2000. Citado na página 30.

WOLPAW, J. R.; BIRBAUMER, N.; MCFARLAND, D. J.; PFURTSCHELLER, G.; VAUGHAN, T. M. Brain-computer interfaces for communication and control. *Clinical neurophysiology : official journal of the International Federation of Clinical Neurophysiology*, v. 113, n. 6, p. 767–791, jun 2002. ISSN 1388-2457. Citado 2 vezes nas páginas 23 and 26.

WOLPAW, J. R.; MCFARLAND, D. J. Multichannel EEG-based brain-computer communication. *Electroencephalography and Clinical Neurophysiology*, v. 90, n. 6, p. 444–449, 1994. ISSN 00134694. Citado na página 49.

WOLPAW, J. R.; MCFARLAND, D. J.; NEAT, G. W.; FORNERIS, C. A. An EEG-based brain-computer interface for cursor control. *Electroencephalography and Clinical Neurophysiology*, v. 78, n. 3, p. 252–259, 1991. ISSN 00134694. Citado na página 48.

YGER, F.; BERAR, M.; LOTTE, F. Riemannian Approaches in Brain-Computer Interfaces: A Review. *IEEE Transactions on Neural Systems and Rehabilitation Engineering*, v. 25, n. 10, p. 1753–1762, 2017. Citado na página 28.

YUAN, H.; HE, B. Brain–computer interfaces using sensorimotor rhythms: Current state and future perspectives. *IEEE Transactions on Biomedical Engineering*, Institute of Electrical and Electronics Engineers (IEEE), v. 61, n. 5, p. 1425–1435, may 2014. Citado na página 35.

ZHANG Z. ZHANG, D. W.-Y. D. Y. Centrality measure in weighted networks based on an amoeboid algorithm. *Journal of Information & Computational Science*, Binary Information Press, v. 9, n. 2, p. 369–376, 2012. Citado na página 98.

ZHOU, B.; WU, X.; ZHANG, L.; LV, Z.; GUO, X. Robust Spatial Filters on Three-Class Motor Imagery EEG Data Using Independent Component Analysis. n. April, p. 43–49, 2014. Citado na página 52.

Annex

ANNEX A – Published work

Journal Publications

CARVALHO, S. N.; COSTA, T. B. S.; URIBE, L. F. S.; SORIANO, D. C.; YARED, G. F. G.; CORADINE, L. C.; ATTUX, R. Comparative analysis of strategies for feature extraction and classification in ssvep bcis. Biomedical Signal Processing and Control, Elsevier Ltd, v. 21, p. 34–42, 2015.

Conference Publications

URIBE, L. F. S.; STEFANO FILHO, C. A.; OLIVATTO, V.; OLIVEIRA, V.; SORIANO, D. C.; BOCCATO, L.; CASTELLANO, G.; ATTUX, R. A comparative analysis of correlation and correntropy in graph-based brain computer interfaces. In: XXXV Simpósio Brasileiro de Telecomunicações, São Pedro, Brasil. [S.l.]: Sociedade Brasileira de Telecomunicações, 2017.

URIBE, L. F. S.; KERSANACH, M. B.; COSTA, T. B. S.; CARVALHO, S. N.; SORIANO, D. C.; ATTUX, R. Deterministic and stochastic wrappers for motor imagery BCIs. In: . [S.l.]: Conference: 4th BRAINN Congress, Campinas-SP, Brazil, 2017.

URIBE, L. F. S.; COSTA, T. B. S.; CARVALHO, S. N.; SORIANO, D. C.; SUYAMA, R.; ATTUX, R. Two-class motor imagery BCI based on the combined use of ICA and feature selection. In: XXV Congresso Brasileiro de Engenharia Biomédica, Foz do Iguaçu, Brazil. [S.l.]: Sociedade Brasileira de Engenharia Biomédica, 2016.

STEFANO FILHO, C. A.; CAMPOS, B. M. de; COSTA, T. B. S.; URIBE, L. F. S.; BARRETO, C. S. F.; ATTUX, R.; CASTELLANO, G. Graphs metrics as features for an LDA based classifier for motor imagery data. In: . [S.l.]: Conference: 3rd BRAINN Congress, Campinas-SP, Brazil, 2016.

SILVA JÚNIOR, J. I. da; CARVALHO, S. N.; COSTA, T. B. S.; URIBE, L. F. S.; SUYAMA, R.; ATTUX, R.; SORIANO, D. C. Spectral vs. canonical correlation analysis for feature extraction in BCI-SSVEP systems. In: . [S.l.]: Conference: 3rd BRAINN Congress, Campinas-SP, Brazil, 2016.

URIBE, L. F. S.; COSTA, T. B. S.; CARVALHO, S. N.; STEFANO FILHO, C. A.; SORIANO, D. C.; SUYAMA, R.; ATTUX, R. Two-class motor imagery BCI based on the combined use of ICA and feature selection: preliminary results. In: . [S.l.]: Conference:

CARVALHO, S. N.; COSTA, T. B.; URIBE, L. F.; SORIANO, D. C.; ALMEIDA,

S. R.; MIN, L. L.; CASTELLANO, G.; ATTUX, R. Effect of the combination of different numbers of flickering frequencies in an ssvep-bci for healthy volunteers and stroke patients. International IEEE/EMBS Conference on Neural Engineering, NER, v.2015-July, p. 78–81, 2015.